

AN ANALYTICAL AND COMPUTATIONAL INVESTIGATION INTO THE EFFECT OF  
SURFACE FRICTION ON THE BEHAVIOR OF A CENTRIFUGAL PENDULUM VIBRATION  
ABSORBER

By

Alina Berkowitz

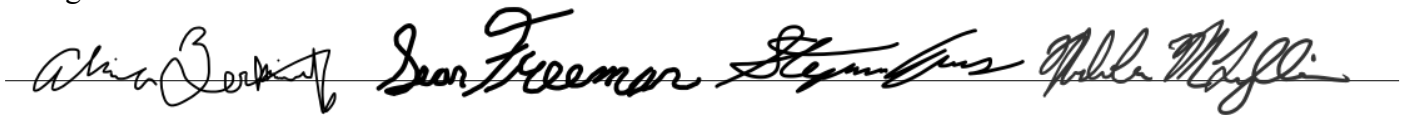
Stefanie Evans

Sean Freeman

Nicholas McLaughlin

SUBMITTED AS PART OF THE CAPSTONE PROJECT  
DEPARTEMENT OF MECHANICAL ENGINEERING  
COLLEGE OF ENGINEERING  
UNIVERSITY OF MASSACHUSETTS LOWELL  
24-April-2020

Signatures of Authors:

The image shows four handwritten signatures in black ink, arranged horizontally from left to right. The first signature is 'Alina Berkowitz', the second is 'Sean Freeman', the third is 'Stefanie Evans', and the fourth is 'Nicholas McLaughlin'. Each signature is written in a cursive style and is positioned above a thin horizontal line.

Capstone Advisor: Murat Inalpolat

Assistant Professor, Structural Dynamics and Acoustic Systems, Department of Mechanical Engineering

## 1 Abstract:

This paper is a continuing investigation of the centrifugal pendulum vibration absorber (CPVA). The CPVA model in question was designed and machined by a prior capstone group in 2018. At the time of this writing, the system resides in the University of Massachusetts Lowell Structural Dynamics and Acoustics Laboratory. CPVAs fundamentally exist to minimize high frequency torsional vibrations through a given drive shaft. In this text fixture, a CPVA assembly is attached to a model transmission shaft than can be run by servomotors.

The subject of inquiry for this report is the effect of friction on the CPVAs performance. In the current models of CPVAs, there are no rigorous considerations for these effects. So, this project aims to develop some methodology by which reliable analytical or experimental results may be ascertained about the frictional influence in the current CPVA configuration. Ultimately, this is to better understand the mechanics behind a CPVA's operation.

This was first attempted through experimental testing. Utilizing the ASTM Standard D1894, a friction test was devised to determine the coefficients of friction for aluminum coupons. A sandblaster was used to generate coupons with a variety of different surface roughness's. These surface profiles were planned to then be measured with an optical profilometer. This would then enable the team to develop a correlation between the surface roughness and the coefficient of friction measured.

However, due to an unanticipated university closure, the experimental testing methodology had to be abandoned. In its stead, a computational MATLAB model was developed to approximate the friction coefficients that would be expected for a given surface roughness. This model required several assumptions and generalizations that may not be appropriate in a more rigorous approach, but it proved to be a consistent framework for this investigation.

From this model, a correlation between the coefficient of friction and the surface roughness of two identical contacting surfaces. The MATLAB model was the most consistent for friction coefficients between 0.15 and 0.45. These results enabled further analysis in ANSYS of the CPVA within this frictional coefficient range.

In ANSYS, the CPVA was modeled and its response analyzed with the range of friction coefficients specified. The frequency responses from ANSYS then informed the team on a surface roughness range that would be feasible for adequate vibration reduction. It was determined that a coefficient of friction of 0.35 was acceptable for reducing the amplitude of the frequency response for the first 6 modes in the ANSYS model. Of all the friction coefficients tested, 0.35 exhibited the lowest overall amplitude and was therefore chosen. Though, coefficients of friction from 0.25 to 0.35 are similarly within an acceptable range.

It is therefore determined that a friction coefficient of 0.35 should be utilized in the CPVA configuration. This should be done by maintaining the current absorber shapes, masses, and materials and by tightening the bolts to achieve the desired interfacing normal force. A friction coefficient of 0.35 corresponds to a surface roughness of  $R_a = 3.020 \mu\text{m}$  and  $R_{ms} = 1.024 \mu\text{m}$ . This is approximately the equivalent roughness of 120 grit sandpaper. Further work is required to develop a process that can accurately and repeatedly produce this surface roughness for all absorbers.

## **2 Acknowledgements:**

This capstone team would like to thank Professor Murat Inalpolat for his support, guidance, and assistance for this project. Undoubtedly, the team would not be as successful without his efforts uniquely. As a great educator and a great researcher, his skills were invaluable in helping to navigate our team through the obstacles experienced. It was an easy choice when we decided to pursue working with him at the end of the Fall 2019 semester. Now, we know that we made the right choice.

We would also like to thank Bahadir Sarikaya for his support of this project throughout its duration. Though we were certainly an imposition to his work and efforts as a doctoral student, he remained helpful, kind, and supportive with any question or problem we faced. His expertise with the CPVA system enabled us to quickly understand the problem we faced and his prowess as an academic mind helped guide us to solutions faster than we could independently.

### 3 Table of Contents

<b>1</b>	<b>ABSTRACT:</b> .....	<b>2</b>
<b>2</b>	<b>ACKNOWLEDGEMENTS:</b> .....	<b>3</b>
<b>3</b>	<b>TABLE OF CONTENTS</b> .....	<b>4</b>
3.1	LIST OF TABLES .....	6
3.2	LIST OF FIGURES .....	6
<b>4</b>	<b>INTRODUCTION</b> .....	<b>8</b>
4.1	CPVA FUNDAMENTALS .....	8
4.2	DESIGN OF CPVAs .....	10
4.3	INTRODUCTION TO FRICTION.....	11
<b>5</b>	<b>LITERATURE REVIEW</b> .....	<b>11</b>
5.1	CONTACT MECHANICS FUNDAMENTALS .....	11
5.2	ROUGH SURFACE MODELING AND ANALYSIS .....	13
5.3	PRIOR COURSE HISTORY .....	14
<b>6</b>	<b>PROJECT SCHEDULE</b> .....	<b>14</b>
6.1	GANTT CHART.....	14
6.2	HOLISTIC APPROACH TO CAPSTONE.....	15
<b>7</b>	<b>DESIGN METHODOLOGY</b> .....	<b>16</b>
7.1	DESIGN CONSTRAINTS.....	16
7.2	DESIGN PROCEDURE.....	17
7.3	SURFACE ROUGHNESS METHODOLOGY .....	18
7.3.1	Surface Modification Method Options .....	18
7.3.2	Surface Modification Method Decision.....	21
7.3.3	Surface Roughness Modification Procedure Design .....	21
7.3.4	Surface Roughness Modification - Sandblasting .....	22
7.4	NORMAL FORCE MODIFICATION METHODOLOGY .....	22
7.4.1	Rotor Compressing Method .....	22
7.4.2	Pressure Vessel .....	24
7.4.3	Absorber Compressing Method .....	24
7.4.4	Ball Bearing Pressure.....	25
7.4.5	Existing Bolt Preload Method.....	26
7.4.6	Design Decision Matrix .....	26
7.5	PROPOSED NORMAL FORCE MODIFICATION DESIGN.....	27
7.6	DESIGN METHODOLOGY OF ANSYS MODELS .....	27
7.7	MATLAB SURFACE GENERATION.....	29
<b>8</b>	<b>DESIGN SOLUTION</b> .....	<b>31</b>
8.1	DEVELOPMENT OF A CONTACT MODEL:.....	32



8.1.1	Derivation of Contact Model: .....	33
8.1.2	Effect of the Radius in the Contact Model.....	35
8.1.3	Effect of Interpolation Resolution.....	38
8.1.4	Establishing a Relationship between the Input Parameters and the Output Coefficient of Friction.....	39
8.2	ANSYS SIMULATION DESIGN SOLUTION.....	40
8.2.1	Modal Analysis .....	40
8.2.2	Harmonic Response .....	42
<b>9</b>	<b>RESULTS.....</b>	<b>42</b>
9.1	MATLAB SURFACE ROUGHNESS RESULTS .....	42
9.2	ANSYS SIMULATION RESULTS .....	45
9.3	DESIGN RESULTS .....	48
<b>10</b>	<b>COST ANALYSIS .....</b>	<b>48</b>
<b>11</b>	<b>SUMMARY AND CONCLUSIONS.....</b>	<b>50</b>
<b>12</b>	<b>RECOMMENDATIONS FOR FURTHER STUDY.....</b>	<b>51</b>
<b>13</b>	<b>PROJECT POSTMORTEM .....</b>	<b>52</b>
13.1	TEAMWORK .....	52
13.2	TECHNICAL COMMUNICATION SKILLS .....	52
13.3	PROJECT SCHEDULE.....	53
13.4	ETHICAL STANDARDS .....	54
13.5	INDUSTRIAL/COMMERCIAL STANDARDS .....	54
13.6	PROFESSIONAL SOCIETIES, CODES, AND STANDARDS .....	54
13.7	SAFETY .....	54
13.8	ENVIRONMENTAL IMPACT .....	55
13.9	SOCIETAL/SOCIAL IMPACT .....	55
13.10	MULTI-DISCIPLINARY ISSUES.....	55
<b>14</b>	<b>BIBLIOGRAPHY .....</b>	<b>56</b>

### 3.1 LIST OF TABLES

TABLE 1. DESIGN CONSTRAINTS CONSIDERED THROUGHOUT THE DURATION OF THIS PROJECT .....	17
TABLE 2. MECHANICAL SURFACE PREPARATION METHODS CONSIDERED.....	19
TABLE 3. CHEMICAL SURFACE PREPARATION METHODS CONSIDERED.....	20
TABLE 4. FULL FACTORIAL DESIGN FOR THE COUPON FRICTION TESTS [26] .....	22
TABLE 5. FACTORS WITH MULTIPLE LEVELS CHOSEN FOR DESIGN OF EXPERIMENTS .....	22
TABLE 6. DECISION MATRIX FOR COMPETING DESIGNS.....	26
TABLE 7. LEGEND FOR THE DECISION MATRIX IN TABLE 8 .....	27
TABLE 8. MATERIAL PROPERTIES OF PRESET MATERIALS IN ANSYS .....	28
TABLE 9. FREQUENCIES AT WHICH THE SIX MODES OCCUR AT FOR EACH COEFFICIENT OF FRICTION .....	41
TABLE 10 RESULTS FROM CALCULATING THE COEFFICIENT OF FRICTION FOR VARIABLE INPUT SURFACE HEIGHT STANDARD DEVIATIONS (6 REPLICATIONS PER RESULT) .....	43
TABLE 11. FIRST 6 MODE PEAKS CALCULATED FOR COEFFICIENTS OF FRICTION FROM 0.15 TO 0.45 (HIGHER COLOR SATURATION CORRESPONDS WITH LARGER MAGNITUDE).....	48
TABLE 12. COST ANALYSIS LEDGER OF CURRENT AND ESTIMATED COSTS .....	49
TABLE 13. ESTIMATED LABOR COSTS INCURRED DURING PROJECT DEVELOPMENT .....	50

### 3.2 LIST OF FIGURES

FIGURE 1. MASS PENDULUM SYSTEM [2] .....	9
FIGURE 2 . CENTRIFUGAL PENDULUM [2] .....	9
FIGURE 3. SINGULAR POINT HINGED PENDULUM [1] .....	10
FIGURE 4. BIFILAR SUSPENSION CPVA [1].....	10
FIGURE 5. HERTZ CONTACT BETWEEN TWO ELASTIC BODIES [5] .....	12
FIGURE 6. 6A - "SURFACE ROUGHNESS PROFILE OF A GLASS-CERAMIC SUBSTRATE MEASURED USING AN ATOMIC FORCE MICROSCOPE", 6B - MATLAB GENERATED RANDOM NORMAL DISTRIBUTION OF POINTS [3] .....	13
FIGURE 7. FINAL GANTT CHART .....	15
FIGURE 8. OVERALL PROJECT FLOW CHART.....	16
FIGURE 9 ENGINEERING DESIGN FLOW CHART UTILIZED THROUGHOUT THIS PROJECT .....	17
FIGURE 10 ABSORBER DESIGNED FOR ROTOR COMPRESSING METHOD .....	23
FIGURE 11. ABSORBER IN CPVA ASSEMBLY AND ALTERNATE ABSORBER VIEW .....	23
FIGURE 12. PRESSURE VESSEL DESIGN WITH CPVA ASSEMBLY ENCASED.....	24
FIGURE 13. ABSORBER COMPRESSING METHOD DESIGN .....	25
FIGURE 14. ABSORBER COMPRESSING METHOD, ALTERNATE VIEW .....	25
FIGURE 15. BALL BEARING METHOD, ANGLED AND ORTHOGONAL VIEW .....	25
FIGURE 16. 25MM SQUARE ROUGH SURFACE GENERATED IN MATLAB WITH ONE ASPERITY PER MM <sup>2</sup> (RA = 3.2MM, RMS = 1 MM).....	30

FIGURE 17. 25MM SQUARE ROUGH SURFACE GENERATED IN MATLAB WITH ONE ASPERITY PER MM <sup>2</sup> WITH AN INTERPOLATION FACTOR OF 5 (RA = 2.9MM, RMS = 0.21MM) .....	30
FIGURE 18. HEIGHT DISTRIBUTION OF THE SURFACES GENERATED IN FIGURE 16 (LEFT) AND FIGURE 17 (RIGHT) .....	31
FIGURE 19. PROCESS FLOW OF CREATING A MATLAB SURFACE TO BE IMPORTED INTO ANSYS.....	31
FIGURE 20. PICTURED LEFT, ORTHOGONAL VIEW OF A GENERATED ROUGH SURFACE IMPORTED INTO SOLIDWORKS WITH VERTICES SHOWING; PICTURED RIGHT, THE SAME SURFACE WITHOUT VERTICES SHOWING .....	32
FIGURE 21. SCHEMATIC REPRESENTATION OF TWO SURFACE PROFILES WITH SPLINE INTERPOLATION BETWEEN ASPERITIES ..	32
FIGURE 22. SCHEMATIC REPRESENTATION OF TWO SURFACE PROFILES WITH SPLINE INTERPOLATION BETWEEN ASPERITIES ..	34
FIGURE 23. DIAGRAM OF ASPERITY CONTACT FORCES DECOMPOSED INTO X AND Z DIRECTIONS .....	34
FIGURE 24. COMPARISON BETWEEN VARIOUS INPUT PARAMETERS (ASPERITY VS INTERPOLATED, RADIUS SIZE) TO BE USED IN THE FINAL CONTACT MODEL. SURFACE PARAMETERS: $\Sigma = 0.25$ MM, ASPERITY DENSITY = 4/MM <sup>2</sup> , WIDTH = 10 MM .....	37
FIGURE 25. COMPARISON BETWEEN COEFFICIENT OF FRICTION RESULTS WITH VARIABLE INTERPOLATION RESOLUTION FACTORS (SURFACE PARAMETERS: $\Sigma = 0.25$ MM, ASPERITY DENSITY = 1/MM <sup>2</sup> , WIDTH = 10 MM) .....	38
FIGURE 26. SURFACE ROUGHNESS (RA) VS INPUT STANDARD DEVIATION (SIGMA) OF SURFACES GENERATED UTILIZING MATLAB'S NORMRND FUNCTION .....	39
FIGURE 27. ROOT MEAN SQUARED (RMS) VS INPUT STANDARD DEVIATION (SIGMA) OF SURFACES GENERATED UTILIZING MATLAB'S NORMRND FUNCTION .....	40
FIGURE 28. TOTAL DEFORMATIONS FOR THE SIX MODES FOUND IN ANALYSIS FOR A COEFFICIENT OF FRICTION OF 0.35 .....	41
FIGURE 29. FREQUENCY RESPONSE DEFORMATION RESULT FOR A COEFFICIENT OF FRICTION OF 0.35 .....	42
FIGURE 30. RESULTING PLOTS FROM SIMULATING 10 MM WIDE SURFACES IN CONTACT UNDER VARIABLE INCREMENTALLY INCREASING LOADS .....	44
FIGURE 31. FREQUENCY RESPONSE DEFORMATION OF THE SELECTED COEFFICIENTS OF FRICTION .....	46
FIGURE 32. FREQUENCY RESPONSE OF CPVA FOR COEFFICIENTS OF FRICTION FROM 0.15 TO 0.45 .....	47

## 4 Introduction

In recent years, a large push has been made to develop increasingly efficient engines. A primary method of achieving this is by reducing the number of active cylinders. However, increased torsional vibrations are produced as a result of the fewer cylinders firing on the same side of the crankshaft. These vibrations can result in lasting fatigue damage to the engine and car alike. Unsurprisingly, as the market demands more efficient vehicles, there has been a simultaneous demand to protect the car against these high frequency vibrations.

One method by which torsional vibrations can be reduced is using mass-pendulums moving on a rotor in rotation. This mass-pendulum system is known as a Centrifugal Pendulum Vibration Absorber, or CPVA. The masses are located on the rotor and freely move along a prescribed path. This results in a counteracting torque, which is fundamentally how these CPVAs operate [1]. Unlike a conventional pendulum system (i.e. a mass on a string), these masses are in constant frictional contact with the rotor and are attached by rollers instead of a string.

Frictional contact between two interfacing surfaces is a well-researched but complicated process. This becomes doubly complicated when considered in a dynamic model. Due to this, the effect of friction in a dynamic situation, such as the motion of a CPVA, requires dedicated efforts to understand. So far, the influence of the frictional contact in a CPVA is not well characterized. Hence, it is the subject of investigation throughout this project. To better understand the behavior of the CPVA, the behavior of friction within the CPVA needs to be understood. So, to further research the CPVA method of damping vibrations, an investigation into the effect of surface friction on the behavior of the CPVA must be conducted.

### 4.1 CPVA Fundamentals

The need for vibration damping became more prevalent as reciprocating engines became more popular. In short, reciprocating machines apply a force on one side of the shaft so that all forces are contributing towards the same direction of rotation. This mechanism leads to heavy and potentially harmful torques on the crankshafts, resulting in less reliability. Other methods of damping the vibrations have been attempted, but result in compromises like increased inertia, dissipated energy, or only working at specifically tuned frequencies. Research in rotational dynamics lead to the development of CPVAs which proved to be extremely useful in reducing the vibrations of reciprocating machines.

CPVAs are essentially a suspended mass acting as a pendulum hinged to a rotor. This mass is free to move along a prescribed path determined by the number of fixed points and the securing method. The mass, also known as the absorber, moves separately, but relative to the rotor. This allows for the damping of overall vibrations in the system. What sets CPVAs apart from other vibration reduction systems is that it does not have to be tuned to specific frequencies. Studies found that CPVAs were able to dampen vibrations over wide ranges of frequencies which has contributed to their popularity.

In a mass pendulum system, gravity acts as the restoring force. This means that when the mass swings to one side or the other, gravity is the force that will pull it back toward the center, inciting cycles of oscillatory motion. In Figure 1, the force of gravity is denoted by  $g$  and can be broken into two components:  $pg \cdot \sin(\theta)$ , and  $pg \cdot \cos(\theta)$ . The mass is represented by  $P$  and it is attached to a fixed-point  $A$  at a distance  $L$  away. In this figure, it is at a position of angle  $\theta$  away from its natural state represented by the dotted line [2].

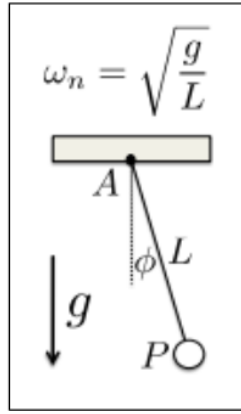


Figure 1. Mass pendulum system [2]

The natural frequency of this system can be determined by the force of gravity experienced, and the length between the mass and fixed point, represented by Equation 1 [2].

$$\omega_n = \sqrt{\frac{g}{L}} \quad (1)$$

In CPVAs, the absorber is the equivalent pendulum mass. In Figure 2 the mass is represented by  $P$ , which is distance  $L$  away from the fixed-point  $A$ . This fixed point is separated from the center of the rotor  $O$  by a distance  $R$ . The system is moving at a rotational (angular) velocity  $\Omega$  also represented by  $\omega$ . In this system, the restoring force is the centrifugal force on the absorber and is indicated by the outward arrows in the figure. The natural frequency of this system is calculated differently than the pendulum previously because of its rotational dynamics. The natural frequency is represented by Equation 2 [2].

$$\omega_n = \Omega \sqrt{\frac{R}{L}} \quad (2)$$

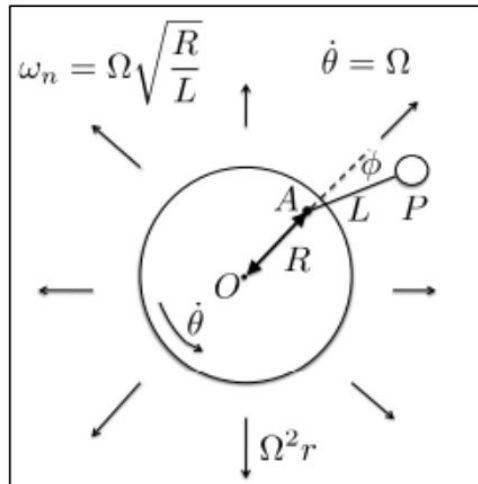


Figure 2 . Centrifugal pendulum [2]

## 4.2 Design of CPVAs

There are two main designs for current CPVAs, which are the Singular Point Hinged Pendulum and the Bifilar Suspension. The Singular Point Hinged Pendulum operates as named. The absorber is attached to the rotor at a singular point and therefore must follow a circular path dependent on the length of the absorber to the fixed point [1].

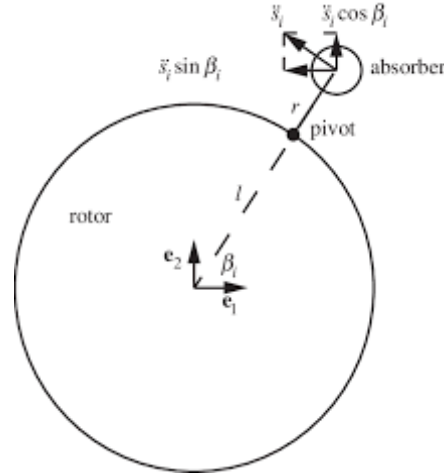


Figure 3. Singular point hinged pendulum [1]

This design is not commonly used because it has a few drawbacks. The natural frequency of a single point hinged pendulum system changes with the amplitude of the pendulum. When the CPVA is operating, the natural frequency will decrease as the amplitude increases. At high amplitudes, this problem can lead to what is known as “under tuning”. To avoid this problem the absorber can be attached to the rotor in two locations, resulting in what is known as a bifilar suspension CPVA. This design has two cutouts on both the rotor and absorber that are inverted from each other. A “roller” links the rotor and absorber together and allows the absorber to freely move within the prescribed path of the cutout [1].

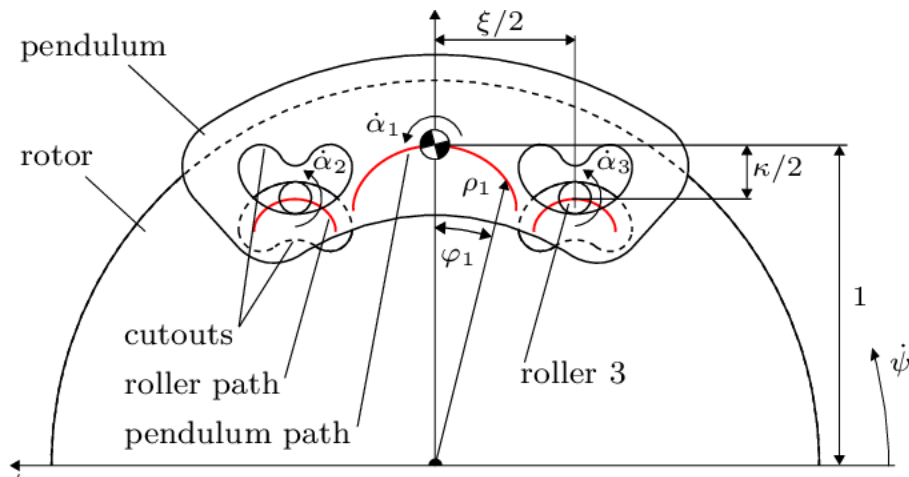


Figure 4. Bifilar suspension CPVA [1]

It is assumed that the roller will roll without slipping, thus making the motion of the absorber purely translational. The cutouts in the rotor and the absorber also allow for customization of the path the absorber follows. The bifilar design cutouts can be made circular, elliptical, cycloidal, etc., to meet the requirements of the application. Research has found elliptical and cycloidal shapes to apply to most scenarios and are commonly used in CPVAs today [1].

### 4.3 Introduction to Friction

In true engineering applications, there are no frictionless surfaces. There is always some amount of resistance between two contacting surfaces. Even flawlessly smooth surfaces are still subject to intermolecular forces at the microscopic level (though these are typically negligible for practical applications). So, in designing any mechanical system, it is critical to consider the impact of and mechanisms behind friction.

Friction is caused by complicated microscopic interactions between two surfaces in contact. Generally, the cause of these interactions can be attributed to the topology of the surfaces, the mechanical properties of the materials, and the conditions by which the surfaces are in contact. Since these properties are unique to each system, they cannot be tabularized and must be evaluated either computationally or experimentally for each application and interaction [3].

Experimental determination of frictional properties is relatively straightforward. The coefficient of friction ( $\mu$ ) is defined by the ratio of the macroscopic shear force ( $F_s$ ) divided by the macroscopic normal force ( $F_N$ ), as shown below in Equation 3 [4]. Experiments to determine the coefficient of friction are typically constructed to measure the translational force required to move an object while a known load is applied normal to the contacting interface.

$$\mu = \frac{F_s}{F_N} \quad (3)$$

In the absence of empirical data, computational models must be developed. These models typically consist of two simulated rough surfaces interacting, deforming, yielding, and otherwise reacting to the influence of the other. For most surfaces, these interactions occur on the scale of micrometers. To examine macroscopic surface interactions, such as two blocks sliding against each other, all the microscopic interactions must be summed and considered.

## 5 Literature Review

### 5.1 Contact Mechanics Fundamentals

Contact mechanics is the field of study that aims to understand the mechanisms by which surfaces interact. Heinrich Hertz pioneered this field in the late 1800s with his classical solution of the deformation, stress, and contact area of two solid, elastic bodies in contact [5]. A diagram of this so-called Hertz contact is shown below in Figure 5.

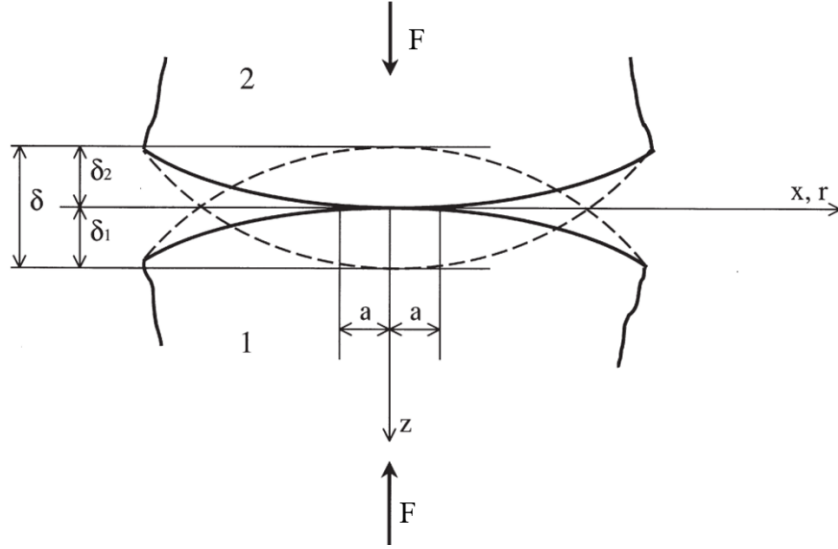


Figure 5. Hertz contact between two elastic bodies [5]

In this diagram, two elastic spheres are under some normal contact load,  $F$ . The total interference between the two bodies is denoted by  $\delta$ .  $\delta_1$  and  $\delta_2$  represent the peak deformations of bodies 1 and 2, respectively. The contact area is a circle of radius  $a$ , as shown above.

The deformation caused by this interaction is calculated using Equation 4 [6].

$$\delta = \left( \frac{9F^2}{16RE^*} \right)^{1/3} \quad (4)$$

$R$  is the composite radius of the undeformed spheres, and  $E^*$  is the composite modulus of elasticity of the two bodies. Both  $R$  and  $E^*$  are given by

$$\frac{1}{R} = \frac{1}{R_1} + \frac{1}{R_2}, \quad \frac{1}{E^*} = \frac{1 - \nu_1^2}{E_1} + \frac{1 - \nu_2^2}{E_2} \quad (5)$$

where  $R_1$  and  $R_2$  are the radii of curvature for bodies 1 and 2,  $E_1$  and  $E_2$  are the moduli of elasticity for bodies 1 and 2, and  $\nu_1$  and  $\nu_2$  are the Poisson's ratios for bodies 1 and 2, respectively [5].  $R$  and  $E^*$  are also known as the radius and modulus of elasticity of the equivalent rough surface [6].

The contact radius can similarly be calculated by Equation 6 [6].

$$a = \left( \frac{3FR}{4E^*} \right)^{1/3} \quad (6)$$

This theory of contact between two spherical, elastic bodies has become the foundation for contact mechanics. Today, far more complex models exist to explain the contacts between bodies. However, Hertz contact continues to be useful for computational models and remains a valid assumption.

Computational contact mechanics is a relatively new method that has come alongside finite element analysis (FEA). The discretization of a complex surface where each element can be analyzed has become possible due to the increases in computational power. In turn, to accurately represent two rough surfaces in contact, rather large element arrays must be made to accommodate the surface's inherent complexity.



The surfaces are then overlaid and compressed while the resulting loads, deflections, stresses, and strains are recorded.

## 5.2 Rough Surface Modeling and Analysis

With regards to modeling, a rough surface can be thought of as a topology of peaks (asperities) and valleys. For many real surfaces, the probability distribution of the peaks and valleys tend to be Gaussian [4]. Figure 6a shows the measured surface profile of a ceramic surface using an atomic microscope. In this figure, the evidence of asperities and valleys are apparent. The jagged nature is due to the sampling of the atomic microscope only being able to capture elevation data at discrete points. Though it does not capture the entirety of the surface phenomena, it still provides an accurate approximation of what kind of roughness exists.

So, to modeling a rough surface, a Gaussian distribution of random heights can be generated and assigned to points in an array. These heights create a surface profile that is a reasonably close approximation to the kind of signal measured by the atomic microscope. Figure 6b shows a random distribution using MATLAB's *normrnd* function. By visual comparison, it is apparent that these two signals achieve the same type of result. Furthermore, this is the method used by computational tribology experts to generate their surfaces [5], [6], [7].

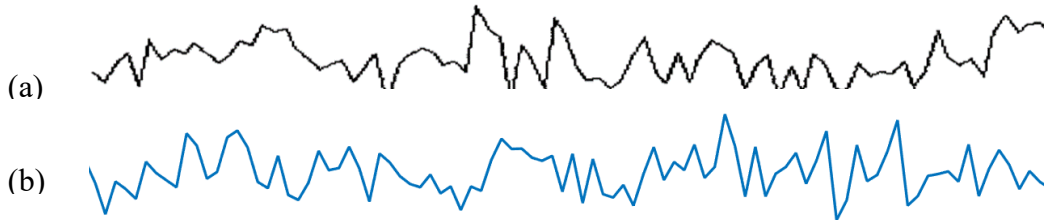


Figure 6. 6a - “Surface roughness profile of a glass-ceramic substrate measured using an atomic force microscope”, 6b - MATLAB generated random normal distribution of points [3]

Surfaces are measured primarily through two parameters: Ra and Rms. Ra is the arithmetic average of height deviation from the centerline of the profile. This is calculated by

$$Ra = \frac{1}{n} \sum |z_i - \bar{z}| \quad (7)$$

where  $z_i$  is the height of the  $i^{\text{th}}$  element,  $\bar{z}$  is the average element height (i.e. the centerline height), and  $n$  is the total number of elements considered [8]. Ra is the standard and most frequently used measurement for surface roughness.

Less frequently used is the Rms, or root mean square, value. This is calculated using Equation 8 [8].

$$Rms = \sqrt{\frac{\sum y_i^2}{n}} \quad (8)$$

These two properties can effectively define and describe any rough, reasonably flat surface. Though other parameters, like the maximum valley depth or maximum peak height are certainly applicable, they tend to be extraneous and provide little substantive benefit in measurement. It should be noted that skewness and kurtosis are also useful parameters when describing real surfaces but will not be used here where a Gaussian distribution is assumed.

### 5.3 Prior Course History

*MECH.2010 Computer Aided Design.* An introduction to solid modeling and mechanical design in SOLIDWORKS. Also teaches the fundamentals of engineering drawings.

*MECH. 2020 Manufacturing Laboratory.* Basic introduction to machine tool practices to familiarize students with the complexities of manufacturing an item. Accurate usage of measuring tools, along with increasing familiarity with both manual and CNC lathes and milling machines. This course was beneficial to the capstone project to provide the context and knowledge on how to approach the development of the experimental test coupons

*MECH. 2960 Materials Science for Engineers.* Understanding the behaviors and properties of materials. Stress, strain, stiffness, thermal expansion, and yielding criteria were considered. The metal chosen for the rotor and absorber were based on the previous capstone groups CPVA, the price of the material, and its response to varying stresses.

*MECH 2060. Strength of Materials.* Thoroughly introduces how the geometry and material properties effect the behavior of an element. Also, and in-depth introduction to how various loading methods can affect a system's response.

*MECH. 4510. Dynamic Systems Analysis.* Introduces how to describe system responses due to initial conditions. Dynamic modeling using both time and frequency domain. This was very helpful when obtaining and understanding the frequency response plots of the CPVA in ANSYS.

*MECH. 4730. Design Theory and Constraints.* Design quality and a basic introduction to design of experiments were taught. The crucial aspects of Six Sigma quality control and considerations to be made when designing a project were similarly taught.

*MECH. 5130 Theory of Finite Element Analysis.* Matrix algebra and Rayleigh-Ritz technique were taught and applied to finite element method. Also, an introduction to ANSYS Workbench, static structural, modal analysis, and harmonic response were taught. This was useful in the analysis of coefficients of friction on the frequency response of the absorbers.

## 6 Project Schedule

### 6.1 Gantt Chart

The final Gantt chart developed for this project is presented below in Figure 7. This Gantt chart was subject to several major revisions throughout the semester especially when the university shifted to a virtual learning environment.

Task	1	2	3	4	5	6	7	8	9	10	11	12	13	14	15	16	Phase
	19-Jan	26-Jan	2-Feb	9-Feb	16-Feb	23-Feb	1-Mar	8-Mar	15-Mar	22-Mar	29-Mar	5-Apr	12-Apr	19-Apr	26-Apr	3-May	
<i>Establish Requirements and Deliverables</i>																	Preplanning and Organization
<i>Project Proposal</i>																	
<i>Background Literature Review</i>																	
<i>Determine Best Mode to Generate Artificial Friction</i>																	Design and Progress in Friction Test
<i>Source Friction Test</i>																	
<i>Design Friction Test</i>																	
<i>Order and Manufacture Coupons</i>																	
<i>Sandblast</i>																	
<i>Sandblast Aluminum Coupons</i>																	Numerical Simulation of Coefficient of Friction
<i>Generate Probablistic Surfaces in MATLAB</i>																	
<i>Simulate Contact Between Rough Surfaces to Obtain a Coefficient Of Friction</i>																	
<i>Design Systems to Modify the Clamping Force</i>																	Design of System
<i>Construct Decision Matrix and Decide on Best Design</i>																	
<i>Simulate Best Design</i>																	
<i>Write Capstone Report/ Prepare Presentation</i>																	Final Report and Presentation
<i>Final Capstone Report and Presentation Due</i>																	
<i>Present Project</i>																	

Figure 7. Final Gantt chart

## 6.2 Approach to Capstone

There were two branches in the project tasks: administrative and engineering. These were both equally important to the project's success. They operated concurrently, according to the flow chart in Figure 8. The administrative branch is provided as the top flow chart and considers the project on an administrative level. Weekly, an updated Gantt chart was produced, containing the updated date and tasks for the overall project. Each chart was kept in an archive for future reference if needed. This weekly update provided the group with direction for the coming week and a review of the total progress of the project.

The other branch of this project was the engineering design, fabrication, and assembly. This branch was split into sections of competing designs for different absorbers to be used on the fixture and how to analyze the varying coefficients of friction. Due to the shift from experimental to analytical investigation in this project, the research done was predominantly simulations. These simulations consisted of a MATLAB model which focused on generating random surface roughness and then evaluating the resulting coefficient of friction. It was then to be considered with the different absorber designs in SolidWorks. The last section of the simulation branch is the ANSYS simulation which used the MATLAB results, to simulate the frequency response deformation for varying coefficients of friction.

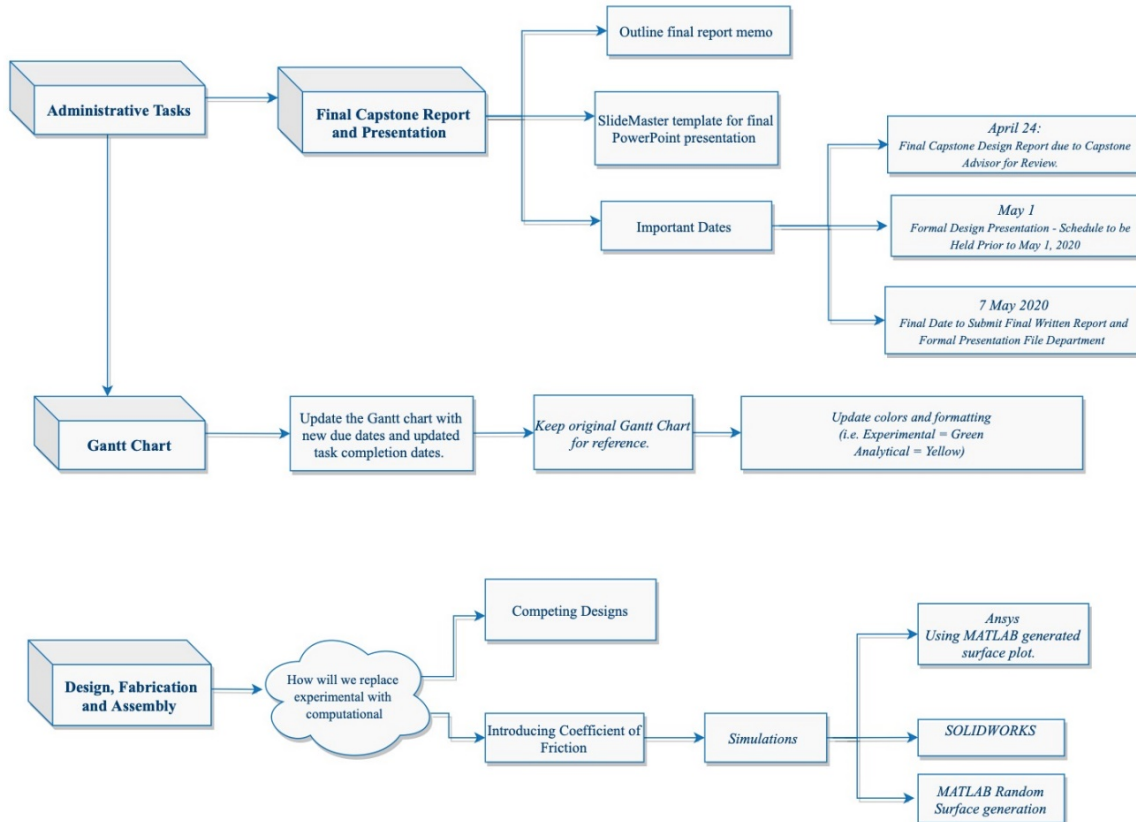


Figure 8. Overall project flow chart

## 7 Design Methodology

### 7.1 Design Constraints

Some of the biggest constraints in actual engineering systems are performance, rate, and cost. For the applicational purposes of this project, the mass of the absorber is a major factor in the performance of the CPVA system. Increasing this mass would reduce vibrations. With that said, increased mass typically leads to a larger system. Since CPVA's were developed to improve the quality of low-cylinder, high power engines, increasing the mass, and enlarging the system would be counterproductive. of the mechanical components in the system will result in improved performance. The vibration constraints and friction related hysteresis must be monitored in parallel with these high-power engines. A table of design constraints was generated to make sure these limitations were not surpassed.

The design constraints, as determined by Professor Inalpolat and the capstone team, are presented below in Table 1. These are ultimately the evaluative parameters used when considering the feasibility of designs.

Table 1. Design constraints considered throughout this project

Design Constraints	Description
<b>Cost of Materials</b>	<i>Materials and production cost cannot exceed \$400 (can be extended if justifiable)</i>
<b>Cost</b>	<i>Method to generate surface roughness must cost under \$100 for all four absorbers</i>
<b>Mass</b>	<i>Absorbers need to have the same dynamic mass as the current model</i>
<b>Maintenance</b>	<i>Fewer than 2 disassembly steps to access the CPVA for adjustments</i>
<b>Reliability</b>	<i>Design needs to run continuously for extended periods with no adjustments required</i>
<b>Repeatability</b>	<i>Method to generate surface roughness must be consistent within <math>Ra = \pm 0.25 \mu m</math></i>
<b>Safety</b>	<i>No conceivable source of harm can be imposed on the system. The risk of operation should remain constant</i>
<b>Size</b>	<i>Must fit within the preexisting CPVA configuration</i>

These design constraints were constantly revisited during this project to ensure compliance with these requirements.

## 7.2 Design Procedure

The engineering design process used in this capstone is presented below in Figure 9.

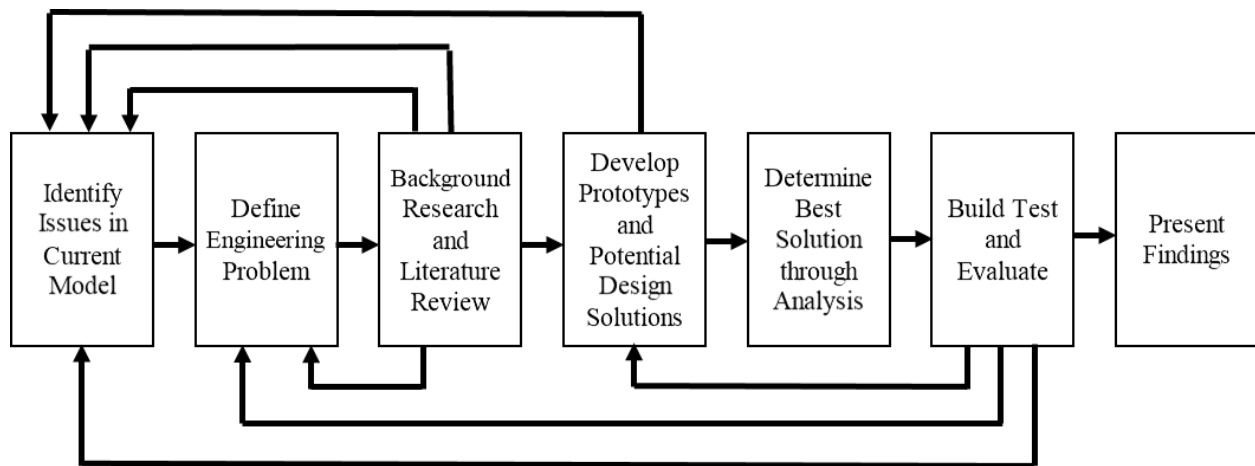


Figure 9 Engineering design flow chart utilized throughout this project

This flow chart has some slight alterations from the typical engineering flow chart. For this specific application, the problem identification comes directly from the CPVA model being investigated. In this situation, the CPVA model was lacking any consideration for friction between the absorbers and rotor.

From this, the team determined that some methodological approach must be made to analyze the influence and impact of dynamic friction on the system. Extensive research was then conducted on the mechanics of a CPVA as well as frictional interactions between surfaces.

In the development of prototypes and design solution stage, it was intended to conduct an experiment that would illustrate the correlation between the coefficient of friction and the surface roughness. Since this was not able to be done, the team effectively had to start at the beginning to approach the problem

from an analytical and computational stance. Once this setback was mitigated, the project progressed relatively smoothly.

This design process was also utilized in the development of the MATLAB and ANSYS models. In any software, numerous iterations are needed. Each of these iterations begins in the identification stage and proceed up until the build and test phase. This process continued until an adequate solution was found and the design could proceed to the presentation stage. This happened frequently and consistently.

### **7.3 Surface Roughness Methodology**

#### **7.3.1 *Surface Modification Method Options***

To control and change the coefficient of friction between the rotor and absorber, it was necessary to choose a method to modify the surface roughness of the aluminum absorber pieces. The team considered different options to introduce a controlled and varied surface roughness between the surfaces in contact. These experimental conclusions will correlate the coefficient of friction with some surface roughness that will result in the most feasible CPVA design. For the category of metal alloys aluminum 6061 is grouped in, there are two main categories of preliminary surface preparation: mechanical and chemical surface preparation. ASTM and industry standards for the metal alloys utilized in this project were referred to repeatedly throughout this process.

The following table summarizes the pros and cons considered for mechanical surface modification techniques that could be used on the aluminum coupons. Surface blasting, brushing, grinding, and polishing were the mechanical surface modification procedures that were studied. These methods require different tools and machinery which produce distinctive surfaces.

Table 2. Mechanical surface preparation methods considered

Method	Mechanical Surface Prep [9]	Surface Blasting [10]	Brushing [11]	Grinding [12]	Polishing
<b>ASTM Standard</b>	D2651-011 D1730 - 09	D1730	D1730		
<b>Notes:</b>	-Should use a nonmetallic abrasive - <u>Example:</u> Aluminum-oxide impregnated nylon matting, glass-bead blasting, and aluminum oxide cloth - Different finishes achieved by different grit [13]	-Relatively low pressures, fine silica sand or aluminum oxide -Cannot use steel-based media – impregnates in surface of aluminum -50-60 psi	- Method of pressing and moving metal brushes onto material surfaces to create directional lines - "Hairline finishing"  -Stainless steel wire brush: 0.5~0.8mm – Coarse 0.12~0.36mm – Medium 0.05~0.1mm – Fine 0.05 or less - Gloss	- "The use of a grinding wheel to abrasively machine the material that you wish to cut" -Each grain of the abrasive material serves as an individual cutting edge. As the grinder is applied to the material to be cut, the abrasive shears tiny chips.	-Various processes including hand buffing with a metal polish, electro-polish, Stoning (320-400 grit), 0.25- $\mu$ m diamond powder, to produce a smooth finish [14]
<b>Pros:</b>		-Abrasive Media can be reused	-Various levels of finishes can be achieved	-Very fine finishes and accurate shapes -Large volumes in mass productions	-Produce a smooth surface -Can produce an accurate surface finish
<b>Cons</b>		-Can warp larger surfaces if pressure is too high -Disrupts oxide film -Can be dangerous if inhaled [15]	- Wire fragments and powder of the bushes get ingrained into the surfaces of soft metal such as aluminum - Pretreatments to remove these ingrained fragments must be applied -Disrupts oxide film	- Aluminum is one of the hardest materials to grind -Heat and sparks created so the right equipment must be used - Aluminum dust can be combustible or explosive if it becomes suspended in the air at the right concentration [16]	-Multi-step process -Can be too smooth for our application if using diamond powder [17]

As seen in Table 2, there are multiple ways of mechanically modifying the surface of the aluminum coupons. The required machinery for surface blasting, otherwise known as sandblasting, would be a sandblaster, air compressor, and the abrasive media. Though complex, sandblasting is an easy method to introduce roughness to an aluminum surface. Brushing can also be used to introduce a controlled surface roughness, but since aluminum is a soft metal, this method would be hard to achieve with metal brushing. Grinding can similarly be used; however, aluminum is a very difficult material to grind and the access to necessary equipment is costly. Finally, polishing is a surface preparation method that results in a very low coefficient of friction. Polishing does not introduce significant roughening to the surface of the coupons so this would not be beneficial for the project. The goal of modifying the surface roughness of these aluminum samples is to produce a quantifiable and controllable coefficient of friction.

Chemical methods of introducing and modifying surface roughness were also considered. Aluminum can be surface etched with chemical solutions as well as electrochemically modified with an induced current while submerged in a chemical solution. Aluminum has been treated with these methods for many years, and many different chemical solutions have been used – sulfuric acid with sodium dichromate (“chromic” etching), sulfuric acid with ferric sulfate, and anodizing using phosphoric acid. There exists plentiful research about these chemical methods, and a summary of the team’s deliberation is provided in Table 3.

Table 3. Chemical surface preparation methods considered

Method	Aluminum surface Etching	Sulfuric Acid/ Sodium Dichromate [18]	Sulfuric Acid / Ferric Sulfate [19]	Phosphoric Acid Anodizing [20]	Electrochemical Machining (ECM) [21]
<b>ASTM Standard</b>	<i>ASTM D2651</i>	<i>ASTM D2674</i>		<i>ASTM D3933</i>	<i>ASTM G150 - 18</i>
<b>Notes:</b>	<i>General standard for surface prep of aluminum  Lightly abraded surfaces give a better profiled surface for adhesive bonding than do highly polished surfaces. Properly abraded surfaces show no smooth, polished areas.</i>	<i>Chromic Acid → a layer of aluminum oxide is formed “chromic acid etching”  Distilled Water 700 mL plus balance of liter Sodium Dichromate 28 to 67.3 grams Concentrated Sulfuric Acid 287.9 to 310.0 grams</i>	<i>“P2 Etch” (15% by weight FeSO<sub>4</sub>, 37% H<sub>2</sub>SO<sub>4</sub> and 48% water)</i>	<i>Anodizing → widely used surface treatments of metals (aerospace)  Bath of 9-12 weight % phosphoric acid at 19-25 degrees Celsius between a voltage from 9 to 16 V under a direct current</i>	<i>“controlled anodic dissolution at atomic level”  Varying the time changes the average surface roughness Ra (micro m)</i>
<b>Pros:</b>		<i>The industrial go-to method for chemical etching for surface prep</i>	<i>-uses ferric sulfate in place of the toxic sodium dichromate as the oxidizer - produces an oxide with a similar morphology to those obtained using the various chromic-Sulphur etches</i>	<i>-Less dependent on time between treatment and rinsing -Thicker layer of oxide than chromic</i>	<i>-Negligible tool wear -lower thermal/mechanical wear on the part</i>
<b>Cons:</b>				<i>-Takes longer than chromic [22]</i>	<i>-Generation of hydrogen bubbles that effects material removal rate -prediction of electrolyte flow pattern</i>

As shown in the above table, these methods provide a controlled and methodic way of introducing surface roughness to the surface of aluminum alloy while also introducing the protective oxide layer that the mechanical methods disrupt. The amount of time exposed to the solution and amount of current used for anodizing and electrochemical machining can be controlled to vary the surface roughness in a repeatable manner.

These chemical methods have been successfully applied to aluminum surfaces in industry but proved to be impractical for the scope of this project. The accessibility of the apparatuses and supplies necessary for mechanical surface preparation was significantly more abundant than the resources, setup, and materials required for chemical surface etching. Proceeding with a mechanical method, the modification of the aluminum surfaces could be completed faster and cheaper because of the accessibility of required tools and materials. Performing this step sooner in the semester would have provided the team ample time to perform the friction test on the aluminum coupons and develop conclusions had the university not closed.



### **7.3.2 *Surface Modification Method Decision***

After considering all the options and the resources available, the team decided to move forward with sandblasting as the surface preparation method. This decision was based on other mechanical surface modifications requiring machinery and tools not available on campus. Therefore, sandblasting was the cheapest and most practical method for the team to use, as well as a repeatable process for future developments. The team acquired a sandblaster from the Plastics Engineering department labs on campus and part of the capstone budget was used to order the other materials necessary such as the sandblasting media. The sandblaster came with standard coarse sand as the blasting media, which was of unknown grit to the team at the time. Should the university not have closed, the size of the sand would have been measured. However, the team ordered a finer abrasive media of smaller grit – multipurpose glass bead abrasive media with mesh size 170-325 and grits of 180-280. This gave the team a coarse and fine abrasive grit to work with.

### **7.3.3 *Surface Roughness Modification Procedure Design***

To modify the surface roughness via sandblasting, several pertinent factors were considered:

- Time of coupon's exposure to sandblasting media
- Pressure (in psi) of the sandblasting media
- Grit of the media used
- Distance between the coupon and the sandblaster nozzle.

After research and deliberation, the team settled on two factors for the current modification of the surface roughness that could be quantified and documented in a repeatable manner – pressure and grit. According to existing research, the factor with the most impact on surface roughness was the pressure of the sandblasting media, whereas the observed impact of the exposure time was imperceptible, and therefore was considered negligible [23]. Based on this research, the team chose pressure and grit as the two factors for this study since they have the most impact on the resultant surface roughness. Additionally, the setup of this experiment did not allow for a controlled variation of distance from the coupon surface, so the team decided to keep that factor at a constant for all samples. This is the best solution devised considering that research shows distance is an important factor in surface roughness [24].

After considering all these factors, the team decided to proceed with two factors, one with two levels and one with three, based on the availability of resources. The following table shows the full factorial Design of Experiments array for these factors. If three levels were chosen, an L9 orthogonal array would have been used [25]. Instead, two different types of grit, fine and large, and could vary the pressure as seen in the second table below:

Table 4. Full factorial design for the coupon friction tests [26]

Full Factorial Array			
Experiment Number	Factor Symbols		Results
	A	B	
1	1	1	Y1
2	1	2	Y2
3	1	3	Y3
4	2	1	Y4
5	2	2	Y5
6	2	3	Y6

Table 5. Factors with multiple levels chosen for Design of Experiments

Factor B	Pressure	Factor A	Grit Size
1	60 psi	1	Fine
2	70 psi	2	Coarse
3	80 psi		

As seen in Table 4, the team designed a full factorial Design of Experiments, meaning that every combination of factors will be tested. This resulted in 6 total pieces being modified according to the factors chosen – grit, either fine or coarse, and air compressor pressure, varying between 60 psi, 70 psi, and 80 psi.

#### 7.3.4 Surface Roughness Modification - Sandblasting

The team proceeded with the experimental design described above. The sandblaster was acquired and set up, and the coupons were subjected to the abrasive media with the grit and pressure described in the DoE above.

### 7.4 Normal Force Modification Methodology

The team designed and considered five methods of modifying the normal force applied to the absorbers. This would in turn, vary the frictional force on the rotor and absorber according to Equation 3.

#### 7.4.1 Rotor Compressing Method

The goal of this design was to create an assembly that could vary the clamping force of the absorbers on the rotor. This would result in a change in the frictional force between the rotor and absorber, without changing the coefficient of friction of the material. This would allow for quick adjustments of the friction force between tests to test different configurations. This design has an absorber on each side of the rotor. It also had two “arms” that protruded away from the rotor and were fixed together with an assembly of nuts and bolts.

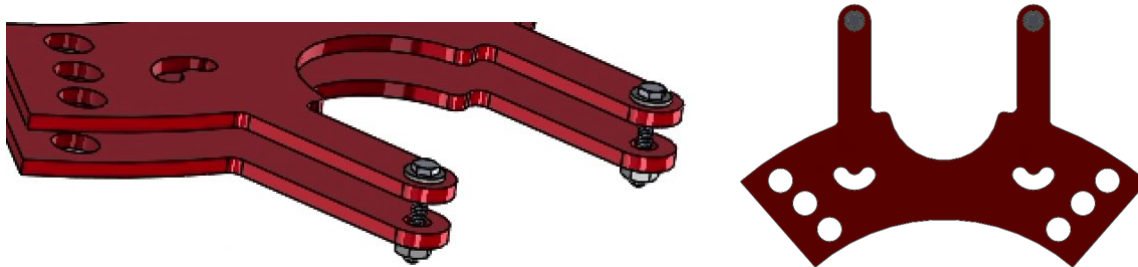


*Figure 10 Absorber designed for rotor compressing method*

The hardware chosen was 4-40 1-1/2" screws, with 4-40 hex nuts, washers, and split washers. The sizing allowed for appropriate fixing of the two components, and the split washers would reduce the change of the nuts "backing out" due to vibrations, a primary concern on this project. The initial design had only the two arms on the original absorber, however, holes and cutouts were added in order to balance the model. The center of mass of the absorbers and the mass of the absorbers were a critical to maintain since a slight change would directly impact the damping of the system. The intention of the large half circle cutout in the middle, and the 6 holes on the sides of the absorber were to balance the mass of the arms. Additionally, the absorber was reduced to half the thickness to account for the mass of a second absorber. The original mass was 103.796 g, and the new mass of both absorbers and hardware was 103.47 g, a difference of 0.3%. The center of mass did not change from the original model. Figure 11 shows the full configuration of the rotor and absorbers.

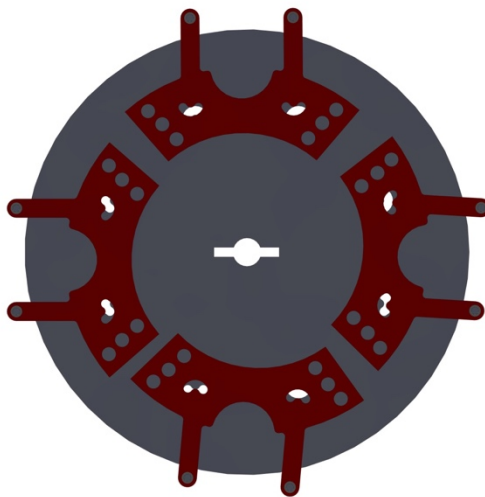


*Figure 11. Absorber in CPVA assembly and alternate absorber view*

The absorbers would remain in the same position around the rotor. The benefit of the arms is that they can be easily accessed when in the top position on the rotor. The screws can be tightened or loosened, and the rotor can be rotated to allow the next absorber to be in the top position for adjustment. To determine the desired clamping force, an excel sheet was created to calculate the torque on the bolts and convert it to the clamping force on the rotor (in Appendix D). The torque could be controlled with a torque wrench and set to the desired torque according to the test being performed.

### 7.4.2 Pressure Vessel

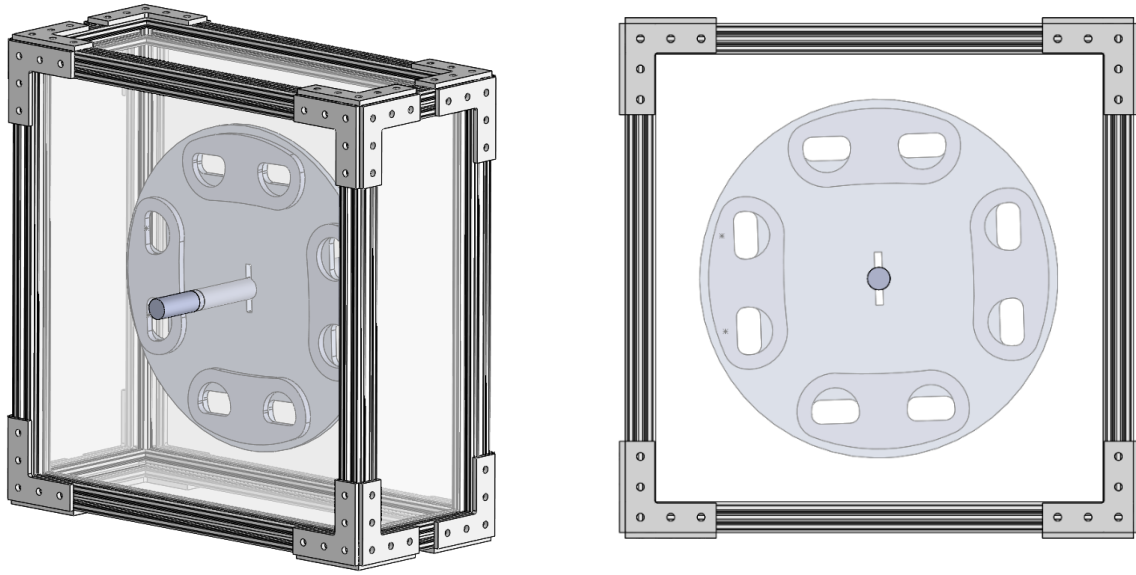


Figure 12. Pressure vessel design with CPVA assembly encased

In this methodology, the general design intent was to force the absorbers and rotor together by increasing the ambient pressure. This would be done by encasing the CPVA into a pressurized vessel that could be loaded to the desired pressure. The assembly designed is shown in the previous figure.

In this assembly, aluminum extrusions are utilized to build a frame around the CPVA with polycarbonate plates. Polycarbonate, acrylic, and aluminum plates were tested under 30 PSI of pressure and the only material that did not reach the yield stress was polycarbonate. Note, this design does not have the appropriate hardware for pressurizing a container as it was designed to visualize the configuration and test the mechanical properties thereof.

For this system with the polycarbonate plates, it was calculated that the total assembly as it is shown above would cost approximately \$300.

This design has a critical flaw that if the rotor and absorbers do not make a perfect seal, they may separate, and any pressure advantage would be lost. There is also a concern of safety since a pressure vessel would be created that could explode or have components explode.

### 7.4.3 Absorber Compressing Method

Another design considered by the team is the opposite of the Rotor Compressing Method mentioned above. In this design, the rotor would be split into two pieces, with the absorbers placed in between. This way, the normal force can be modified by tightening the rotors against the absorbers. The configuration can be seen in the following figures.

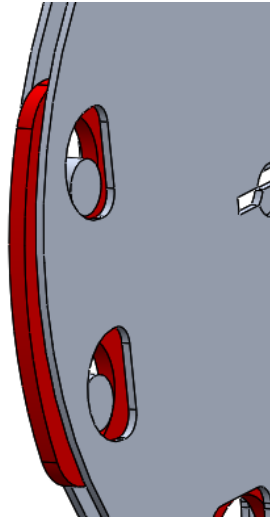


Figure 13. Absorber compressing method design



Figure 14. Absorber compressing method, alternate view

This method would be rather costly in that new rotor pieces need to be manufactured. However, tightening the two rotor pieces closer together would increase the normal force on the absorbers, and thus modifying the force of friction between their surfaces and the rotor surfaces.

#### 7.4.4 Ball Bearing Pressure

This design applies normal force in the absorbers via a ball bearing against each of the four absorbers. These ball bearings would be attached to a plate that is part of the frame design around the rotors. This plate can be adjusted to apply a specific amount of normal force on these absorbers against the rotor, and thus modifying the friction force between them. This setup can be seen in the following figure.

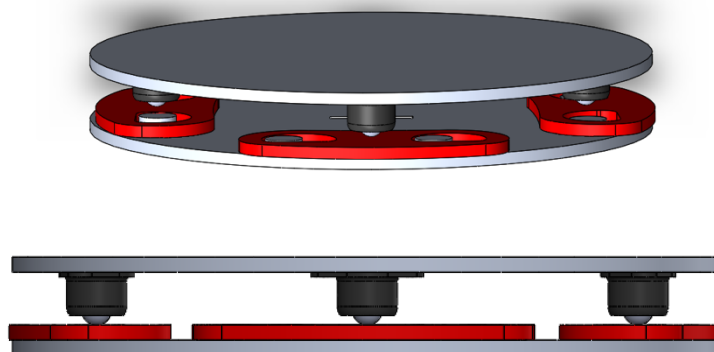


Figure 15. Ball bearing method, angled and orthogonal view

### 7.4.5 Existing Bolt Preload Method

This design takes advantage of the pre-existing bolts in the current CPVA design, and either increases or decreases the torque to vary the normal force. The cost of this design modification would be negligible as no new parts would need to be purchased or manufactured. Torqueing the bolts would produce a clamping force between the rotor and absorbers. Whether there is a load being applied to the system or not, the tightening of the bolts will create a preload. A higher preload is desired because that will help prevent the bolts from loosening from the vibrations the system experiences. Any deformation and yielding to the system will correspond to the strength of the materials being used. Depending on the material properties, a higher preload can be applied and result in elastic or plastic deformation which, in the case of vibrations, is less likely to cause wear.

Aluminum 6061 is the material being used, which is a common material used in the automotive industry. This Aluminum alloy tends to be corrosion resistant and does not deform when exposed to ambient pressures or temperatures unless they are under extreme conditions. Fewer deformations resulting from the environment will increase the lifecycle of the system [26].

The normal force can be defined as the magnitude of the frictional force divided by the coefficient of friction. Tightening or loosening the bolts will allow the desired normal force to be achieved which can then be related to the coefficient of friction [26].

### 7.4.6 Design Decision Matrix

The team carefully considered all the benefits and drawbacks of these designs, using a decision matrix to quantify these considerations. A decision matrix assigns a fair and equal scale to be used for all the designs, showing how the designs rank against each other. Using a variety of analytical and evaluative techniques, the rankings of each design are presented below in Table 6.

Table 6. Decision matrix for competing designs

Design	Price	Complexity	Resource Intensity	Safety	Feasibility	Reliability	Maintenance	Durability	Total
<i>Rotor Compressing Method</i>	3	8	7	9	8	9	10	8	62
<i>Pressure Vessel</i>	6	7	5	2	2	4	3	2	31
<i>Absorber Compressing Method</i>	2	8	7	9	8	9	9	8	60
<i>Ball Bearing Pressure</i>	6	7	8	8	8	9	9	9	64
<i>Existing Bolt Preload</i>	9	9	10	10	8	7	8	7	68

Table 7 contains the metrics used for scoring these designs.

Table 7. Legend for the decision matrix in Table 6

Criteria	Description	"0" Rating	"10" Rating
<b>Price</b>	<i>Upfront cost of the assembly (Bill of Materials)</i>	<i>~\$1,000</i>	<i>~\$0</i>
<b>Complexity</b>	<i>Number of pieces in the assembly/resources, skills required to put together assembly</i>	<i>20 or greater additional components</i>	<i>no additional resources required</i>
<b>Manufacturing Intensity</b>	<i>Unique pieces in assembly, tools required for assembly (e.g. torque wrench)</i>	<i>10 hours of processing time required for the most complicated component</i>	<i>No processing time required</i>
<b>Safety</b>	<i>Probability/danger if pieces malfunction and potential hazards</i>	<i>Unsuitable to be operated in the presence of people</i>	<i>No additional safety hazards are imposed</i>
<b>Feasibility</b>	<i>Estimated likelihood of success informed by engineering analysis</i>	<i>Highly unlikely to work</i>	<i>Highly likely to operate as intended</i>
<b>Reliability</b>	<i>Will this design consistently deliver the results expected for this configuration</i>	<i>Several anticipated inconsistencies</i>	<i>No anticipated inconsistencies</i>
<b>Maintenance</b>	<i>Ease of access to components for modifications/replacements during lifetime</i>	<i>Requires more than 2 steps for disassembly</i>	<i>Easy to access and modify</i>
<b>Durability</b>	<i>Withstanding long term use, considering yielding, structural integrity, wear</i>	<i>Anticipated failure within 6 months</i>	<i>Useful life expected beyond 5 years</i>

## 7.5 Proposed Normal Force Modification Design

The most straightforward and simple method to modify the normal force, as seen in Table 6, is using the existing bolt preload design. All the designs considered, this would be the easiest method, in theory, costing very little and requiring no unique pieces. The only potential issue with this design modification is the amount of control this would give since the CPVA vibrates, the bolts can loosen, not providing a steady normal force on the absorbers.

To mitigate this issue, the current bolting should be augmented with 222 Threadlocker Purple Loctite. This Loctite variant is specifically designed to prevent the loosening of screws under vibratory loads while still being adjustable by hand. Since the CPVA needs to be modifiable, a permanent thread locker cannot be employed, so this purple variant is an excellent alternative.

## 7.6 Design Methodology of ANSYS Models

After a final absorber design was chosen, analysis to obtain an appropriate coefficient of friction began. The plots produced in MATLAB was able to calculate the specific surface roughness that would achieve a specific coefficient of friction. The range of coefficients that were determined to be accurately modeled by the MATLAB results were from 0.15 to 0.45. These were evaluated in increments of 0.05 in the ANSYS model. This was then able to produce a modal analysis in order to determine which coefficient would produce the most feasible results.

The goal of a CVPA is to reduce the overall vibrations transmitted from an engine. So, the results from ANSYS were considered by how well they disallowed the transmittance of these vibrations. It was determined that a modal analysis on the design, along with the frequency response of deformation from the absorbers, would provide enough data to determine the most feasible coefficient of friction. The modal analysis was performed on ANSYS workbench 19.2, following an ANSYS workshop tutorial on modal analysis of a spinning flywheel [27]. The dynamics of the flywheel were modified from the tutorial to fit the specifications of the project.

First, the engineering data was entered into the workbench, the rotor and absorbers were given Aluminum Alloy for material, a preset material in ANSYS workbench. The pins, or rollers, of the CPVA were set to stainless steel, another preset material in the workbench. Preset values can be observed in Table 7.

*Table 8. Material properties of preset materials in ANSYS*

Material	Density (kg/m <sup>3</sup> )	Compressive Yield Strength (Pa)	Tensile Yield Strength (Pa)	Tensile Ultimate Strength (Pa)	Youngs Modulus (Pa)	Poisson Ratio	Bulk Modulus (Pa)	Shear Modulus (Pa)
<i>Aluminum Alloy</i>	2770	2.8 e08	2.8 e08	3.1 e08	7.1 e10	0.33	6.9608 e10	2.6692 e10
<i>Stainless Steel</i>	7750	2.07 e08	2.07 e08	5.86e08	1.93 e11	0.31	1.693 e11	7.3664 e10

Geometry was imported into the model from SolidWorks, using given files of the current design for the CPVA test rig. The geometry used in this analysis was only the rotor, absorbers, and rollers. Once imported, ANSYS Mechanical was opened, and the initial conditions were given to the model. The contact tool was used to assign contact between each piece of the model. Most importantly, the contact between the absorbers and rotor was set as “frictional” with a coefficient of friction of 0.15. The frictional contact requires one body to be the “contact” body, and one to be the “target” body. The target body is the body that is rigid in the structure, so the rotor was chosen to be the target body. The contact bodies were set to the absorbers. It is important to note that at this point the modal analysis being performed was for a 0.15 coefficient of friction. The other coefficient analyses were produced by reopening the same model and resetting the coefficient of friction between the absorbers and rotor to the desired amount, then solving. Once set, the contacts between the roller bodies in the model were left as their default “bonded” state.

Contacts between the roller and absorber/rotor were set to “frictionless,” “Rough,” and “No Separation.” These were attempted as it would be closer to the type of contact experienced in the actual test rig. The frictionless contact setting allowed for the separation and sliding of the components in contact with the rollers. The rough contact setting would not allow slippage and in theory would allow the rollers to roll in static friction. However, after several tests with other simple models, it became clear that the motion desired could not be achieved by this setting. Finally, the no separation contact setting would allow for the slippage of the rollers, without separating from the walls of the cutouts in the rotor and absorbers. The no separation configuration would be the ideal contact setting, as it would allow for a “linear” contact which is necessary to solve for the modal analysis in ANSYS. Due to the lack of time and familiarity with ANSYS, these attempts did not produce functional models capable of producing simulations. The computational power of the current system could no longer meet the demands, and more experience with ANSYS workbench tools like the “rigid dynamics” or “transient structural” would be needed. It was determined that since the coefficient of friction could still be varied between the rotor and absorber, the results produced would still be adequate and relevant.

Once the contacts were set, a fixed support was placed in the center of the rotor, to act as the axel that it would be rotating on. Next, a rotational velocity of 1000 RPM around the positive Z axis (a potential RPM of an automobile operating at low revolutions) was placed on the rotor. The solution was set to



solve for the total deformation of the system, as a check of reasonable results, and to ensure simulation was set up correctly.

The modal analysis was performed next. The analysis was set to inherit all the supports from the static structural branch. No further loading was placed on the model as the rotational velocity would be accounted for by an increase in stiffness automatically performed by ANSYS. The Modal analysis was set to find the first six natural frequencies. This was chosen because the previous capstone performing a modal analysis on the structure of the entire testing rig determined that the first five modes would be sufficient since it is operating at relatively low RPM. So, this capstone team used a default of the first six modes to add a factor of safety in case a significant mode was missed in the previous analysis. The model was solved, and the deformation plots for the six modes were produced.

The next analysis that was performed was the harmonic response. In the same fashion as the modal analysis, the harmonic response would inherit the supports and solutions of the previous analysis. An excitation acceleration of  $20 \text{ m/s}^2$  (recommended by the tutorial analysis was based on) was applied around the positive Z axis. The minimum frequency was set to 0 Hz, and the maximum to 700 Hz. The range of 0 - 700 Hz was determined as satisfactory because 700 Hz is far greater than any frequency that our test rig and any automobile would be experiencing. A damping of 5% was applied because the peak responses at resonant frequencies would be unbounded. The solution intervals were set to 1000, which would result in enough data points to extract the peaks and be able to perform a thorough analysis of the data.

A frequency response deformation was scoped to the four absorbers. This allowed the software to analyze directly how the absorbers would interact at the modal frequencies. The model was solved, and plots of the frequency response on the absorbers for each of the coefficients were produced. The seven plots produced were then plotted against each other so they could be directly compared. In this study, the ideal coefficient of friction would be one that had the smallest magnitude of amplitude on the frequency response graphs at the resonant frequencies. This would produce absorbers that propagate the least magnitude of vibrations when the system is run at those frequencies.

## 7.7 MATLAB Surface Generation

Figure 16 shows a 3D surface generated in MATLAB. This surface, like Figure 6b, utilizes MATLAB's *normrnd* function to assign a unique height to each element while the standard distribution and population mean of the heights are specified.

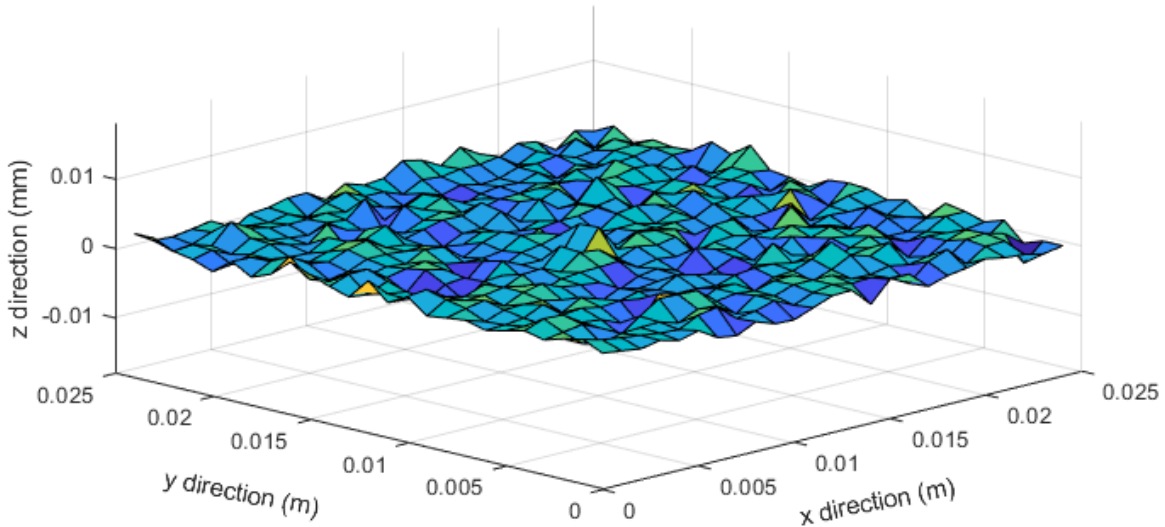


Figure 16. 25mm square rough surface generated in MATLAB with one asperity per mm<sup>2</sup> ( $R_a = 3.2\mu\text{m}$ ,  $R_{ms} = 1\mu\text{m}$ )

This plot, though, considers only the asperities of the surface. Hence, this is not an accurate illustration of a real rough surface, rather an approximation thereof. For a more realistic representation of what a rough surface looks like, the resolution between asperities needs to be increased. In MATLAB, this can be done using the interp2 function. Figure 17 shows a surface with identical input parameters as Figure 16 but overlays a grid with 5 times the resolution of the original asperity matrix for an interpolated surface. The interp2 function is then utilized, with the interpolation method set to 'spline.' The spline setting is preferred over the other methods (linear, cubic, nearest, etc.) due to its moderate computational intensity and smooth output. This type of surface is preferred for finite element analysis (FEA) since the mesh is smoothed and there are not any unrealistically jagged points as seen in Figure 16.

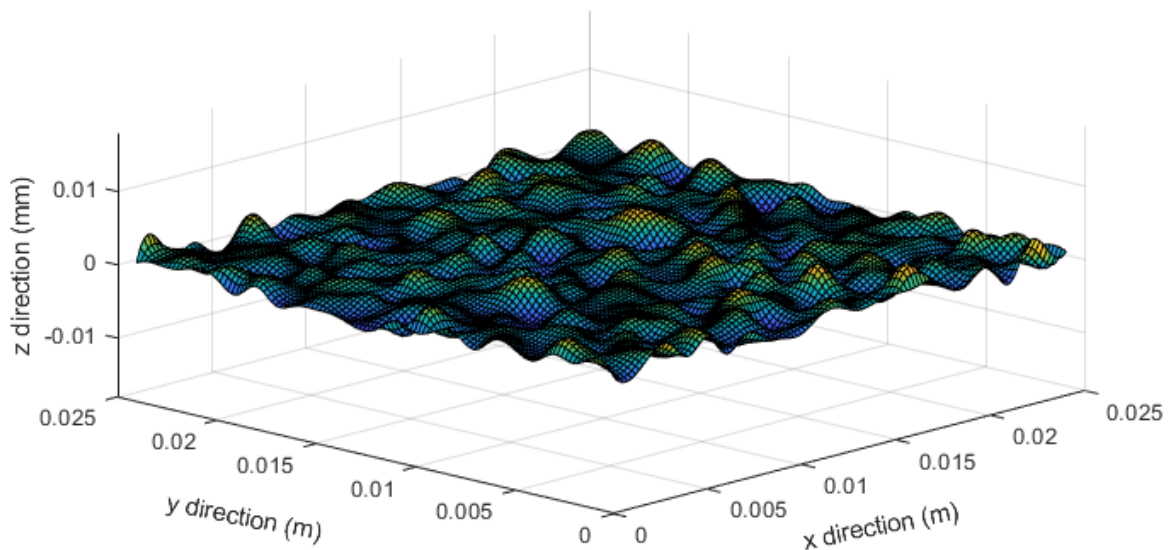


Figure 17. 25mm square rough surface generated in MATLAB with one asperity per mm<sup>2</sup> with an interpolation factor of 5 ( $R_a = 2.9\mu\text{m}$ ,  $R_{ms} = 0.21\mu\text{m}$ )

Histograms of these Figures 16 and 17 are provided below in Figure 18.

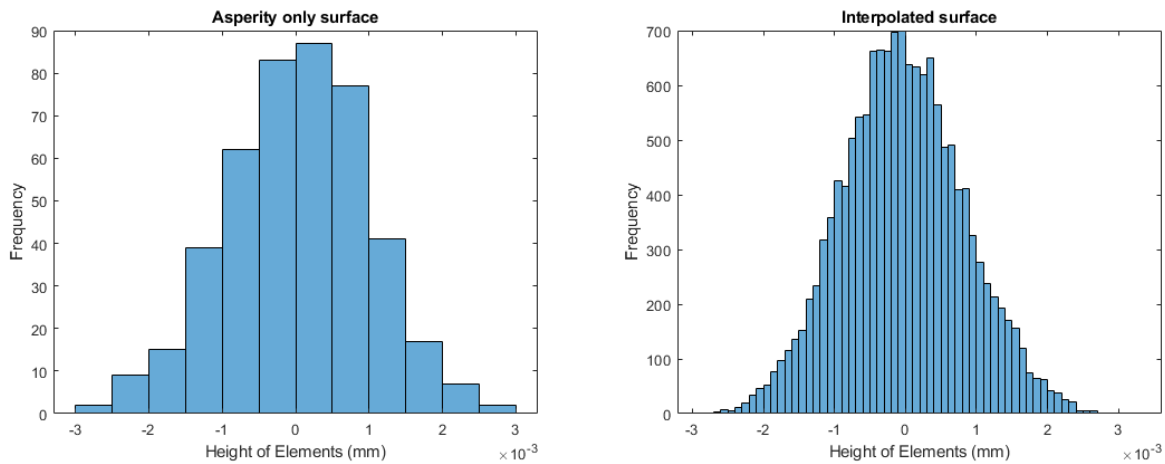


Figure 18. Height distribution of the surfaces generated in Figure 16 (left) and Figure 17 (right)

It is evident that there is a far greater resolution of the surface with the interpolation. Accordingly, the histogram generated with the interpolated surface represents a Gaussian distribution more accurately than the asperity only surface. The surface in Figure 17 has an interpolation factor of 5, meaning that there are 5 additional data points between successive asperities. Since the surface mesh is generated in two dimensions, the increase in resolution is  $5^2$  or 25 times greater. This is reflected in Figure 18 where the asperity only surface (left) has 25 times fewer data points than does the interpolated surface (right).

Due to this increased resolution, it would be prudent to utilize the interpolated method of generation. As the resolution increases of the surface, it is assumed the accuracy of the model does as well. Though, there is some computational efficiency cost to be considered with the surface of higher resolution.

## 7.8 Finite Element Approach

To import these surfaces into a finite element software, the surfaces must first be exported as a 3D file. To do this from MATLAB, the surface generated must be decomposed into a mesh of triangles and saved as a stereo-lithography file (.STL). The code for exporting a surface model to an .STL file is exceptionally complicated, thus it was sourced from Paul Kassebaum on mathworks.com [28]. This type of file, commonly used in 3D printing, can be opened by most commercial modeling software packages, such as SolidWorks. This part is then edited to extrude a volume behind the surface and subsequently exported as a SolidWorks part. This file, now, can be imported into ANSYS for analysis. The following figure displays this process visually. Of note, SolidWorks' simulation suite was not used for this application due to the large amount of faces causing the mesh to fail consistently.

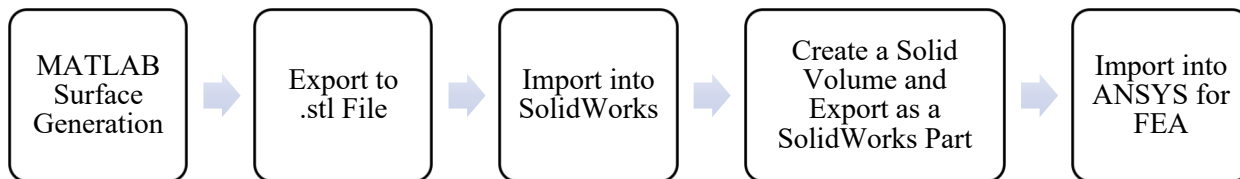


Figure 19. Process flow of creating a MATLAB surface to be imported into ANSYS

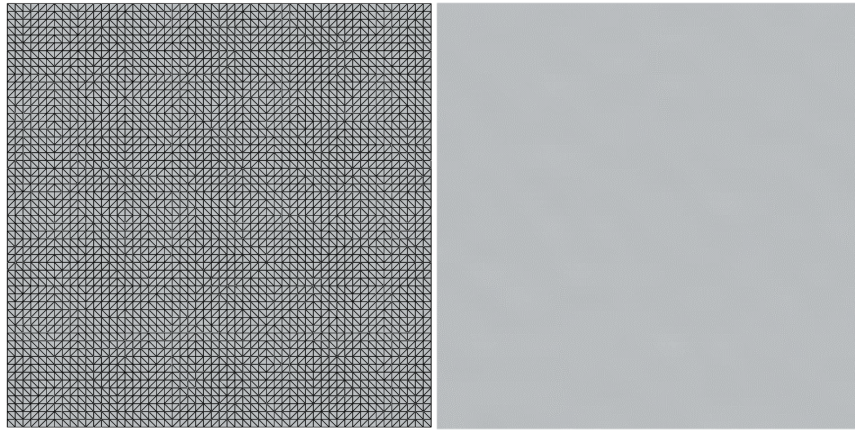


Figure 20. Pictured left, orthogonal view of a generated rough surface imported into SolidWorks with vertices showing; pictured right, the same surface without vertices showing

When came the process of simulating and evaluating the rough surfaces in ANSYS, considerable difficulty was had. ANSYS had difficulty accommodating the substantial amount of faces and the surfaces were difficult to constrain and load as intended. Considerable time was spent trying to develop a FEA model that could accurately deform the micrometer high asperity protrusions. Ultimately though, due to technical difficulties with ANSYS, the second option of developing a code to compute the contact mechanics was prioritized.

## 8 Design Solution

### 8.1 Development of a Contact Model:

The first approach to developing a contact model was to create a MATLAB script that could calculate the load of two interfering asperity elements.

To do this, some method must be instituted to record the interference between the undeformed asperities in contact. As shown below in Figure 21, the surfaces can be thought of being some distance, or distillation,  $d$  apart. As the surfaces are compressed together, eventually the free lengths of the  $i^{\text{th}}$  asperity of surfaces 1 and 2, given by  $L_{1,i}$  and  $L_{2,i}$ , will interfere. This interference is denoted by  $\delta$  and is the same as shown in Figure 5. So, for the  $i^{\text{th}}$  element, the interference  $\delta$  can be determined by Equation 9.

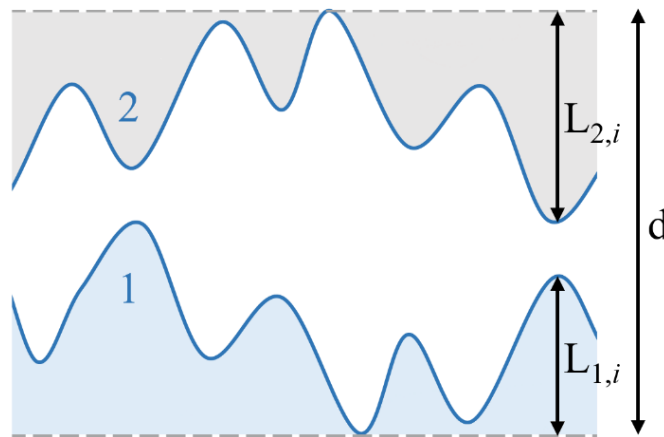


Figure 21. Schematic representation of two surface profiles with spline interpolation between asperities

$$\delta_i = \begin{cases} [(L_{1,i} + L_{2,i}) - d] & \text{if } [(L_{1,i} + L_{2,i}) - d] > 0 \\ 0 & \text{else} \end{cases} \quad (9)$$

To find the resulting force due to an element's deformation, F can be solved for from Equation 4 yielding

$$F_i = \frac{4E^*}{3} (\delta_i^3 R)^{1/2} \quad (10)$$

which considers the force at the  $i^{th}$  element. The resulting  $\delta_i$  from Equation 9 is then inserted into this equation to yield the corresponding force.

Now that formulations for the force and displacement exist as a function of the distillation, a script can be written to evaluate the interference at every asperity and the corresponding force for some given distillation. The sum of the resulting force matrix is the macroscopic normal force ( $F_{N,0}$ ).

However, this is not particularly useful in this form as surfaces are not typically compressed to achieve a certain distillation, rather, they are subjected to a load. What is more useful is to specify a given normal force ( $F_N$ ) and to use a root finding method to find at what distillation the macroscopic normal force is equal to the specified normal force. To do this, the implementation of Steven C. Chapra's secant method script for MATLAB was modified for use [29]. This, in effect, is the foundation of the code provided in Appendix C entitled *LoadFun.m*.

At this point in formulating the code, the method by which the shear force is evaluated comes into question. The most basic methodology, as suggested by Hulikal, Lapusta, and Bhattacharya, is assuming the shear force is the product of the area in contact and the shear strength [4]. This is provided below in Equation 11.

$$S_i = \tau A_i = \tau(\pi a_i^2) \quad (11)$$

In this equation  $S_i$  is the shear force on the element,  $\tau$  is the shear strength of the deformable surface of interest, and  $A_i$  is the element contact area. Should the Hertz contact model be adopted,  $A_i$  can be expanded as  $\pi a_i^2$  where  $a_i$  is the radius of the element's area of contact as given in Equation 6.

This methodology was utilized, and it exists commented out in *LoadFun.m* (see Appendix C) but proved to be unrealistic. The shear force, since it depends exclusively on the area of contact, is disproportionately large compared to the normal force. The coefficient of friction tended to be in the scale of 5-10 which is far beyond any reasonable experimental result. For this reason, a second, more robust method had to be considered.

### 8.1.1 Derivation of Contact Model:

A new method was derived that attempts to modify the simple Hertz contact model. This new model is designed to consider the curvature of the generated surface when evaluating the contacts between the sphere-tipped asperities. In the general Hertz contact case, as used in the previous methodology, the asperities come into direct, orthogonal contact. This is unacceptable since the shear force can only be considered as it was in Equation 11.

Contact between sphere-tipped asperities can be generalized by Figure 22.

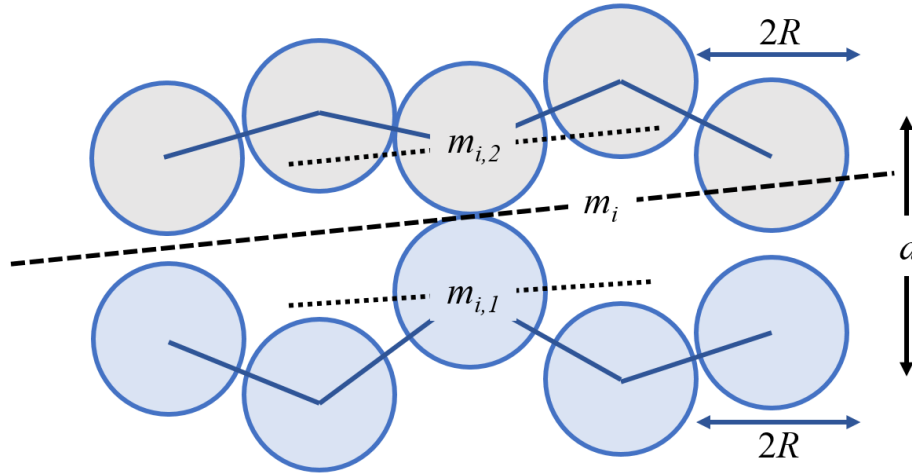


Figure 22. Schematic representation of two surface profiles with spline interpolation between asperities

In this figure, two surfaces are locally contacting at the middle asperity. The slope of the surface at the asperity of interest is given by  $m_{i,1}$  for the first (bottom) surface and  $m_{i,2}$  for the second (top) surface. The average slope is given by  $m_i$  which is simply the arithmetic mean of the asperity slopes of surfaces 1 and 2.

The forces resulting from these asperities contacting can still be thought of as Hertz contact. However, now they are normal to the average slope  $m_i$  rather than normal to the surfaces themselves. The new methodology is shown below for a hypothetical asperity contact in Figure 23.

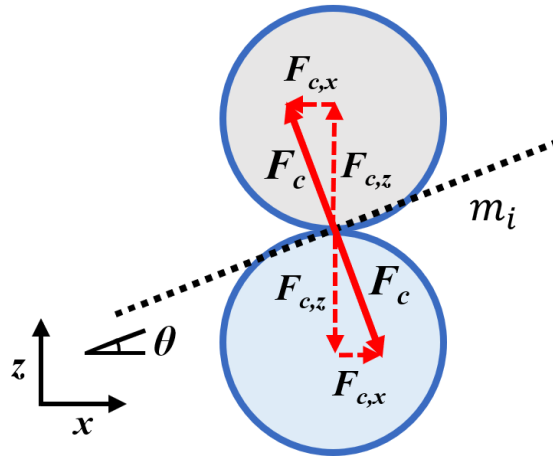


Figure 23. Diagram of asperity contact forces decomposed into  $x$  and  $z$  directions

In this diagram, a supposed instantaneous slope for the asperity contact ( $m_i$ ) is imposed. The angle of this slope, with respect to the  $x$  axis, is simply the arctangent of  $m_i$ , shown in Equation 12. The resultant force vector is orthogonal to  $m_i$ , thus can be decomposed into the appropriate  $x$  and  $z$  components. The interference is still assumed to be normal to the surfaces in contact, so when using the Hertz equation (in Equation 7) the interference from distillation must be adjusted by the angle  $\theta$ . This is provided in Equation 13. Likewise, the formulations for  $F_{c,x}$ , and  $F_{c,z}$  are provided in Equation 14, and 15 respectively.

$$\theta_i = \arctan (m_i) \quad (12)$$

$$\Delta_i = \delta_i(\cos \theta) \quad (13)$$

$$F_{c,z} = F_i = \frac{4}{3} \sqrt{\Delta_i^3 RE^{*2}} \left| \sin\left(\frac{\pi}{2} - \theta\right) \right| \quad (14)$$

$$F_{c,x} = s_i = \frac{4}{3} \sqrt{\Delta_i^3 RE^{*2}} \cos\left(\frac{\pi}{2} - \theta\right) \quad (15)$$

Since  $F_{c,z}$  is the component in the z direction, it is set equal to the normal force of the element. Similarly, since  $F_{c,x}$  is the component in the x direction, it is set equal to the shear force of the element. Note, shear is only considered in the x direction because the surfaces are set to only translate in that direction. Hence, interactions that are occurring along the y axis are not influential to the coefficient of friction being investigated along the x axis.

When evaluating the shear for the surface, the element shear force acting against the direction of investigation needed to be disregarded. For this model, the direction of investigation is set to be the positive x axis, so any shear component calculated to be negative must be set equal to zero. Should this not be done, the resulting coefficient of friction is miniscule. To recapitulate, the overall shear force is a summation of the element shear forces across the surface being investigated. If these negative elements remained in the shear array, the overall shear force is approximately zero, thus making the coefficient of friction approximately zero as well (see Equation 3). Once this modification was made, the resulting coefficients of friction were far more reasonable.

After evaluating the simplified Hertz model and the new, modified Hertz model, it became evident that the modified Hertz model was the more accurate one and should be implemented into all consecutive codes. All codes in Appendix C utilize this contact model.

### 8.1.2 Effect of the Radius in the Contact Model

A critical element of this method is determining the appropriate radius to use. In Equation 3, the radius of the equivalent rough surface is defined by the radii of the asperities in contact. For simplification, it is assumed all asperities have similar radii. This assumption follows a precedent set by Bhushan [6]. However, the matter of determining what identical radius to be used is not clear or intuitive.

Several radius methods were utilized and tested throughout the development of this contact model (see the Figures in Appendix D.3). To do this, a MATLAB script was written to evaluate the coefficient of friction of two random, interfacing surfaces as a function of the input load. This code can be found in Appendix C labeled *Friction\_Test.m*. A slight modification to this code is made in *Friction\_Test\_Evolve.m* which creates a plot of the coefficient of friction vs the normal force applied. The applied normal force is programmed to iterate between 0 to 1000 N. Though, for some surfaces with smaller asperity heights, the iteration fails before 1000 N.

*Friction\_Test\_Evolve.m* was then used to test different methods for calculating the radius. It was determined that the following radius calculating methods produced inconsistent, unrealistic, or otherwise unreasonable coefficient of friction vs load plots: the minimum radius of curvature of the first surface, the maximum radius of curvature of the first surface, and the average radius of curvature of the first

surface. Note, during these calculations, the first and second surfaces were created with the same input parameters, so it is assumed the radius calculated from the first surface can be used for the second.

Ultimately, it was decided to test a fixed radius that is some fraction of the distance between consecutive asperities. Different fractions were tested, including 1, 1/2, 1/4, and 1/10. A comparison between these, as well as the differences between the asperity only and an interpolated surface model, are provided in Figure 24.

In this Figure, there is relatively little variation between the plots generated. Though the shapes of the plots do tend to differ significantly, the numerical range of the steady-state coefficient of friction is reasonably small, about 0.06. From evaluating the average steady-state (or approaching steady-state) coefficients of friction, it is found the standard deviation is 0.022. This is reasonable, considering that the surfaces tested had to be randomly generated between successive tests.

From this, several conclusions can be made. The foremost is that the fraction used for calculating the radius leaves little impact on the result. The second is that the interpolated surface models tend to yield plots that stabilize sooner than the asperity only models. Therefore, when conducting subsequent calculations, a fixed radius some fraction of the distance between consecutive asperities should be chosen and the surfaces should be interpolated.



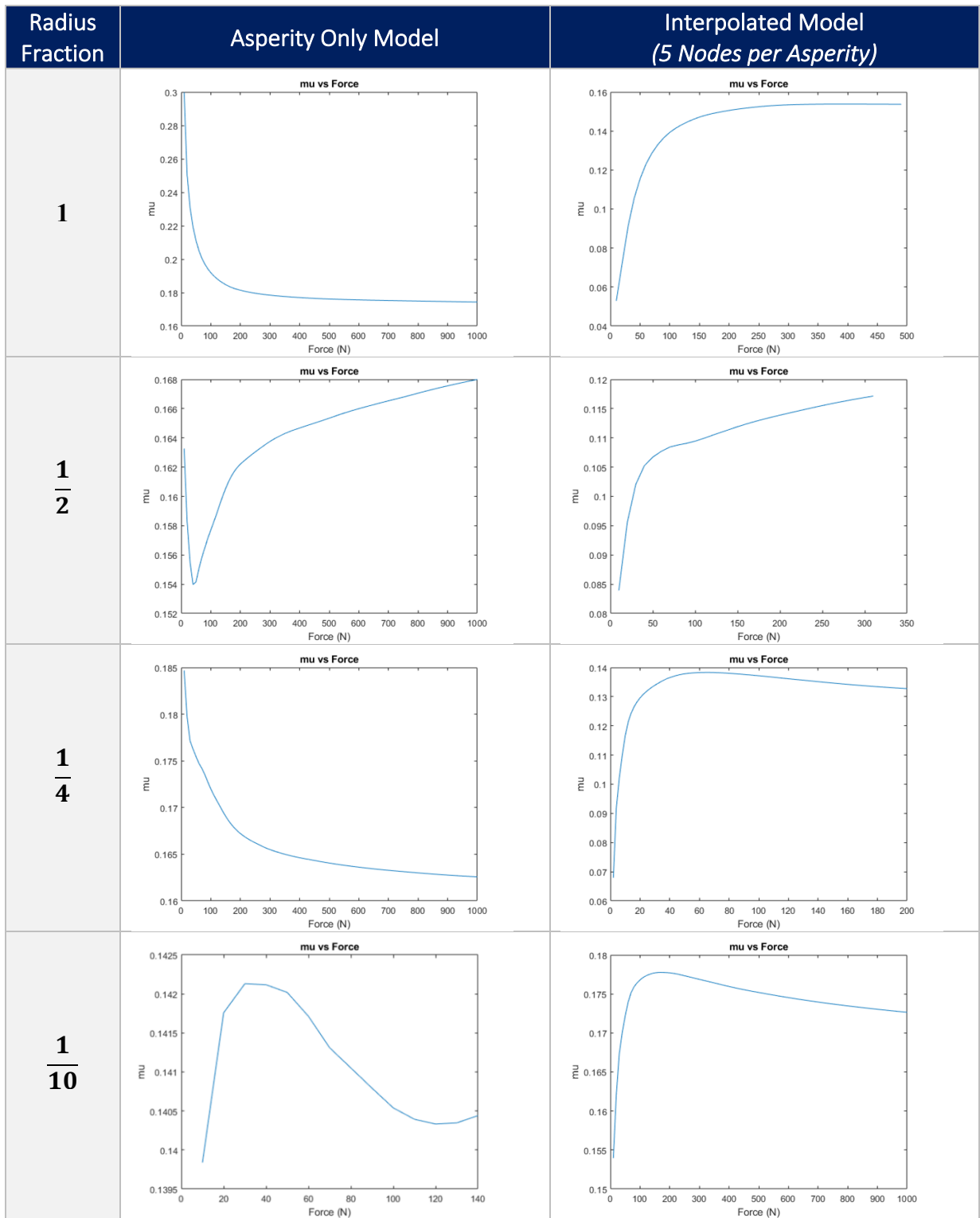


Figure 24. Comparison between various input parameters (asperity vs interpolated, radius size) to be used in the final contact model. Surface parameters:  $\sigma = 0.25 \mu\text{m}$ , asperity density =  $4/\text{mm}^2$ , width =  $10 \text{ mm}$

### 8.1.3 Effect of Interpolation Resolution

In this model, since the surfaces were decided to be interpolated, it is critical to determine what effect the interpolation resolution has on the coefficient of friction. The interpolation resolution is equivalent to the number of new points between asperities. So, the factor of new data points overall is equivalent to the squared interpolation resolution factor.

The figure below compares the friction results and heat maps generated with interpolation resolution factors of 1, 5, and 10.

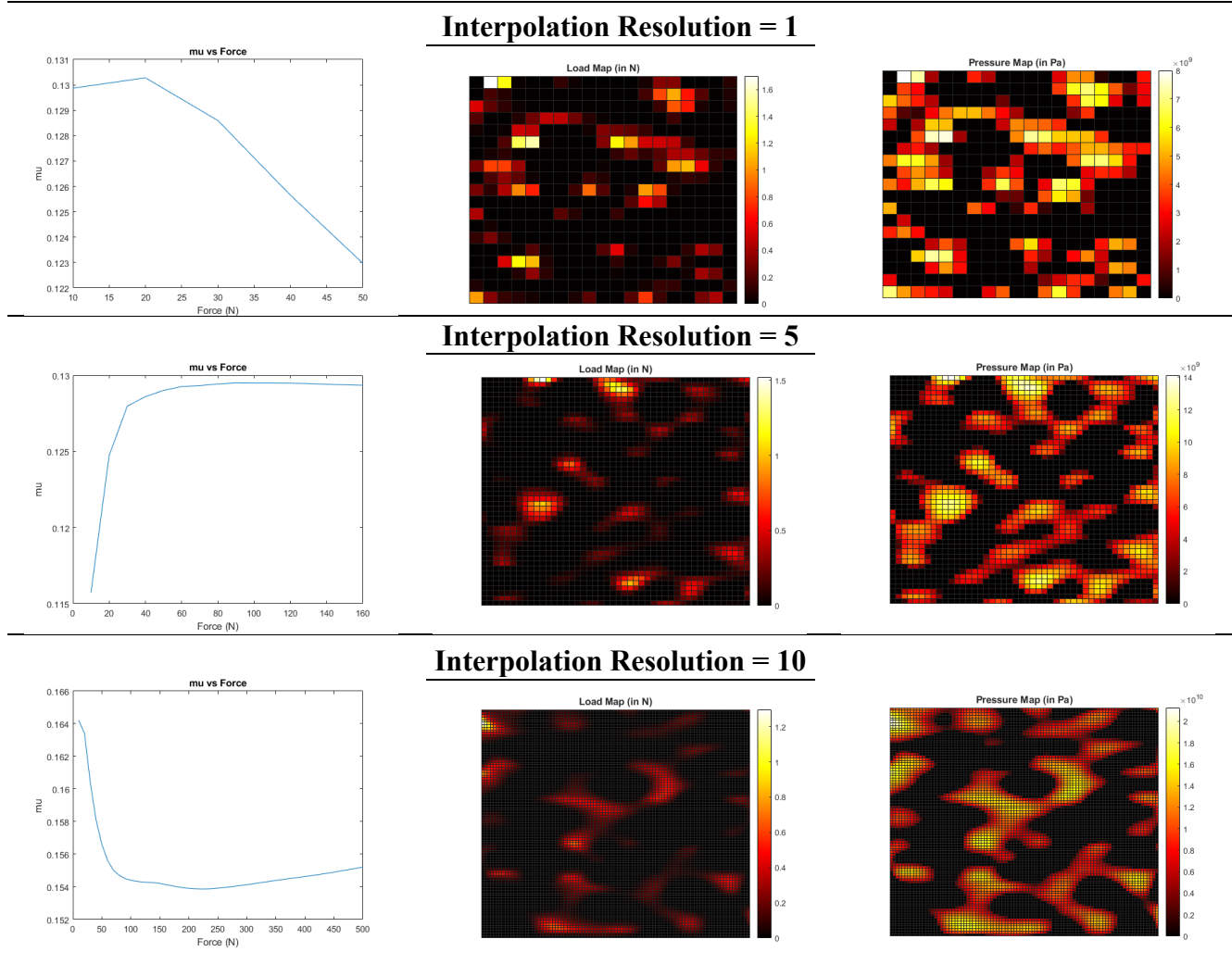


Figure 25. Comparison between coefficient of friction results with variable interpolation resolution factors (Surface parameters:  $\sigma = 0.25 \mu\text{m}$ , asperity density =  $1/\text{mm}^2$ , width = 10 mm)

In this figure, there is relatively little deviation between the resulting coefficient of friction plots amongst the different interpolation resolutions. The range of these coefficients of friction is  $\pm 0.02$  which is a typical deviation between models with identical input parameters (see Appendix D.3.1). So, it can be determined that the interpolation resolution factor has a negligible impact on the friction results. Since this is the case, a high interpolation resolution factor will not be used in further calculations since it increases the computation time needlessly.

### 8.1.4 Establishing a Relationship between the Input Parameters and the Output Coefficient of Friction

It is important to reconcile the relationship between the standard deviation input when generating the random, rough surface and the surface properties thereof. To do this, the MATLAB script *Ra\_Rms\_vs\_Sigma.m* was developed and is provided in Appendix C. This code iterates through hundreds of random surfaces and calculates the Ra and Rms values (Equations 7 and 8) to be plotted. Additionally, linear regressions were added to the average, upper, and lower bounds of these plots. For the results generated, a surface was generated 20 times per standard deviation ( $\sigma$ ) tested. Standard deviations were tested from 0 to 5  $\mu\text{m}$ , at intervals of 10 nm. This results in 10,000 surfaces being plotted.

The surface roughness (Ra) vs input standard deviation plot is provided below in Figure 26. Likewise, the root mean squared (Rms) vs input standard deviation plot is provided in Figure 27.

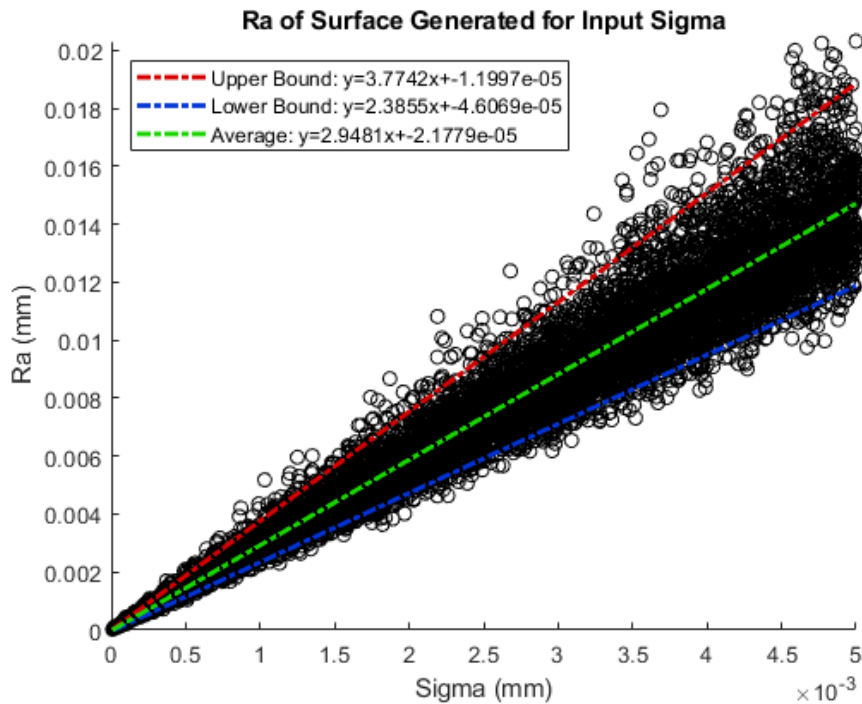


Figure 26. Surface roughness (Ra) vs input standard deviation (sigma) of surfaces generated utilizing MATLAB's normrnd function

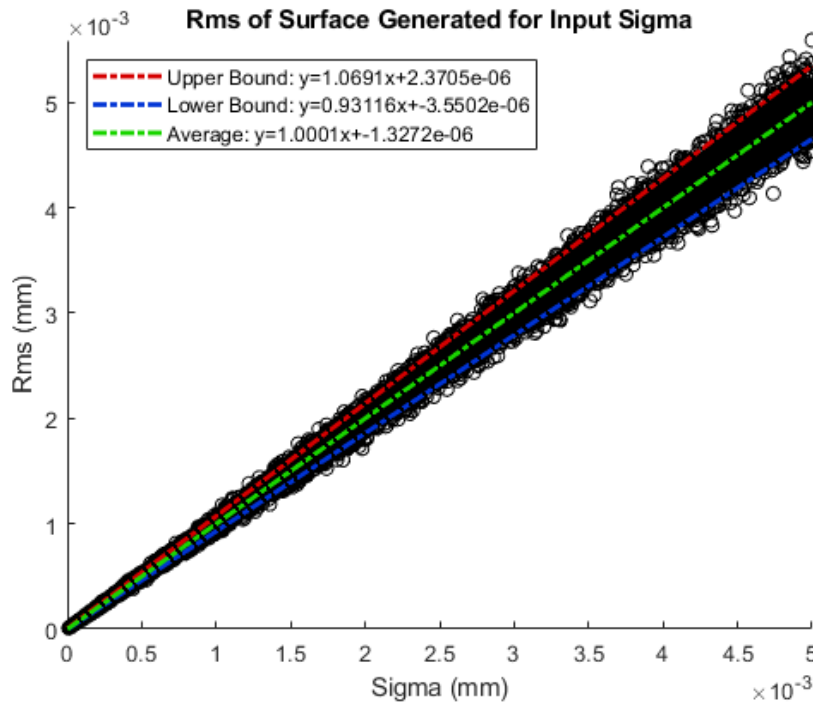


Figure 27. Root mean squared (Rms) vs input standard deviation (sigma) of surfaces generated utilizing MATLAB's normrnd function

Examining Figure 26, it is apparent there are significant deviations between the upper bound and average as well as the average and lower bound. This is not surprising since the process by which these models are generated requires a random distribution of points to be generated. There is a 19% difference between the average and lower bound slopes and a 28% difference between the average and upper bound slopes. This skew towards the lower bound is peculiar and should be noted for considering errors in this model.

Interestingly, the average slope of Figure 27 is  $\sim 1.00$ . Though, this is to be expected since the standard deviation is equivalent to the root mean squared of a sample when the mean is zero. The slope of the upper and lower bound is also of note, being relatively tight to the average, implying the average relationship is accurate. It is also far tighter than Figure 26, with a percent difference of 6.9% between the average and both the lower and upper bounds. Since there is no skew here, this further advances the peculiarity of the skew in Figure 26.

These two plots are essential to the characterization of this computational model. Should empirical tests be pursued, the tools for measuring and characterizing the surfaces tested will be the roughness parameter, Ra, and the root mean squared, Rms. So, these plots will be invaluable to correlate the results from this computational study to those results. This is also useful for the final plots relating the coefficient of friction to  $\sigma$ , Ra, and Rms.

## 8.2 ANSYS Simulation Design Solution

### 8.2.1 Modal Analysis

Given the initial set up of the static structural model in ANSYS, the modal analysis found six frequencies at which the deformation in the structure was the greatest. These frequencies are represented in Table 9. The frequencies did not vary by much depending on the coefficient of friction, which is expected because the geometry and material properties of the absorbers (such as Young's Modulus and Poisson Ratio) are not changing.

Table 9. Frequencies at which the six modes occur at for each coefficient of friction

Mode	0.15	0.2	0.25	0.3	0.35	0.4	0.45	Avg.	Std. Dev.
1	166.31	166.32	166.28	166.28	166.28	166.29	166.29	166.29	0.016
2	197.60	197.61	197.23	197.24	197.25	197.25	197.26	197.35	0.175
3	223.37	223.43	222.85	222.90	222.94	222.98	223.02	223.07	0.233
4	266.99	267.15	266.90	267.03	267.15	267.27	267.38	267.12	0.166
5	304.97	304.91	304.52	304.57	304.63	304.68	304.73	304.72	0.169
6	586.95	587.15	585.68	585.94	586.18	586.42	586.64	586.42	0.532

ANSYS produced six plots of the deformation on the rotor and absorbers. Given below in Figure 28, six deformation plots are shown for a coefficient of 0.35. The overall mode shapes produced were generally similar for each coefficient. These plots are important because it visualizes how each model will be deforming at given frequencies. In these plots, the largest amount of deformation occurs at the areas colored in red, and the smallest in blue according to the gradient on the left side of the plots.

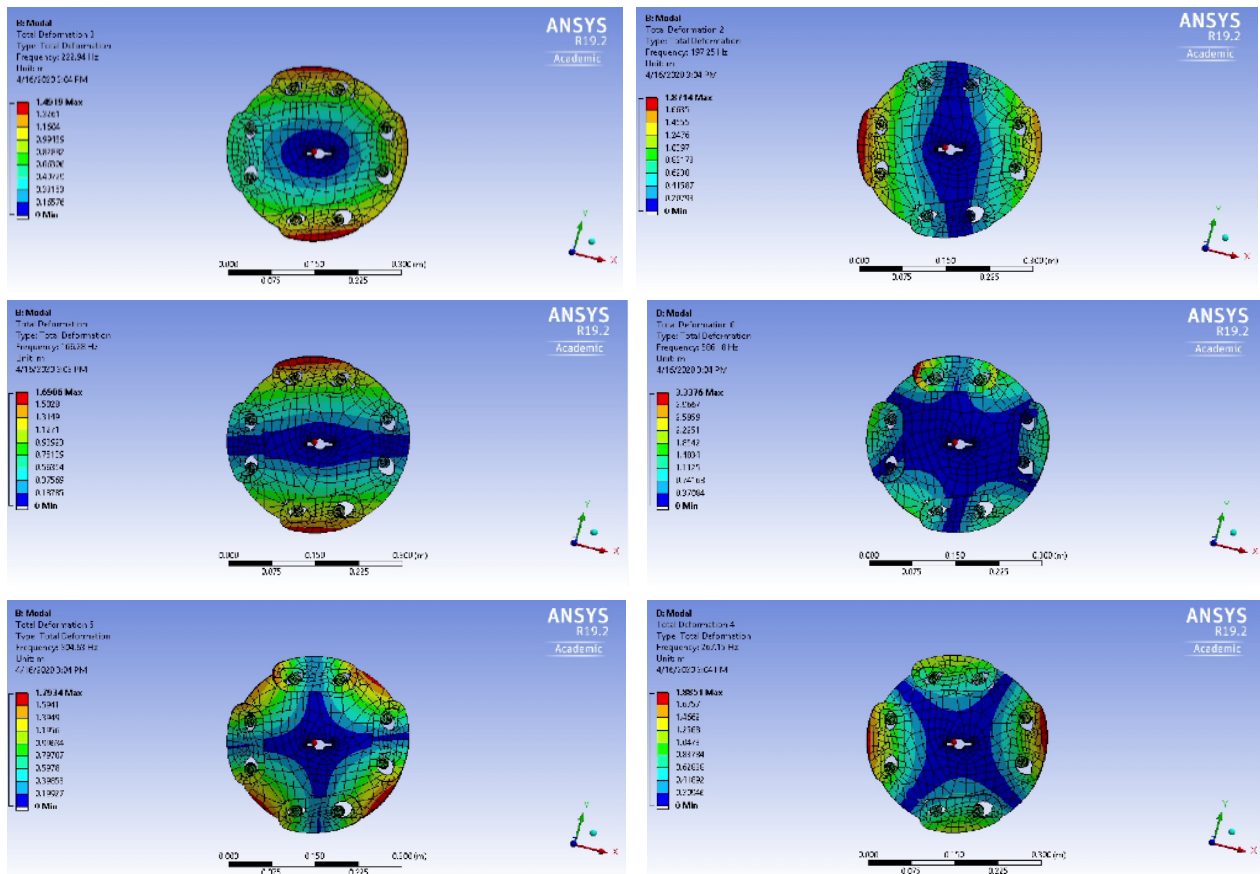


Figure 28. Total deformations for the six modes found in analysis for a coefficient of friction of 0.35

## 8.2.2 Harmonic Response

Using the harmonic response analysis in ANSYS, a further investigation of how each absorber interacted could be pursued. An excitation acceleration of  $20\text{m/s}^2$  was placed on the rotor around the positive z axis, and the model was set to solve for frequency response deformation scoped to the absorbers. This analysis would allow for the direct comparison between of how each absorber would respond. The absorbers had not shown much variation between them for the mode shape, and frequencies they occurred at, but did show variation in their frequency response. The model was set to solve for the frequency response deformation of the absorbers, sweeping across a range of frequencies from 0 to 700 Hz. A plot of the frequency response deformation obtained for absorbers with a coefficient of 0.35 is shown in Figure 29.

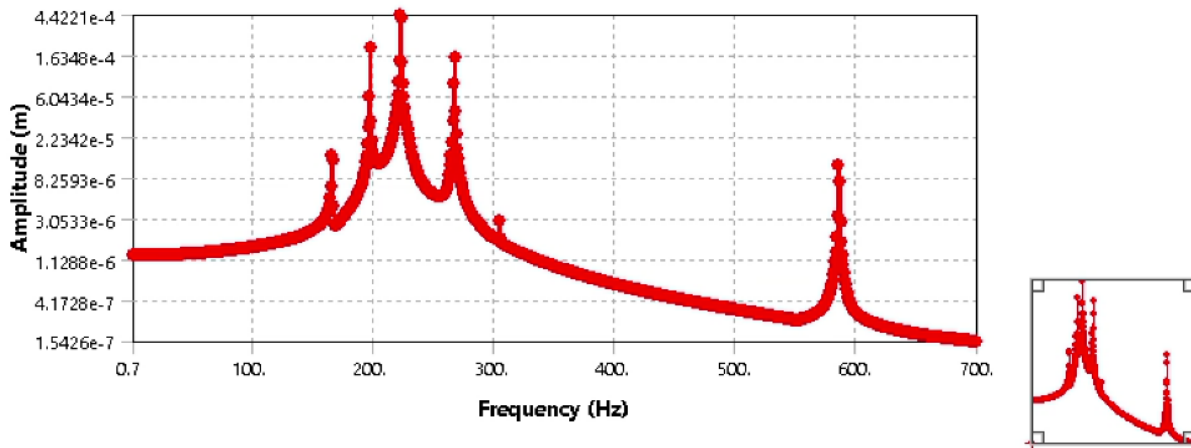


Figure 29. Frequency response deformation result for a coefficient of friction of 0.35

The graph plots the amplitude in meters against the frequency in Hertz. The solution intervals were set to 1000, in order to obtain smooth plots, and ensure that there were no overlooked frequency peaks. For example, the fifth mode has a small response and could have been overlooked in models with small solution intervals. In this analysis, there are six peaks in the data, which align with the modal analysis performed earlier. The added benefit of high sampling is having enough data points when the data was exported to Microsoft Excel for data analysis. Here it can be seen that the highest amplitude occurred in the third mode, represented by the third peak on the graph. This is about 222 Hz, and the deformation was about  $4.4 \times 10^{-4}$  meters or about .44 millimeters. The ideal absorber would be the absorber that produces the smallest deformation across the six modes.

## 9 Results

### 9.1 MATLAB Surface Roughness Results

To develop a relationship between the surface roughness and friction coefficient, many simulations had to be run. With the assumptions and conclusions made, a series of analyses were run using varying input standard deviations. In these analyses, two 10 mm wide square, rough surfaces were generated in MATLAB using *Surfaces.m*. They were then tested in *Friction\_Test\_Int\_Evolve.m* to generate a plot of the coefficient of friction as a function of the applied normal force (ranging from 0 to 1000 N). The average coefficient of friction across the range was recorded and 6 replications were performed for each input sigma tested. The results from these analyses are presented below in Table 10.

Table 10. Results from calculating the coefficient of friction for variable input surface height standard deviations (6 replications per result)

Surface Characteristics			Coefficient of Friction Results		
Sigma ( $\sigma$ ) [ $\mu\text{m}$ ]	Roughness ( $Ra$ ) [ $\mu\text{m}$ ]	Root Mean Squared ( $Rms$ ) [ $\mu\text{m}$ ]	Avg. Coefficient of Friction ( $\mu$ ) [ ]	Sample Standard Deviation ( $\sigma_{\mu}$ ) [ ]	Coefficient of Variation ( $CV_{\mu}$ ) [%]
0.100	0.295	0.100	0.058	0.012	20.8%
0.250	0.737	0.250	0.165	0.017	10.3%
0.500	1.474	0.500	0.250	0.033	13.2%
0.750	2.211	0.750	0.282	0.029	10.4%
1.000	2.948	1.000	0.335	0.049	14.8%
1.250	3.685	1.250	0.388	0.058	14.9%
1.500	4.422	1.500	0.394	0.058	14.7%
2.000	5.896	2.000	0.466	0.061	13.2%
3.000	8.844	3.000	0.498	0.082	16.4%
4.000	11.792	4.000	0.528	0.134	25.3%
5.000	14.740	5.000	0.550	0.117	21.2%

In Table 10, the roughness and root mean square parameters are calculated using the average line of best fit from Figures 26 and 27. It should be noted there is some expected variability in the true roughness and root mean squared, as evidenced by the variability in Figures 26 and 27. However, it remains an appropriate approximation since the surfaces are randomly generated.

These results are presented graphically in Figure 30. In the first three plots, which relate the coefficient of friction to the input sigma, surface roughness, and root mean squared value, a logarithmic trend line fits the data with an  $R^2$  value of 0.9912. This is exceptional considering the inherent randomness of the surface generation and the assumptions made throughout the development of this model. This  $R^2$  value indicates that this modified Hertz contact model created reliably outputs a coefficient of friction consistent with the logarithmic function. Of note, each leading term has the same coefficient. This is due to how  $Ra$  and  $Rms$  are equivalent to  $\sigma$  scaled by some constant multiple. The variation in this is reflected in the second term in these equations.

The last plot in Figure 30 is a graph of the coefficient of variation for the friction coefficient as a function of the input sigma. There is a loosely increasing trend and the lowest values are within the range of sigma = 0.25 – 2  $\mu\text{m}$  or an equivalent  $Ra$  value of 0.73 – 5.9  $\mu\text{m}$ . For context, this roughness is equivalent to approximately the 30 - 310 sandpaper grit range [30]. This is a reasonable roughness for this model to anticipate as it can be readily achievable using normal mechanical processes such as sanding or abrasive blasting. The corresponding coefficients of friction in this range are 0.165 – 0.466, which is also reasonable and the expected outcome for these surfaces.



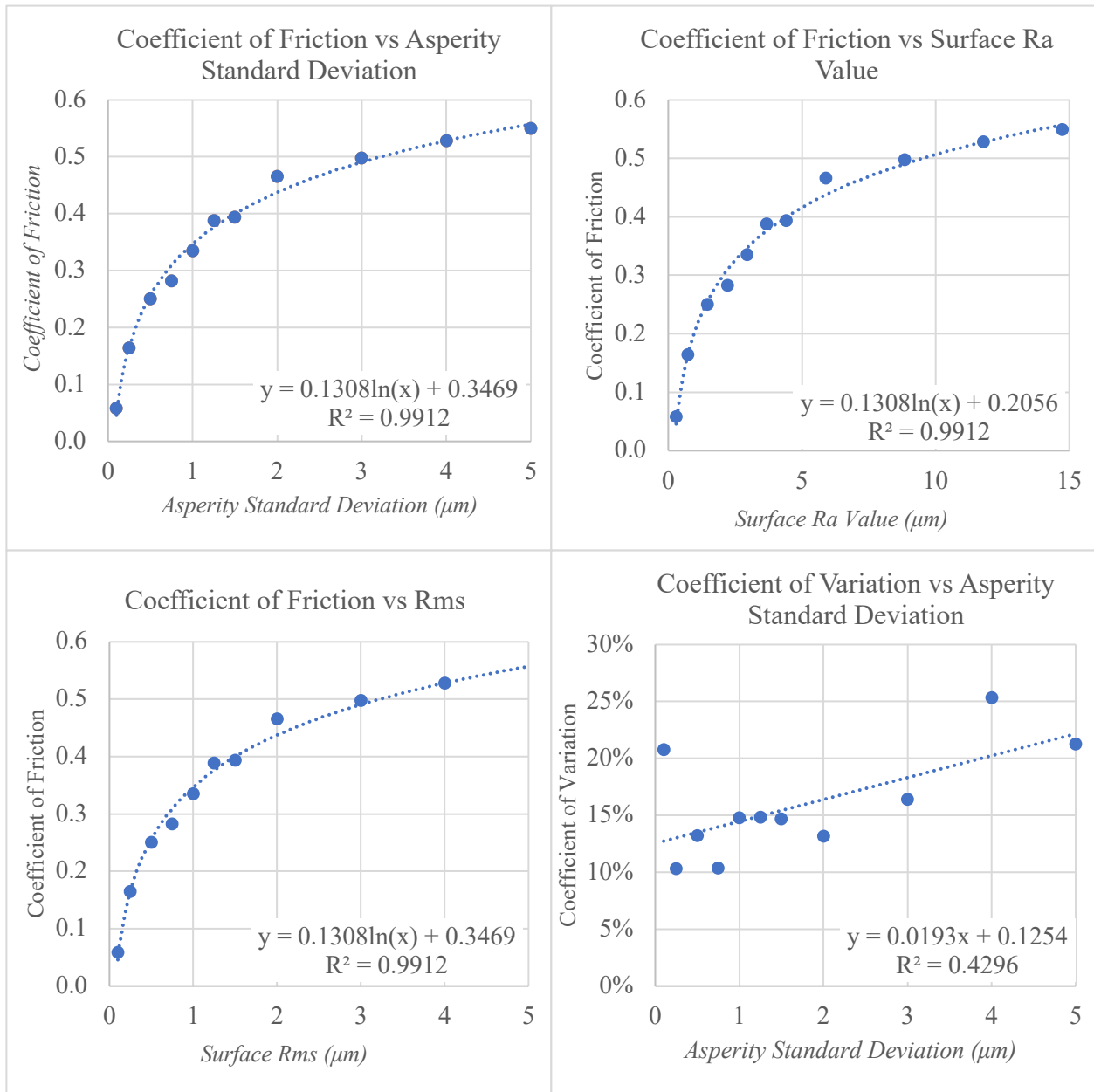


Figure 30. Resulting plots from simulating 10 mm wide surfaces in contact under variable incrementally increasing loads

The results from Figure 30 then enable one to choose a desired coefficient of friction and then find the required input sigma, roughness, or root mean squared value. The equations to convert between the coefficient of friction and these three parameters is a simple algebraic manipulation of the trend line functions provided in the first three plots of Figure 30. These are provided in Equations 16, 17, and 18, for convenience.

$$\sigma = 0.0721e^{7.5803\mu} \quad [\mu m] \quad (16)$$

$$Ra = 0.2127e^{7.5803\mu} \quad [\mu m] \quad (17)$$

$$Rms = 0.0721e^{7.5803\mu} \quad [\mu m] \quad (18)$$



In these equations, the variable  $\mu$  refers to the coefficient of friction desired. Of interest here, each equation presented has the same exponent. This is, as previously pointed out, due to how Ra and Rms are constant multiples of  $\sigma$ . The variation of this constant multiple is reflected in the coefficient of the leading term. Note, Equation 16 is equivalent to Equation 18. This is because there was an exact correlation between sigma and the Rms value. However, this is not necessarily the case, so they are provided as separate equations. Should the mean be anything but 0, Equations 16 and 18 will not be equivalent.

## **9.2 ANSYS Simulation Results**

To further understand how the absorbers are reacting at their natural frequencies, a frequency response deformation plot was created in a harmonic analysis on ANSYS. The frequency response deformation plot was scoped to the absorbers so that only their response would be plotted as the frequency was swept from 0 to 700 Hz. This number was chosen to allow for an overshoot past the highest mode found of 587.15 Hz. The result was a plot of frequency in Hz and the amplitude of the absorber response in meters. Initially, this data was extracted and entered into excel for each coefficient of friction. The plots were difficult to interpret raw and unconventional for frequency response plots. In order to align with convention, the data was plotted with a logarithmic scale, which has the benefit of a more easily comparable set of data. Plotted in Figure 31 is each of the frequency response deformations for the range of coefficients of friction from 0.15 to 0.45, in increments of 0.05. This was an adequate range of coefficients and a sufficient number to determine the most feasible option.

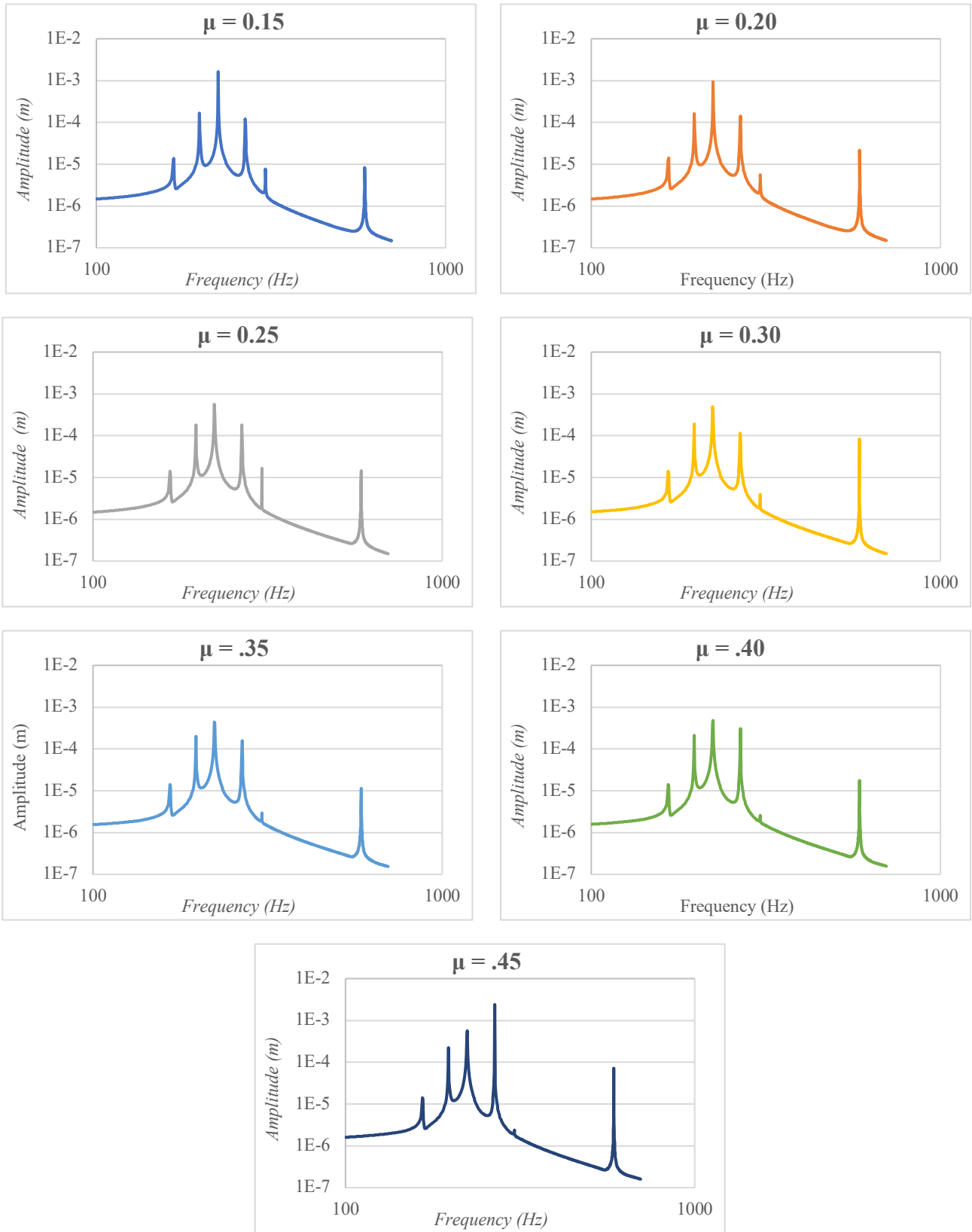


Figure 31. Frequency response deformation of the selected coefficients of friction

From the initial comparison of these graphs, the coefficients on either end of the spectrum seemed to have the highest response, these coefficients are 0.15 and 0.45. This would, in turn, result in more vibrations throughout the system and lead to potential inefficiencies or fatigue failure at these frequencies. The coefficients that had smaller amplitudes were the coefficients in the middle of the range, 0.25, 0.3, and 0.35. For further comparison, these results were plotted against each other, represented in Figure 32.

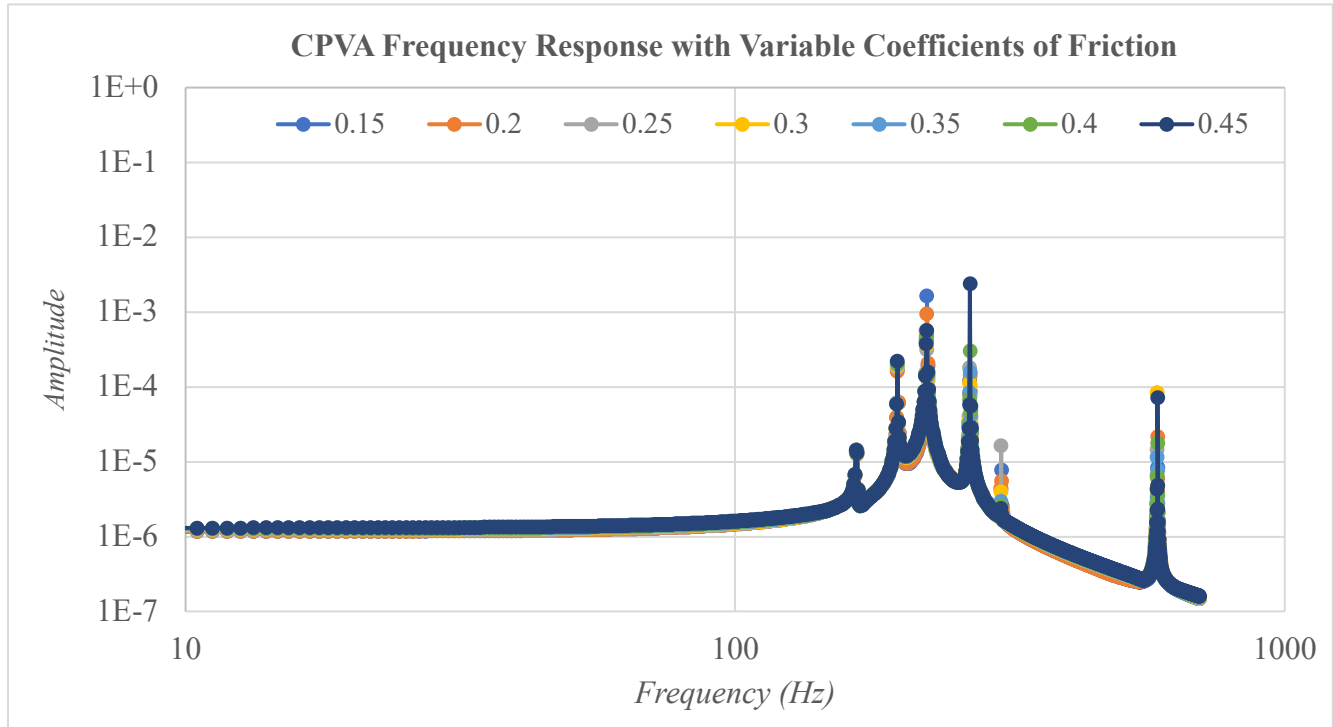


Figure 32. Frequency response of CPVA for coefficients of friction from 0.15 to 0.45

Further analysis of Figure 32 was needed. The peaks were examined with an increased selective scale so that the different coefficient's responses could directly be seen at each peak. Each coefficient appeared to have a certain peak or mode where it had the highest response amongst the coefficients of friction sampled. The most frequent highest responses on the modes came from coefficients of 0.45 and 0.15, followed closely by 0.20 and 0.40. The coefficient with the highest response was different for each mode, but 0.35 was never a peak. This aligns with our initial interpretation of the data, hypothesizing that the most feasible coefficient would be one in the middle range. Further dissection of the peaks is represented in Table 11.

Table 11. First 6 mode peaks calculated for coefficients of friction from 0.15 to 0.45 (higher color saturation corresponds with larger magnitude)

$\mu$	First 6 Modes of the CPVA Frequency Responses						Average
	1 166.3 Hz	2 197.4 Hz	3 223.1 Hz	4 267.1 Hz	5 304.7 Hz	6 586.4 Hz	
0.15	1.38E-05	1.67E-04	1.64E-03	1.20E-04	7.68E-06	8.41E-06	3.26E-04
0.20	1.43E-05	1.61E-04	9.39E-04	1.42E-04	5.51E-06	2.17E-05	2.14E-04
0.25	1.42E-05	1.79E-04	5.63E-04	1.83E-04	1.65E-05	1.46E-05	1.62E-04
0.30	1.42E-05	1.89E-04	4.93E-04	1.14E-04	3.95E-06	8.40E-05	1.50E-04
0.35	1.42E-05	1.99E-04	4.42E-04	1.58E-04	2.95E-06	1.14E-05	1.38E-04
0.40	1.42E-05	2.09E-04	4.80E-04	3.05E-04	2.58E-06	1.76E-05	1.71E-04
0.45	1.42E-05	2.21E-04	5.63E-04	2.40E-03	2.39E-06	7.17E-05	5.45E-04

From this table, it is evident there are two modes where a large response is generated: the third and fourth modes. In the third mode,  $\mu = 0.15$  and  $0.20$  result in relatively large peaks. In the fourth mode,  $\mu = 0.45$  results in the largest response peak calculated. Due to this, the coefficients of friction of  $0.15$ ,  $0.20$ , and  $0.45$  are not being considered. To compare the remaining results, the average response of the first 6 modes was taken into consideration and the smallest was chosen. Ultimately, a coefficient of friction of  $0.35$  resulted in the smallest response magnitudes overall and is the design choice. Though, it should be noted that the range of  $0.25$ - $0.35$  is similar in performance and would also be viable.

Utilizing equations 17, and 18, the Ra and Rms values to achieve are  $Ra = 3.020 \mu\text{m}$  and  $Rms = 1.024 \mu\text{m}$ . This is the equivalent roughness of approximately 120 grit sandpaper.

### 9.3 Design Results

From the normal force assemblies considered, the MATLAB analysis, and the subsequent ANSYS analysis, it was determined that the best configuration to pursue is to: modify the normal force in the existing system by torquing the connecting bolts and applying purple Loctite to ensure no vibration loosening; maintain the same absorber shape, mass, and material; and to create a surface roughness of  $Ra = 3.020 \mu\text{m}$  to achieve a contact coefficient of friction of  $0.35$ .

This is not necessarily the optimal configuration for the CPVA assembly; however, it is certainly a feasible one to be further analyzed. The work set forth in this project provides a foundation for subsequent work to build off and to improve.

## 10 Cost Analysis

The following tables (Tables 12 and 13) record and estimate the costs incurred or would be required for the completion of this project. Table 12 is a cost ledger of the materials purchased during this project as well as the projected materials for the final assembly. Table 13 provides the estimated costs incurred for labor during this project.

Table 12. Cost analysis ledger of current and estimated costs

Purchased Items Ledger						
Part Name	Part Number	Vendor	Description	Quantity	Unit Cost	Cost
Aluminum Bar	89015K236	McMaster-Carr	Multipurpose 6061 Aluminum Sheet 1/8" Thick, 6" x 12"	2	\$ 16.63	\$ 33.26
Aluminum Plate	8975K68	McMaster-Carr	Multipurpose 6061 Aluminum 1/4" Thick x 2-1/2" Wide, 3 Feet Long	2	\$ 16.44	\$ 32.88
Thumb Screws	91745A192	McMaster-Carr	Stainless Steel Spade-Head Thumb Screw 8-32 Thread Size, 3/8" Long	1	\$ 9.38	\$ 9.38
Screw Tap (8-32)	26955A33	McMaster-Carr	General Purpose Tap Plug Chamfer, Uncoated High-Speed Steel, 8-32 Thread Size	1	\$ 4.61	\$ 4.61
Drill Bit (Gauge 29)	2901A203	McMaster-Carr	Black-Oxide High-Speed Steel Drill Bit Wire Gauge 29, 2-7/8" Overall Length	1	\$ 1.86	\$ 1.86
Glass Abrasive Media	3398K15	McMaster-Carr	Abrasive Blasting Media Multipurpose, Glass Bead, 170-325 Mesh Size, 10 lbs.	2	\$ 21.32	\$ 42.64
Sandblaster Kit	N/A	Amazon	Sand Blaster, Sand Blaster Gun Kit, Sandblaster with 2 Replaceable Tips & 1/4" Quick Connect, and Safety Goggles	1	\$ 39.56	\$ 39.56
Sandblasting Gloves	N/A	Amazon	Jewboer 23.6" Rubber Sandblasting Sandblaster Gloves for Sandblast Cabinets	1	\$ 17.99	\$ 17.99
Sandpaper	N/A	Amazon	120 To 3000 Assorted Grit Sandpaper for Wood Furniture Finishing, Metal Sanding and Automotive Polishing	1	\$ 7.99	\$ 7.99
					<b>Total</b>	<b>\$190.17</b>

Final Design Proposed Ledger						
Part Name	Part Number	Vendor	Description	Quantity	Unit Cost	Cost
Aluminum Bar	8975K87	McMaster-Carr	Multipurpose 6061 Aluminum 1/4" Thick x 3" Wide x 3' Long	1	\$ 19.68	\$ 19.68
Threadlocker	1810A27	McMaster-Carr	Adjustable Threadlocker, Loctite® 222, 0.3 4 oz. Bottle	1	\$ 15.35	\$ 15.35
					<b>Total</b>	<b>\$ 35.03</b>

*Table 13. Estimated labor costs incurred during project development*

<b>Task</b>	<b>Hourly Cost</b>	<b>Estimated Hours</b>	<b>Total Cost</b>
<b>Management</b>	\$ 36.00	60	\$ 2,160.00
<b>Design</b>	\$ 30.00	270	\$ 8,100.00
<b>Manufacturing</b>	\$ 24.00	4	\$ 96.00
<b>Assembly</b>	\$ 15.00	2	\$ 30.00
<b>Documentation</b>	\$ 30.00	40	\$ 1,200.00
		<b>Total</b>	<b>\$ 11,586.00</b>

In total, combining the cost from Table 12, and the labor costs incurred from Table 13, the total cost of developing this project is \$11,811.20. Though, as it is with most engineering projects, most of this cost comes from the labor. The project has remained within the materials budget as specified by the engineering department.

## **11 Summary and Conclusions**

The main objective of this capstone project was achieved in several steps. The starting point of this project was to learn about and work to understand the effects of friction between two surfaces in a CPVA system. The team worked with both experimental and analytical approaches for finding an adequate coefficient of friction for the predesigned CPVA. These approaches were tasked to measure and control the frictional forces exhibited during operation. This then would enable further research into how the dynamics of the system would be impacted by the friction observed.

Part of this project was to develop a system that could modify the frictional force observed in the CPVA. 5 designs were developed with varying feasibilities and complexities. The best design of those ideated was simply torqueing the existing bolts to the desired preload. The benefits of this design option include simplicity, frugality, and safety. Though the other design options may be appropriate in a different situation, with the design constraints of this project, torqueing the bolts proved ideal.

The unpredicted restrictions of in person laboratory time for experimental testing limited the team to mainly analytical models. A sandblaster was acquired before spring break, which allowed the team to produce aluminum coupons with variable surface roughnesses. In its place, random surfaces were generated in MATLAB, and a method of characterizing and measuring the surfaces based on roughness parameter Ra, and the root mean squared Rms, was developed. A relationship between the frictional coefficient and surface roughness was determined and proved to be exceptionally reliable. A range of frictional coefficients was determined to be ideal within the MATLAB model and was selected for further study.

A modal and harmonic response analysis was performed for each of the selected coefficients of friction. The frequency response deformation for each mode was found and was directly compared between the different coefficients of friction. The goal was to dampen the vibrations in the system, so the coefficient that had the overall smallest responses across all modes out of the range of coefficients was chosen. This analysis indicated that 0.35 was the most reasonable coefficient of friction to move forward with.

## 12 Recommendations for Further Study

There are several things that should be investigated further by anyone pursuing this research project in the future. Due to the extreme circumstances caused by the pandemic this semester, it is recommended that future investigations involve the physical testing and observation of the effects of surface friction on the CPVA system. Although the analytical portion of this research is crucial, experimental testing is necessary to fully understand the system's behavior and will lead to more efficient prototypes to be developed. Moving forward, physical testing should be performed when possible, and the results of these friction tests should be compared with the MATLAB analytical models generated in this project. Continuing to sandblast the aluminum coupons with varying grit sizes would allow a thorough comparison of the experimental and analytical results. The coupons with the varying surface roughness generated by the sandblasting should be inspected with a profilometer to determine the average surface roughness coefficient (Ra). The friction testing proposed in this report should be performed with these coupons, and the resultant coefficients of friction should be compared to those generated by the analytical model.

Furthermore, the impact on the performance of the full CPVA assembly by the effects of friction should be further pursued. Similar to the comparison between physical testing and analytical modeling intended by this semester's research, the physical testing of the CPVA assembly with the modified absorbers should be compared to the computational analysis. The preliminary ANSYS simulation results are provided in this report, however, this should be investigated in more detail.

The reduction of torsional vibrations can be further investigated using modal analysis. If the laboratory space is available, experimentation modeling the system in COMSOL or Femap is encouraged, which may be better suited for modeling the nonlinear characteristics of frictional factors. A free response analysis with no torque or excitations on the rigid body of the CPVA can be performed, and the natural modes of the CPVA can be obtained by knowing the stiffness, mass, and geometric orientation of the structure. Once these natural modes are obtained, they can be used in a harmonic analysis. Future research in this unfamiliar territory should include understanding how frictional hysteresis and the damping effects on the system can be controlled with the methods proposed in this report to reduce vibrational effects.

Regarding the analytical model developed, there are several shortcomings that were not addressed in its current form. The foremost of these is the neglect of a time-dependent, evolving model of contact. In real frictional interactions, the deflection, deforming, and restitutive forces are dynamic. The model developed exists as quasi-static and does not capture the time evolution in any capacity. This ultimately was due to the time constraints incurred in this project. In future developments, the first effort should be made to include an evolving contact system. Some infrastructures for this exist in the code but is not being implemented.

There should also be a more accurate contact model utilized. The one developed is a decent approximation but makes some sweeping generalizations that may not be appropriate in a more rigorous model. Many contact theories exist in varying levels of complexity and accuracy. The contact model used in this project compromised the complexity of more advanced contact models for the actual functioning of the code. In future works, a more rigorous contact model could seamlessly be integrated into the current code.

There are likely computational inefficiencies in the current iteration of the code as well. Though these are inevitable, efforts would be well spent to refine the current code into a speedier and less computationally intensive version.

## **13 Project Postmortem**

### **13.1 Teamwork**

Retrospectively, from the standpoint of both the capstone advisor and all the team members, everyone in this group has a strong and unique set of skills. The team's ability to openly communicate with one another has resulted in substantiated experimental and analytical conclusions.

The main factors that allowed the group to remain on task is dedication and reliability. Since there was always one weekly meeting with Professor Inalpolat, along with anywhere between 1 and 3 team weekly meetings, it was hard to fall behind. Each group member worked to attend every meeting. Each meeting was thoroughly annotated so there was no fallout if anyone had to miss a meeting. The OneDrive folder was also a reliable and consistent source for progress updates that allowed the group to remain up to date on each individual team member's progress so there was no overlap or repetition when it came to getting ahead of the planned tasks of the week.

The structure of each meeting consisted of revisiting the overarching project goals and assuring that all the intermediate steps planned for the week were being completed. The goal of the project was revisited at the beginning of every meeting as design decisions and cost analyses were completed. This meeting strategy allowed us to adapt to new project and design constraints as they appeared. Revisiting the project objectives allowed us to modify things relatively quickly when the unexpected changes in the academic calendar occurred.

The communication platforms utilized from January to the beginning of March were mainly email, text message, and in person meetings. After the change in academic setting that occurred mid-March, there was an adjustment period for students and faculty to transition to online learning with the main mode of communication being text message and Zoom. Moving forward, although in person meetings were no longer feasible, the team dynamic remained unchanged. A strong foundation was built at the beginning of the project which eliminated most, if not all, collaboration, communication, and work distribution obstacles that arose.

### **13.2 Technical Communication skills**

There were a few preliminary group meetings with the team members and the capstone advisor. Prior to winter break, there were four recommended readings for the team intended to steer us in the right direction and further our understanding of the CPVA built by the previous capstone group. Completing these readings assured that when the project began in January, everyone was on the same page and had the same technical understanding of the system.

Shortly after the semester began, a meeting with one of Professor Inalpolat's PhD students, Bahadir, was arranged. The meeting took place in the Acoustics lab and Bahadir explained his knowledge of how the testing apparatus operated, what materials were used, and gave us spare parts and showed us which resources were at our disposal. Bahadir also emailed us the previous capstone group's CAD files for the CPVA, along with their final report so we could understand the project in its entirety and what had been completed.

After these initial steps were completed and each person had a more concrete understanding of CPVA's and the project objective, technical communication and organization as a group could begin. Technical communication did not differ significantly from the team's general communication skills. Some of the most important aspects of technical communication were documentation, organization, and task distribution.



The OneDrive folder initially consisted of just the research papers professor Inalpolat had encouraged us to read before starting the project. Shortly after the spring semester began, CAD files from Bahadir were added to the folder, along with documents containing notes from the multiple weekly meetings along with the weekly presentation. We quickly realized the best way to keep track of the work being done was to create a new folder for each week in the OneDrive. This allowed us to easily find information during group meetings and maintain organization and fluid communication throughout the semester.

### 13.3 Project Schedule

The initial project description was relatively vague because it was more analytical than experimental. In the initial stages of developing a reasonable project schedule, there were a handful of meetings with professor Inalpolat where the project objectives and goals were revisited. A solid outline for the project was created and was referred to and updated in all the weekly meetings.

A major change that occurred during this project is the switch from experimental testing to completely simulation-based testing.

Luckily, before spring break, Aluminum 6061 coupon samples were cut in the Makerspace and there was ample time to work with a monitor to figure out how to use a CNC milling machine to find the center of the side of each Aluminum specimen. This process was more complex than anticipated, so it was incredibly beneficial that the team was proactive when it came to ordering material. This allowed the team to spend time working to acquire a sandblaster. A refurbished sandblaster was acquired for free from one of the lab spaces in the basement of Ball Hall. We successfully sandblasted 9 Aluminum coupons along with a tenth sample specimen that was used as a practice to get a feel for what variables were able to be controlled.

The next stage of the design process was planned to consist of getting trained or finding someone who was already trained on the surface roughness testing apparatus in the baseball lab. Due to the COVID – 19 outbreaks leading to a global pandemic, all courses were moved to be online for the foreseeable future and campus including labs and such were closed and off limits to both students and faculty.

The project goals were being met accordingly. Since we had acquired the sandblaster before spring break, we were somewhat ahead of schedule because that eliminated the process of either purchasing a sandblaster or looking into other chemical or mechanical ways to modify surface roughness. The materials needed for the testing procedure were already ordered, sandblasting some of the specimens, and had a solid working plan moving forward. It was disappointing to no longer be able to do any hands-on experimental tests in the lab, but under the circumstances, we were incredibly happy with the progress that had been made.

The planned tests in the baseball lab were now going to be simulation based. We moved forward with generating random surface profiles in MATLAB to obtain a coefficient of friction from those surfaces to then evaluate in ANSYS. These simulations were completed as oppose to sandblasting multiple aluminum coupons with different grit sizes and physically testing those samples in the baseball lab to measure the coefficient of friction.

Although some monetary assets were lost with the purchasing of materials, in the long run, the materials obtained can be used for further studies and were not wasted in the least bit. Also, the largest sum of money would be spent on training or getting access to the profilometer to measure the resulting surface roughnesses of the aluminum coupons. The cost of having access to the profilometer is hundreds of dollars an hour. The simulations may take more time and be less accurate because we do not have the ability to physically alter the surface roughness of the coupons in the test setup. That error can be accounted for by being able to produce more iterations of surface roughnesses and run more simulations

which would take time as opposed to doing that with experimental testing which would take time and be a large monetary sink.

### **13.4 Ethical Standards**

All the software used for modeling and computational analysis of the project was used under the University's licenses available to students and accessible to students through the UMass Lowell virtual desktops or student licenses available to download. The articles and resources used for research for the project were accessed with permission, on public domains or on the UMass Lowell Database, and no sources were accessed illegally or without permission. All the resources used were referenced properly within this report, all information taken from other sources to support design decisions were cited. Proper consideration was given to the intellectual property of all team members, advisors, and university staff. All project supplies, sources, and developments were documented and collected in an accessible and easy to use manner to assist any further work and development on this project by any team or staff moving forward.

### **13.5 Industrial/Commercial Standards**

The team referenced multiple industrial standards throughout this project, structuring procedures and decisions around existing ASTM standards. Following standardized procedures helps create a repeatable process for procedures that generate more reliable and credible results and will help teams in the future that will continue this research capstone design project.

Specifically, this project referenced ASTM D2651-011, the Standard Guide for Preparation of Metal Surfaces under the Aluminum Alloys subsection and ASTM D1730 – 09, Standard Practices for Preparation of Aluminum and Aluminum-Alloy Surfaces for Painting as a guideline in choosing and deciding on methods of surface roughness modification for the coupons.

The team also referenced ASTM D-2674, ASTM D-3933, and ASTM G150-18 in researching chemical and electrochemical surface preparation for aluminum as alternatives compared to mechanical surface roughness modification.

### **13.6 Professional Societies, Codes, and Standards**

ASTM D2651-011 and ASTM D1730 – 09 were followed to prepare the aluminum surface to be modified

ASTM D-2674, ASTM D-3933, and ASTM G150-18 were followed while the potential of chemical surface alteration was still being considered

ASTM D1894 standard for friction testing was followed when the friction test was designed.

### **13.7 Safety**

Through the entire timeline of the project the safety of all members, faculty, and persons near the project were held as a priority. All meeting, experiments, and manufacturing were strictly performed under the safety guidelines of the facility they were conducted in. All group members were properly trained and operated under the supervision of certified individuals when required to do so. Prior to using any machines in the Makerspace members were trained, and under direct supervision during the whole process.

### **13.8 Environmental Impact**

In recent years, the trend in the automotive market has been to maximize efficiency. One way to reduce the weight of the vehicle by reducing the size of the engine. This lightening typically consists of reducing the number of cylinders and utilizing less material overall. However, this reduction in cylinders and mass results in the increased magnitude and propagation of vibrations throughout the vehicle. These high frequency vibrations can significantly harm the car's output and reliability. So, in order to keep pursuing fuel efficient automobiles, there must be a focused effort on damping these vibrations.

The CPVA in our study is specifically designed considering an automobile. Hence, our efforts in this project contribute to the furthering of the CPVA which in turn will help advance the fuel-efficient cause. Increased fuel efficiency results in less pollutants being released per mile driven. In turn, this capstone aids in the effort to reduce pollution.

### **13.9 Societal/Social Impact**

Improving the dampening performance of the CPVA increases the efficiency of the vehicles that use it, conserving fuel, saving money, and providing a smoother and more comfortable ride. This will have a positive societal impact by allowing car companies to produce and market more fuel efficient and environmentally conscious luxury vehicles. The improvement to the vehicle's performance offered by the CPVA will increase customer satisfaction by offering more efficient performance and reduction of fuel cost.

### **13.10 Multi-Disciplinary Issues**

In the first half of the semester, the team reached out and was in communication with various departments on campus and external companies in the area. The team reached out to local companies concerning surface preparation methods, before settling on sandblasting in-house and communicating with the laboratory managers both in mechanical and plastics engineering for the proper tools and equipment. Once the sandblasting method was settled on, the team was in contact with the various labs on campus and external companies inquiring about access to profilometry or other methods to analyze the surface roughness of the sandblasted coupons. Unfortunately, the circumstances this semester cut this communication short after spring break.

## 14 Bibliography

- [1] A. Wedin, "Education of Vibrations in Engines Using Centrifugal Pendulum Vibration Absorbers," Chalmers University of Technology, Goteborg, 2011.
- [2] A. Jain, "Experimental Measurement of the Response of Centrifugal Pendulum Vibration Absorbers," University of Michigan, 2013.
- [3] B. Bhushan, N. Axen, S. Hogmaker and S. Jacobson, "Friction and Wear Measurement Techniques," in *Modern Tribology Handbook*, 2000.
- [4] S. Hulikal, N. Lapusta and K. Bhattacharya, "Static and sliding contact of rough surfaces: effect of asperity-scale properties and long-range elastic interaction," Department of Mechanical and Civil Engineering, California Institute of Technology, Pasadena, CA.
- [5] G. Adams and M. Nosonovsky, "Contact modeling - forces," *Tribology International*, vol. 33, pp. 431-442, 2000.
- [6] B. Bushan, "Contact mechanics of rough surfaces in tribology: multiple asperity contact," *Tribology Letters*, no. 4, pp. 1-35, 1998.
- [7] ASTM International, *Standard Test Method for Static and Kinetic Coefficients of Friction of Plastic Film and Sheeting*, West Conshohocken, PA: ASTM International.
- [8] J. T. Black and R. A. Kohser, *Degarmo's Materials and Processes in Manufacturing*, 2012: John Wiley & Sons, Inc..
- [9] Gabrian, "Mechanical Finishes for Aluminum Extrusions: What Are the Options?," Gabrian, 11 October 2019. [Online]. Available: [www.gabrian.com/mechanical-finishes-for-aluminum-extrusions/](http://www.gabrian.com/mechanical-finishes-for-aluminum-extrusions/).
- [10] P. Harmon, "Sandblasting Aluminum- A Complete Guide.," 27 February 2018. [Online]. Available: [pittsburghsprayequip.com/blogs/pittsburgh-spray-equipment-company/sandblasting-aluminum-a-complete-guide](http://pittsburghsprayequip.com/blogs/pittsburgh-spray-equipment-company/sandblasting-aluminum-a-complete-guide).
- [11] MISUMI, "Surface Finishing Tutorial: Technical Tutorial," MISUMI, 2020. [Online]. Available: [www.misumi-techcentral.com/tt/en/surface/2012/03/119-surface-adjustments---brushed-finish.html](http://www.misumi-techcentral.com/tt/en/surface/2012/03/119-surface-adjustments---brushed-finish.html).
- [12] Clinton Aluminum, "Grinding Aluminum Sheets and Plates," Clinton Aluminum, 8 July 2018. [Online]. Available: [www.clintonaluminum.com/grinding-aluminum-sheets-and-plates/](http://www.clintonaluminum.com/grinding-aluminum-sheets-and-plates/).
- [13] Wagner, "Mechanical Finishes - Resources - The Wagner Companies.," Wagner, 2020. [Online]. Available: [wagnercompanies.com/resources/finishes/](http://wagnercompanies.com/resources/finishes/).

- [14] V. Krottner, "How to Optically Polish Aluminum," *MoldMaking Technology*, 2020. [Online]. Available: [www.moldmakingtechnology.com/articles/how-to-optically-polish-aluminum](http://www.moldmakingtechnology.com/articles/how-to-optically-polish-aluminum).
- [15] Occupational Safety and Health Administration, "Protecting Workers from the Hazards of Abrasive Blasting Materials," Occupational Safety and Health Administration, September 2014. [Online]. Available: [www.osha.gov/Publications/OSHA3697.pdf](http://www.osha.gov/Publications/OSHA3697.pdf).
- [16] Occupational Safety and Health Administration, "Hazards Associated with Aluminum Grinding," Occupational Safety and Health Administration, 2020. [Online]. Available: [www.osha.gov/laws-regs/standardinterpretations/2009-10-08](http://www.osha.gov/laws-regs/standardinterpretations/2009-10-08).
- [17] Goddard Space Flight Center, "Process for Polishing Bare Aluminum to High Optical Quality," Goddard Space Flight Center, 29 December 2017. [Online]. Available: [www.techbriefs.com/component/content/article/ntb/tech-briefs/manufacturing-and-prototyping/1831](http://www.techbriefs.com/component/content/article/ntb/tech-briefs/manufacturing-and-prototyping/1831).
- [18] 3M, "Surface Preparation and Pretreatment for Structural Adhesives," October 2018. [Online]. Available: [multimedia.3m.com/mws/media/933332O/surface-prep-pretreatment-for-structural-adhesive-techbulletin.pdf](http://multimedia.3m.com/mws/media/933332O/surface-prep-pretreatment-for-structural-adhesive-techbulletin.pdf).
- [19] A. N. Rider, "Surface Treatment and Repair Bonding," Butterworth-Heinemann, December 8 2017. [Online]. Available: [www.sciencedirect.com/science/article/pii/B9780081005408000078](http://www.sciencedirect.com/science/article/pii/B9780081005408000078).
- [20] S. a. C. E. Ebnesajjad, "Surface Treatment of Materials for Adhesion Bonding," Grand Rapids: William Andrew, 2006.
- [21] J. & M. S. & M. N. Kumar, "Study of Electro Chemical Machining Etching Effect on Surface Roughness and Variation with Chemical Etching Process," 2019.
- [22] WPI, "Adhesive Technology: Surface Preparation Techniques on Aluminum," [Online]. Available: [web.wpi.edu/Pubs/E-project/Available/E-project-031609-134903/unrestricted/Henkel\\_Final\\_MQP.pdf](http://web.wpi.edu/Pubs/E-project/Available/E-project-031609-134903/unrestricted/Henkel_Final_MQP.pdf). [Accessed 2020].
- [23] P. & E. M. & K. A. Horodek, "Studies of stainless steel exposed to sandblasting," 2015.
- [24] S. & G. A. & M. H. & R. A. & G. S. Zeighami, "Effect of Sandblasting Angle and Distance on Biaxial Flexural Strength of Zirconia-based Ceramics," *The Journal of Contemporary Dental Practice*, vol. 18, pp. 443-447, 2017.
- [25] S. G. Shina, *Six Sigma for Electronics Design and Manufacturing*, McGraw-Hill, 2002.
- [26] R. G. Budynas and K. J. Nisbett, *Shingley's Mechanical Engineering Design Tenth Edition*, vol. Tenth Edition, New York: McGraw-Hill Education, 2015.
- [27] ANSYS, Inc., "WS 01.1: Flywheel," ANSYS, Inc., 2019.

- [28] P. Kassebaum, "MathWorks Blogs," The MathWorks Inc., 20 June 2013. [Online]. Available: <https://blogs.mathworks.com/community/2013/06/20/paul-prints-the-l-shaped-membrane/#0d2c8d8b-352f-4b12-a0ba-5b5922a8795e>. [Accessed 2020].
- [29] S. C. Chapra, Applied Numerical Methods with MATLAB for Engineers and Scientists, McGraw Hill Education, 2016.
- [30] MicroGroup, "Grit Finish and Estimated RMS and Ra Values," [Online]. Available: <https://www.microgroup.com/wp-content/uploads/Grit-Finish-and-Estimated-RMS-and-Ra-Values.pdf>. [Accessed May 2020].

# Appendix A

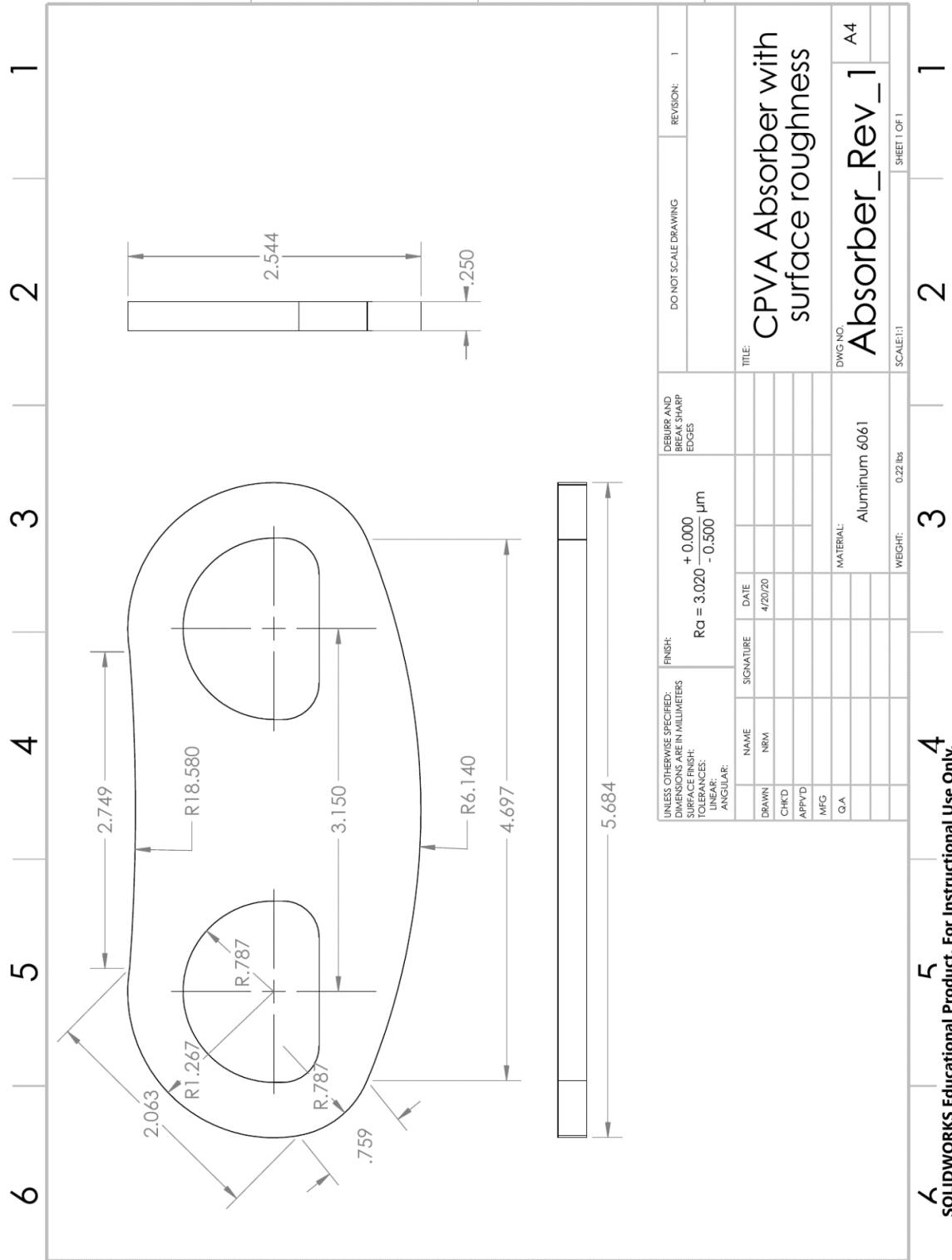


Figure A1 Final Design of CPVA Rotor

# Appendix B

<i>Week</i>	1	2	3	4	5	6	7	8	9	10	11	12	13	14	15	16
<i>Dates</i>	19-Jan	26-Jan	2-Feb	9-Feb	16-Feb	23-Feb	1-Mar	8-Mar	15-Mar	22-Mar	29-Mar	5-Apr	12-Apr	19-Apr	26-Apr	3-May
<i>ME Department Capstone Kickoff</i>	1															
<i>Team Forms</i>	1															
<i>Review and Discuss Topic</i>	1															
<i>Establish Requirements and Deliverables</i>	1															
<i>Project Proposal (Prepare and Present)</i>		1														
<i>Capstone Project Questionnaire</i>			2													
<i>Background Literature Review</i>			1													
<i>Friction Test Preperation</i>			1	1												
<i>Friction Test</i>			1	1	1											
<i>Preliminary Design</i>			1	1	1											
<i>Bill of Materials</i>				1	1											
<i>Resources Needed</i>				1	1											
<i>Design Report</i>						1										
<i>Prepare Preliminary Design Review</i>						1										
<i>Preliminary Design Review</i>							1									
<i>Order Materials/Request Resources</i>							1	1	2							
<i>Design Fabrication/Assembly</i>									1	1	1					
<i>Prepare Capstone Report</i>												1	1			
<i>Final Capstone Report and Presentation</i>														2		
<i>Capstone Presentation</i>																2

Figure B1. Initial Project Gantt Chart



Post Project Gantt Chart																		
Task	1	2	3	4	5	6	7	8	9	10	11	12	13	14	15	16	Phase	
	19-Jan	26-Jan	2-Feb	9-Feb	16-Feb	23-Feb	1-Mar	8-Mar	15-Mar	22-Mar	29-Mar	5-Apr	12-Apr	19-Apr	26-Apr	3-May		
<i>Establish Requirements and Deliverables</i>								S P R I N G  B R E A K									Preplanning and Organization	
<i>Project Proposal</i>																		
<i>Background Literature Review</i>																		
<i>Determine Best Mode to Generate Artificial Friction</i>																		Design and Progress in Friction Test
<i>Source Friction Test</i>																		
<i>Design Friction Test</i>																		
<i>Order and Manufacture Coupons</i>																		
<i>Sandblast</i>																		
<i>Sandblast Aluminum Coupons</i>																		
<i>Generate Probabalistic Surfaces in MATLAB</i>																		Numerical Simulation of Coefficient of Friction
<i>Simulate Contact Between Rough Surfaces to Obtain a Coefficient Of Friction</i>																		
<i>Design Systems to Modify the Clamping Force</i>																		Design of System
<i>Construct Decision Matrix and Decide on Best Design</i>																		
<i>Simulate Best Design</i>																		
<i>Write Capstone Report/ Prepare Presentation</i>																		Final Report and Presentation
<i>Final Capstone Report and Presentation Due</i>																		
<i>Present Project</i>																		

Figure B2 Final Gantt Chart

## Appendix C: All MATLAB Code

### C.1: Surfaces.m

```
function [Ra1,Rms1,Ra2,Rms2,L1,L2,LI1,LI2] =  
Surfaces(sigma1,sigma2,width,title1,title2,resolution,interpolateresol  
ution)  
% This function generates two random surfaces. The surfaces are  
exported to  
%   an array of elements and a 3D (.stl) file. These may be  
interpolated to any  
%   degree of resolution utilizing MATLAB's interp2 command, thereby  
enabling  
%   the use of cubic, linear, nearest, spline, etc. for interpolation.  
Spline  
%   is used in this code for its computational efficiency and its  
accuracy to  
%   a continuous, rough surface.  
%  
% A new folder is made in the current directory to store the .stl  
files of  
%   each generated surface and the histograms of the element  
distributions. This  
%   is done to prevent the cluttering of the current directory.  
%  
%   Simgal and Sigma2 are input in microns  
%   title1 and title2 must be input as '' (a string)  
%   Resolution is default 0.5 <- this specifies the density of  
asperities  
%       per square mm  
%   interpolate is either 'Y' (yes) or 'N' (no)  
%   interpolateresolution is default 2  
interpolate = 'Y'; % In previous iterations, there was a for loop  
considering whether or not to interpolate  
%       in this version, it is default set to  
interpolate  
  
% this code below makes a new folder in the existing directory to  
store  
%   the files generated  
foldname = datetime("now");  
foldname = datestr(foldname,30);  
mkdir(foldname)  
  
%If mu is set to be 0, then the Ra and Rms values are accurate  
%   For any other values of mu, the mean must be subtracted from the  
%   z values, which is easier not to do  
mu = 0;  
  
%This acceptablesigma specifies how many standard deviations are  
acceptable
```

```

%   in the final distribution. It was postulated that having an
unlimited
%   range of the distribution created asperities that were excessively
tall
%   for the surface intended
acceptablesigma = 3;

%Sigma is the standard deviation of the surface roughness
if isempty(signal)
sigma = 0.5; % [microns] : Default Sigma
else
    sigma = signal; % [microns] : Specified Sigma
end

sigma = sigma/1000; % [mm] : Converts to mm

%This specifies the width of the surface generated in mm
%   Note, because of the way MATLAB indexes, the width is Width-1 so
the true
%   width is actually 9 mm when specified to be 10
if isempty(width)
Width = 10; % Default width is 10 mm
else
    Width = width;
end

% Resolution refers to the asperity density per square mm This
provides the step size between
%   successive points. So to convert between Resolution (R) and
asperity
%   density (p), use the formula  $p = R^{-2}$ 
if isempty(resolution)
Resolution = 0.5; % Default resolution is .5.
else
    Resolution = resolution;
end

% This sets up the asperity matrix
i = 1:Resolution:Width;
x = i;
y = i;
[Xa,Ya] = meshgrid(x,y);

% This is the heart of this code. This is what defines the probability
%   distribution. normrnd is a normal distribution. The reason Xa and
Ya
%   are divided by an obscenely large number, is because this ensures
that
%   for each point in the matrix a random point is generated while
having a
%   negligible impact to the average and standard deviation specified
La = normrnd(mu+(Xa/1000000000),sigma+(Ya/10000000000));

```

```

% This code looks for any asperities outside of the acceptable range
% previously specified and sets them equal to zero.
for i = 1:Ya
    for j = 1:Ya
        if abs(La(i,j)) > acceptablesigma*sigma
            La(i,j) = 0;
        end
    end
end

% This is an vestigial remenant of a previous code iteration. The code
is
% set to always interpolate.
L1 = La;
if interpolate == 'Y'
if isempty(interpolateresolution)
    InterpolationResolutionFactor = 2; % Default interpolation
resolution
else
    InterpolationResolutionFactor = interpolateresolution;
end

% Creates the grid for the interpolation matrix
X = 1:(Resolution/InterpolationResolutionFactor):Width;
Y = X;
[X,Y] = meshgrid(X,Y);
L = interp2(Xa,Ya,La,X,Y,'spline');
LI1 = L;
% Methods that can be input into interp2
% cubic, linear, nearest, spline

% This is an vestigial remenant of a previous code iteration.
elseif interpolate == 'N'
    X = Xa;
    Y = Ya;
    L = La;
end

% The following code section calculates the arithmetic mean of the
% asperity heights (Ra) and Root mean squared (Rms)
zmax = max(max(L));
sumz = sum(sum(L));
SizeL = size(L);
Ra = zmax - sumz/(SizeL(1)*(SizeL(2)));
Ra1 = Ra;
Lsq = La.^2;
SumLsq = sum(sum(Lsq));
Rms = sqrt((1/(SizeL(1)*SizeL(2)))*SumLsq);
Rms1 = Rms;

% Set up the histogram to display the asperity height

```

```

% distribution of the surface generated
figure
histogram(L)
xlabel('Height of Elements (mm)');
ylabel('Frequency');
histname = append(title1, '_Histogram.fig');
savefig(histname)
movefile(histname, foldname)
close

% Credit for the following code goes to the person who provided this
code
% on mathworks.com, with some modifications, additions and
subtractions
% for this application
% https://blogs.mathworks.com/community/2013/06/20/paul-prints-the-l-shaped-membrane/#0d2c8d8b-352f-4b12-a0ba-5b5922a8795e
figure
n = Width; % number of partitions in each dimension.
mesh(X,Y,L)
colormap pink;
faces = delaunay(X,Y);
patches = trisurf(faces,X,Y,L);
vertices = get(patches, 'vertices');
facets = vertices';
facets = reshape(facets(:,faces'), 3, 3, []);
edge1 = squeeze(facets(:,2,:) - facets(:,1,:));
edge2 = squeeze(facets(:,3,:) - facets(:,1,:));
normals = edge1([2 3 1],:) .* edge2([3 1 2],:)...
    - edge2([2 3 1],:) .* edge1([3 1 2],:);
normals = bsxfun(@times,...
    normals, 1 ./ sqrt(sum(normals .* normals, 1)));
meanNormal = zeros(3,length(vertices)); % pre-allocate memory.
for k = 1:length(vertices)
    % Find all faces shared by a vertex
    [sharedFaces,~] = find(faces == k);
    % Compute the mean normal of all faces shared by a vertex
    meanNormal(:,k) = mean(normals(:,sharedFaces),2);
end
meanNormal = bsxfun(@times, meanNormal,...
    1 ./ sqrt(sum(meanNormal .* meanNormal, 1)));
shellThickness = 0.05;
underVertices = vertices - shellThickness*meanNormal';
underFaces = delaunay(underVertices(:,1),underVertices(:,2));
trisurf(underFaces,...
    underVertices(:,1),...
    underVertices(:,2),...
    underVertices(:,3));
boundaryIndices = ...
[find(vertices(:,2) == min(vertices(:,2))); % min y
find(vertices(:,1) == max(vertices(:,1))); % max x
find(vertices(:,2) == max(vertices(:,2))); % max y

```

```

    find(vertices(:,1) == min(vertices(:,1)))];% min x
boundaryIndices = [...
    boundaryIndices(1:floor(end/4-1)); % semi open interval [1, end/4).
    boundaryIndices(floor(end/4+1):floor(end/2));%[end/4, end/2)
    boundaryIndices(floor(end*3/4-1):-1:floor(end/2+1));%[end/2,end*3/4)
    boundaryIndices(end-1:-1:floor(end*3/4+1))]; % [end*3/4, end)
constrainedEdges = [boundaryIndices(1:end-1), boundaryIndices(2:end)];
underFaces = DelaunayTri(...
    [underVertices(:,1),underVertices(:,2)],constrainedEdges);
inside = underFaces.inOutStatus; % 1 = in, 0 = out.
underFaces = underFaces.Triangulation(inside,:);
underFaces = fliplr(underFaces);
trisurf(underFaces,...
    underVertices(:,1),...
    underVertices(:,2),...
    underVertices(:,3));
set(gca,'dataAspectRatio',[1 1 1],...
    'xLim',[0 1],'yLim',[0 1]);
wallVertices = [vertices(boundaryIndices,:);
    underVertices(boundaryIndices,:)];
% Number of wall vertices on each surface (nwv).
nwv = length(wallVertices)/2;
% Allocate memory for wallFaces.
wallFaces = zeros(2*(nwv-1),3);
% Define the faces.
for k = 1:nwv-1
    wallFaces(k, :) = [k+1, k, k+nwv];
    wallFaces(k+nwv-1, :) = [k+nwv, k+1+nwv, k+1];
end
trisurf(wallFaces,...
    wallVertices(:,1),...
    wallVertices(:,2),...
    wallVertices(:,3));
% Shift indices to concatenate with the original surface.
underFaces = underFaces + length(vertices);
wallFaces = wallFaces + 2*length(vertices);
% Concatenate the results.
shellVertices = [vertices; underVertices; wallVertices];
shellFaces = [faces; underFaces; wallFaces];
minZ = min(shellVertices(:,3));
shellVertices = shellVertices...
    - repmat([0 0 minZ],length(shellVertices),1);
trisurf(shellFaces,...
    shellVertices(:,1),...
    shellVertices(:,2),...
    shellVertices(:,3));

% This subsection generates the title for the saved .stl file
if isempty(title1)
    filename = surfacel;
else
    filename = append(title1, '.stl');

```

```

end

% Create the facets.
shellFacets = shellVertices';
shellFacets = reshape(shellFacets(:,shellFaces'), 3, 3, []);
% Compute their normals.
edge1 = squeeze(shellFacets(:,2,:) - shellFacets(:,1,:));
edge2 = squeeze(shellFacets(:,3,:) - shellFacets(:,1,:));
shellNormals = edge1([2 3 1],:) .* edge2([3 1 2],:)...
    - edge2([2 3 1],:) .* edge1([3 1 2],:);
shellNormals = bsxfun(@times,...
    shellNormals, 1 ./ sqrt(sum(shellNormals .* shellNormals, 1)));
% Associate each facet with its normal.
shellFacets = cat(2, reshape(shellNormals, 3, 1, []), shellFacets);
% Open the file for writing
fid = fopen(filename, 'wb+');
fprintf(fid, 'solid %s\r\n', filename);
fprintf(fid, [...
'facet normal %.7E %.7E %.7E\r\n' ...
'outer loop\r\n' ...
'vertex %.7E %.7E %.7E\r\n' ...
'vertex %.7E %.7E %.7E\r\n' ...
'vertex %.7E %.7E %.7E\r\n' ...
'endloop\r\n' ...
'endfacet\r\n'], shellFacets);
fprintf(fid, 'endsolid %s\r\n', filename);

fclose(fid);
% This is the conclusion of code sourced from the man in the link
below
% https://blogs.mathworks.com/community/2013/06/20/paul-prints-the-l-shaped-membrane/#0d2c8d8b-352f-4b12-a0ba-5b5922a8795e
% -----
% -----
% THIS IS THE CONCLUSION OF THE GENERATION OF THE FIRST SURFACE
% -----
% -----

%Sigma is the standard deviation of the surface roughness
if isempty(sigma2)
    sigma = 0.455172414; % [microns] : Default Sigma
else
    sigma = sigma2; % [microns] : Specified Sigma
end

sigma = sigma/1000; % [mm] : Converts to mm

%This specifies the width of the surface generated in mm
% Note, because of the way MATLAB indexes, the width is Width-1 so
the true
% width is actually 9 mm when specified to be 10

```

```

if isempty(width)
Width = 10; % Default width is 10 mm
else
    Width = width;
end

% Resolution refers to the asperity density per square mm This
provides the step size between
% successive points. So to convert between Resolution (R) and
asperity
% density (p), use the formula  $p = R^{-2}$ 
if isempty(resolution)
Resolution = 0.5;
else
    Resolution = resolution;
end
movefile(filename, foldname)
close

% This sets up the asperity matrix
i = 1:Resolution:Width;
x = i;
y = 1:Resolution:(2*Width);
[Xa, Ya] = meshgrid(x, y);

% This is the heart of this code. This is what defines the probability
% distribution. normrnd is a normal distribution. The reason Xa and
Ya
% are divided by an obscenely large number, is because this ensures
that
% for each point in the matrix a random point is generated while
having a
% negligible impact to the average and standard deviation specified
La = normrnd((Xa/1000000000), sigma+(Ya/1000000000));

% This code looks for any asperties outside of the acceptable range
% previously specified and sets them equal to zero.
for i = 1:Xa
    for j = 1:Ya
        if abs(La(i, j)) > acceptablesigma*sigma
            La(i, j) = 0;
        end
    end
end

% This is an vestigial remenant of a previous code iteration. The code
is
% set to always interpolate.
L2 = La;
if interpolate == 'Y'
if isempty(interpolateresolution)

```



```

        InterpolationResolutionFactor = 2;
else
    InterpolationResolutionFactor = interpolateresolution;
end

% Creates the grid for the interpolation matrix
X = 1:(Resolution/InterpolationResolutionFactor):Width;
Y = 2*X;
[X,Y] = meshgrid(X,Y);
L = interp2(Xa,Ya,La,X,Y,'spline');
LI2 = L;
% Methods that can be input into interp2
% cubic, linear, nearest

% This is an vestigial remenant of a previous code iteration.
elseif interpolate == 'N'
    X = Xa;
    Y = Ya;
    L = La;
end

% The following code section calculates the arithmetic mean of the
% asperity heights (Ra) and Root mean squared (Rms)
zmax = max(max(L));
sumz = sum(sum(L));
SizeL = size(L);
Ra = zmax - sumz/(SizeL(1)*(SizeL(2)));
Ra2 = Ra;
Lsq = La.^2;
SumLsq = sum(sum(Lsq));
Rms = sqrt((1/(SizeL(1)*SizeL(2)))*SumLsq);
Rms2 = Rms;

% Set up the histogram to display the asperity height
% distribution of the surface generated
figure
histogram(L)
xlabel('Height of Elements (mm)');
ylabel('Frequency');
histname = append(title2,'_Histogram.fig');
savefig(histname)
movefile(histname,foldname)
close

% Credit for the following code goes to the person who provided this
code
% on mathworks.com, with some modifications, additions and
subtractions
% for this application
% https://blogs.mathworks.com/community/2013/06/20/paul-prints-the-l-shaped-membrane/#0d2c8d8b-352f-4b12-a0ba-5b5922a8795e
figure

```

```

n = Width; % number of partitions in each dimension.
mesh(X,Y,L)
colormap pink;
faces = delaunay(X,Y);
patches = trisurf(faces,X,Y,L);
vertices = get(patches,'vertices');
facets = vertices';
facets = reshape(facets(:,faces'), 3, 3, []);
edge1 = squeeze(facets(:,2,:) - facets(:,1,:));
edge2 = squeeze(facets(:,3,:) - facets(:,1,:));
normals = edge1([2 3 1],:) .* edge2([3 1 2],:) ...
    - edge2([2 3 1],:) .* edge1([3 1 2],:);
normals = bsxfun(@times,...
    normals, 1 ./ sqrt(sum(normals .* normals, 1)));
meanNormal = zeros(3,length(vertices)); % pre-allocate memory.
for k = 1:length(vertices)
    % Find all faces shared by a vertex
    [sharedFaces,~] = find(faces == k);
    % Compute the mean normal of all faces shared by a vertex
    meanNormal(:,k) = mean(normals(:,sharedFaces),2);
end
meanNormal = bsxfun(@times, meanNormal, ...
    1 ./ sqrt(sum(meanNormal .* meanNormal, 1)));
shellThickness = 0.05;
underVertices = vertices - shellThickness*meanNormal';
underFaces = delaunay(underVertices(:,1),underVertices(:,2));
trisurf(underFaces,...
    underVertices(:,1),...
    underVertices(:,2),...
    underVertices(:,3));
boundaryIndices = ...
[find(vertices(:,2) == min(vertices(:,2))); % min y
 find(vertices(:,1) == max(vertices(:,1))); % max x
 find(vertices(:,2) == max(vertices(:,2))); % max y
 find(vertices(:,1) == min(vertices(:,1)))]; % min x
boundaryIndices = [...
    boundaryIndices(1:floor(end/4-1)); % semi open interval [1, end/4).
    boundaryIndices(floor(end/4+1):floor(end/2)); %[end/4, end/2)
    boundaryIndices(floor(end*3/4-1):-1:floor(end/2+1)); %[end/2, end*3/4)
    boundaryIndices(end-1:-1:floor(end*3/4+1))]; %[end*3/4, end)
constrainedEdges = [boundaryIndices(1:end-1), boundaryIndices(2:end)];
underFaces = DelaunayTri(...
    [underVertices(:,1),underVertices(:,2)],constrainedEdges);
inside = underFaces.inOutStatus; % 1 = in, 0 = out.
underFaces = underFaces.Triangulation(inside,:);
underFaces = fliplr(underFaces);
trisurf(underFaces,...
    underVertices(:,1),...
    underVertices(:,2),...
    underVertices(:,3));
set(gca,'dataAspectRatio', [1 1 1],...
    'xLim',[0 1],'yLim',[0 1]);

```

```

wallVertices = [vertices(boundaryIndices,:);
                underVertices(boundaryIndices,:)];
% Number of wall vertices on each surface (nwv).
nwv          = length(wallVertices)/2;
% Allocate memory for wallFaces.
wallFaces    = zeros(2*(nwv-1),3);
% Define the faces.
for k = 1:nwv-1
    wallFaces(k      ,:) = [k+1 ,k      ,k+nwv];
    wallFaces(k+nwv-1,:) = [k+nwv,k+1+nwv,k+1];
end
trisurf(wallFaces,...
        wallVertices(:,1),...
        wallVertices(:,2),...
        wallVertices(:,3));
% Shift indices to concatenate with the original surface.
underFaces = underFaces + length(vertices);
wallFaces  = wallFaces + 2*length(vertices);
% Concatenate the results.
shellVertices = [vertices; underVertices; wallVertices];
shellFaces    = [faces;    underFaces;    wallFaces];
minZ = min(shellVertices(:,3));
shellVertices = shellVertices...
    - repmat([0 0 minZ],length(shellVertices),1);
trisurf(shellFaces,...
        shellVertices(:,1),...
        shellVertices(:,2),...
        shellVertices(:,3));

% This subsection generates the title for the saved .stl file
if isempty(title1)
    filename = surfacel;
else
    filename = append(title2, '.stl');
end

% Create the facets.
shellFacets = shellVertices';
shellFacets = reshape(shellFacets(:,shellFaces'), 3, 3, []);
% Compute their normals.
edge1 = squeeze(shellFacets(:,2,:) - shellFacets(:,1,:));
edge2 = squeeze(shellFacets(:,3,:) - shellFacets(:,1,:));
shellNormals = edge1([2 3 1],:) .* edge2([3 1 2],:)...
    - edge2([2 3 1],:) .* edge1([3 1 2],:);
shellNormals = bsxfun(@times,...
    shellNormals, 1 ./ sqrt(sum(shellNormals .* shellNormals, 1)));
% Associate each facet with its normal.
shellFacets = cat(2, reshape(shellNormals, 3, 1, []), shellFacets);
% Open the file for writing
fid = fopen(filename, 'wb+');
fprintf(fid, 'solid %s\r\n', filename);
fprintf(fid, [...

```

```

'facet normal %.7E %.7E %.7E\r\n' ...
'outer loop\r\n' ...
'vertex %.7E %.7E %.7E\r\n' ...
'vertex %.7E %.7E %.7E\r\n' ...
'vertex %.7E %.7E %.7E\r\n' ...
'endloop\r\n' ...
'endfacet\r\n'], shellFacets);
fprintf(fid, 'endsolid %s\r\n', filename);

fclose(fid);
% This is the conclusion of code sourced from the man in the link
below
% https://blogs.mathworks.com/community/2013/06/20/paul-prints-the-l-shaped-membrane/#0d2c8d8b-352f-4b12-a0ba-5b5922a8795e

% Move the .stl file to the folder generated
movefile(filename, foldname)
close
end

% End of the code. ('?'-'')?

```

## C.2: LoadFun.m

```
function [f0,s0] = LoadFun(L1,L2,d,UL,iter)
% This function calculates the overall force and overall shear force
% (in
%   one direction) that is expected from a modified Hertzian contact
%   theory
%   when two interfacing rough surfaces are brought together by some
%   distance
%   d.
% L1 is the first rough surface
% L2 is the second rough surface
% d is the distance of seperation between the surfaces
% UL is the "unit length" between elements in the rough surfaecs
% iter is a vestigial code remnant designed to compensate for the time
% evolution of
%   this system if the temporal dynamics were to be considered

% This preallocates the arrays that will be used in this code
[i,j] = size(L1);
Load = zeros(i,j);
Shear = zeros(i,j);
def = zeros(i,j);
delta = zeros(i,j);
Pressure = zeros(i,j);
theta = zeros(i,j);
phi = zeros(i,j);

% Method 1 of determining the radius.
% R = mean(abs((1/i)*(gradient(L1(:,1),UL))))/1000 ; %mm to m

% Method 2 of determining the radius. This averages the instantaneous
% curvature of each point. This is computationally inefficient and
% found to not be consistent
% Fdot = abs(gradient(L1(:,1)));
% Fdotmean = mean(Fdot);
% Fdotdotmean = mean(abs(gradient(Fdot)));
% R = ((1 + Fdotmean^2)^(3/2))/(Fdotdotmean*1000);

% Method 3 of determining the radius. This is the simplest, setting
% the
%   radius equal to 1/4 of the distance between successive heights
%   (dubbed the "unit length" or (UL)"). Tests were run to see if
%   this was
%   an acceptable assumption to make, and it was concluded there is
%   little
%   to no dependence of what fraction of the UL is used, so long as
%   it is
%   a constant fraction
R = .25*UL;
```

```

% Material properties of Aluminum 6061 from matweb.com
E = 68.9e9; % [Pa / N/m^2] : Modulus of Elasticity
tau = 26e9; % [Pa / N/m^2] : Shear Modulus
v = 0.33; % Poisson's Ratio

% EStar is a modified Modulus of Elasticity considering both
interfacing
% materials. Since it is assumed both materials will be aluminum
6061,
% this simplification is made
EStar = 2*E/(1-v^2); % [Pa / N/m^2]

% This provides the slope of each asperity/data point of both surfaces
and
% averages them together to give a compound slope of contact
interfacing
[L1dotx,L1doty] = gradient(L1,UL);
L2i = L2(iter:i,:);
[L2dotx,L2doty] = gradient(L2i,UL);
Ldotytemp = cat(3,L1doty,L2doty);
Ldot = nansum(Ldotytemp,3)./2;

% This converts the slope into an angle in radians (theta) and
subtracts it
% from pi/2 for simplification in subsequent steps. See derivation
of
% contact surface for justification
for a = 1:i
    for b = 1:j
theta(a,b) = atan(Ldot(a,b));
phi(a,b) = pi/2 - theta(a,b);
    end
end

% The for loop that goes through each element to calculate the
interference
% between the associated elements on opposing surfaces
for i = 1:i
    for j = 1:j
dr = ((L2(i,j)+ d) - L1(i,j))/1000; % This is the interference
        if dr >= 0
            def(i,j) = 0;
            delta(i,j) = 0;
        elseif dr < 0
            def(i,j) = -dr;
            delta(i,j) = abs(dr*cos(theta(i,j)));

            % This is a vestigial remnant of a previous solution to
            % calculate the interfacial load and shear. The
assumptions

```

```

% in this are non-ideal and produce markedly incorrect
results
% Load(i,j) = (4/3)*EStar*(R^.5)*abs((dr^1.5));
% Shear(i,j) = tau*pi*R*def(i,j);

CumulativeLoad =
(abs(delta(i,j)^3)*(16/9)*R*(EStar^2))^0.5;
% This a second vestigial remminat of a previous
solution. The
% assumptions in this calculation are more accurate to
what
% was expected, however was not consistent overall
% Load(i,j) = CumulativeLoad;
% Shear(i,j) =
abs(tau*(pi)*((3/4)*(R/EStar)*Load(i,j))^(2/3));

% This is the third solution attempted and provided the
most
% consistent, accurate, and expected results. This
consists
% of decomposing the contact force into a load and shear
% vector. This is, in itself, an assumption, but one
that is
% acceptable in solution.
Load(i,j) = CumulativeLoad*abs(sin(phi(i,j)));
Shear(i,j) = CumulativeLoad*(cos(phi(i,j)));
Pressure(i,j) =
((6*CumulativeLoad*EStar^2)/((pi^3)*(R^2)))^(1/3);

% If the shear is greater than zero, it is immediately set
% equal to 0. This is done such that only the shear in
one
% direction is considered. If this was not done, the
overall
% "Shear" would be approximately zero
if Shear(i,j) > 0
    Shear(i,j) = 0;
else
    Shear(i,j) = -Shear(i,j); % Converts the negative
shear
% into positive shear
end
end
end
end

% These sum the force at each element into the overall force and shear
f0 = sum(sum(Load));
s0 = sum(sum(Shear));
end

% End of the code. ('?-'?)?

```





### C.3: LoadFunHM.m

```
function [f0,s0] = LoadFunHM(L1,L2,d,UL,iter)
% This function calculates the overall force and overall shear force
% (in
%   one direction) that is expected from a modified Hertzian contact
%   theory
%   when two interfacing rough surfaces are brought together by some
%   distance
%   d.
% This code is separate from "LoadFun.m" in that this function
% generates a
%   heat map at the end of it. For hundreds of consecutive
%   calculations, this
%   is needlessly intensive and pointless
% L1 is the first rough surface
% L2 is the second rough surface
% d is the distance of separation between the surfaces
% UL is the "unit length" between elements in the rough surfaces
% iter is a vestigial variable designed to compensate for the time
% evolution of
%   this system if the temporal dynamics were to be considered

% This preallocates the arrays that will be used in this code
[i,j] = size(L1);
Load = zeros(i,j);
Shear = zeros(i,j);
def = zeros(i,j);
delta = zeros(i,j);
Pressure = zeros(i,j);
theta = zeros(i,j);
phi = zeros(i,j);

% Method 1 of determining the radius.
% R = mean(abs((1/i)*(gradient(L1(:,1),UL))))/1000 ; %mm to m

% Method 2 of determining the radius. This averages the instantaneous
% curvature of each point. This is computationally inefficient and
% found to not be consistent
% Fdot = abs(gradient(L1(:,1)));
% Fdotmean = mean(Fdot);
% Fdotdotmean = mean(abs(gradient(Fdot)));
% R = ((1 + Fdotmean^2)^(3/2))/(Fdotdotmean*1000);

% Method 3 of determining the radius. This is the simplest, setting
% the
%   radius equal to 1/4 of the distance between successive heights
%   (dubbed the "unit length" or (UL)"). Tests were run to see if
%   this was
```

```

%    an acceptable assumption to make, and it was concluded there is
little
%    to no dependence of what fraction of the UL is used, so long as
it is
%    a constant fraction
R = .25*UL;

% Material properties of Aluminum 6061 from matweb.com
E = 68.9e9; % [Pa / N/m^2] : Modulus of Elasticity
tau = 26e9; % [Pa / N/m^2] : Shear Modulus
v = 0.33; % Poisson's Ratio

% EStar is a modified Modulus of Elasticity considering both
interfacing
%    materials. Since it is assumed both materials will be aluminum
6061,
%    this simplification is made
EStar = 2*E/(1-v^2); % [Pa / N/m^2]

% This provides the slope of each asperity/data point of both surfaces
and
%    averages them together to give a compound slope of contact
interfacing
[L1dotx,L1doty] = gradient(L1,UL);
L2i = L2(iter:i,:);
[L2dotx,L2doty] = gradient(L2i,UL);

Ldotytemp = cat(3,L1doty,L2doty);
Ldot = nansum(Ldotytemp,3)./2;

% This converts the slope into an angle in radians (theta) and
subtracts it
%    from pi/2 for simplification in subsequent steps. See derivation
of
%    contact surface for justification
for a = 1:i
    for b = 1:j
theta(a,b) = atan(Ldot(a,b));
phi(a,b) = pi/2 - theta(a,b);
    end
end

% The for loop that goes through each element to calculate the
interference
%    between the associated elements on opposing surfaces
for i = 1:i
    for j = 1:j
        dr = ((L2(i,j)+ d) - L1(i,j))/1000; % This is the
interference
        if dr >= 0
            def(i,j) = 0;
            delta(i,j) = 0;
        end
    end
end

```

```

elseif dr < 0
    def(i,j) = -dr;
    delta(i,j) = abs(dr*cos(theta(i,j)));

    % This is a vestigial remnant of a previous solution to
    % calculate the interfacial load and shear. The
assumptions
    % in this are non-ideal and produce markedly incorrect
results
    % Load(i,j) = (4/3)*EStar*(R^.5)*abs((dr^1.5));
    % Shear(i,j) = tau*pi*R*def(i,j);

    CumulativeLoad =
(abs(delta(i,j)^3)*(16/9)*R*(EStar^2))^0.5;
    % This a second vestigial remnant of a previous
solution. The
    % assumptions in this calculation are more accurate to
what
    % was expected, however was not consistent overall
    % Load(i,j) = CumulativeLoad;
    % Shear(i,j) =
abs(tau*(pi)*((3/4)*(R/EStar)*Load(i,j))^(2/3));

    % This is the third solution attempted and provided the
most
    % consistent, accurate, and expected results. This
consists
    % of decomposing the contact force into a load and shear
    % vector. This is, in itself, an assumption, but one
that is
    % acceptable in solution.
    Load(i,j) = CumulativeLoad*abs(sin(phi(i,j)));
    Shear(i,j) = CumulativeLoad*cos(phi(i,j));
    Pressure(i,j) =
((6*CumulativeLoad*EStar^2)/((pi^3)*(R^2)))^(1/3);

    % If the shear is greater than zero, it is immediately
set
    % equal to 0. This is done such that only the shear in
one
    % direction is considered. If this was not done, the
overall
    % "Shear" would be approximately zero
    if Shear(i,j) > 0
        Shear(i,j) = 0;
    else
        Shear(i,j) = -Shear(i,j);
    end
end
end
end
end
end

```

```

% These sum the force at each element into the overall force and shear
f0 = sum(sum(Load));
s0 = sum(sum(Shear));

% This generates a heatmap for the pressure distribution on the first
% surface
figure
heatmap((Pressure), 'ColorMap',hot);
Ax = gca;
Ax.XDisplayLabels = nan(size(Ax.XDisplayData));
Ax.YDisplayLabels = nan(size(Ax.YDisplayData));
title('Pressure Map (in Pa)');

% This generates a heatmap for the load distribution on the first
% surface
figure
heatmap((Load), 'ColorMap',hot);
Ax = gca;
Ax.XDisplayLabels = nan(size(Ax.XDisplayData));
Ax.YDisplayLabels = nan(size(Ax.YDisplayData));
title('Load Map (in N)');
end

% End of the code. ('?'-'')?

```

## C.4: Ra\_Rms\_vs\_Sigma.m

```
% This code iterates through hundreds of generated surfaces and
calculates
%   the arithmetic mean of the asperity heights (Ra) and Root mean
squared
%   (Rms) to correlate these outputs with the input standard deviation
%   (sigma) of the asperity height distribution
% The output of this code is two distinct graphs. One is the Ra vs
sigma
%   and the second is Rms vs Sigma. Lines of best fit are added to the
%   upper and lower bound of these distributions.

clear
close all

%If mu is set to be 0, then the Ra and Rms values are accurate
%   For any other values of mu, the mean must be subtracted from the
%   z values, which is easier not to do
mu = 0;

% The number of times each surface should be generated at a specified
%   sigma
replications = 20;

% How many sigma iterations should be made
SigmaSize = 500;

% This is a factor that, when multiplied by SigmaSize yields the
maximum
%   input sigma (in mm). This is also the factor when multiplied by
the
%   current iteration of the for loop, will determine which
SigmaScale = 0.00001;

for q = 1:SigmaSize
    for r = 1:replications

% Specified standard deviations of the asperity distribution for the
rough
%   surface generated
sigma = SigmaScale*q;
sigmaindex(q) = sigma; % Store sigma

% Width of the surface generated. Note this surface will end up
equally
%   width - 1 due to MATLAB's indexing
Width = 10;
```

```

% Resolution refers to the asperity density per square mm This
provides the step size between
%    successive points. So to convert between Resolution (R) and
asperity
%    density (p), use the formula  $p = R^{-2}$ 
Resolution = 0.5;

% This interpolateresolution specifies how many elements should be
created
%    between successive asperities
InterpolationResolutionFactor = 3;

% This sets up the asperity matrix
i = 1:Resolution:Width;
x = i;
y = i;
[Xa,Ya] = meshgrid(x,y);

% This is the heart of this code. This is what defines the probability
%    distribution. normrnd is a normal distribution. The reason Xa and
Ya
%    are divided by an obscenely large number, is because this ensures
that
%    for each point in the matrix a random point is generated while
having a
%    negligible impact to the average and standard deviation specified
La = normrnd(mu+(Xa/1000000000),sigma+(Ya/10000000000));

% Export data from the rough surface generated
zmax = max(max(La));
sumz = sum(sum(La));
SizeL = size(La);

% The following code section calculates the arithmetic mean of the
%    asperity heights (Ra) and Root mean squared (Rms)
Ra(q,r) = zmax - sumz/(SizeL(1)*(SizeL(2)));
Lsq = La.^2;
SumLsq = sum(sum(Lsq));
Rms(q,r) = sqrt((1/(SizeL(1)*SizeL(2)))*SumLsq);
    end

% Store data about the maximum and minmum Ra and Rms values
minrms(q) = min(Rms(q,:));
minra(q) = min(Ra(q,:));
maxrms(q) = max(Rms(q,:));
maxra(q) = max(Ra(q,:));
end

% Calculat the average rms and ra
for i = 1:SigmaSize
    averagerms(i) = mean(Rms(i,:));
    averagera(i) = mean(Ra(i,:));
end

```

```

end

% Calculate the line of best fit for the max, min, and average Ra and
Rms
linminrms = polyfit(sigmaindex,minrms,1);
linmaxrms = polyfit(sigmaindex,maxrms,1);
linminra = polyfit(sigmaindex,minra,1);
linmaxra = polyfit(sigmaindex,maxra,1);
avgrms = polyfit(sigmaindex,averagerms,1);
avgra = polyfit(sigmaindex,averagera,1);

% Creat a plot of the Rms vs sigma for all data points
figure;
hold on
for i = 1:replications
scatter(sigmaindex,Rms(:,i),'k','HandleVisibility','off')
end
pause

% Adding and formatting the lines of best fit to the Rms figure
fplot(@(x) linmaxrms(1)*x + linmaxrms(2),'-
.', 'color', '#D50000', 'linewidth', 2)
fplot(@(x) linminrms(1)*x + linminrms(2),'-
.', 'Color', '#0034D5', 'linewidth', 2)
fplot(@(x) avgrms(1)*x + avgrms(2),'-.', 'Color', '#1AD500', 'linewidth',
2)
axis([0 max(sigmaindex) 0 max(maxrms)])

% Final formatting of the figure
legend(['Upper Bound: y=' num2str(linmaxrms(1)) 'x+'
num2str(linmaxrms(2))], ['Lower Bound: y=' num2str(linminrms(1)) 'x+'
num2str(linminrms(2))], ['Average: y=' num2str(avgrms(1)) 'x+'
num2str(avgrms(2))], 'Location', 'northwest')
xlabel('Sigma (mm)')
ylabel('Rms (mm)')
title('Rms of Surface Generated for Input Sigma')

% Creat a plot of the Ra vs sigma for all data points
figure;
hold on
for i = 1:replications
scatter(sigmaindex,Ra(:,i),'k','HandleVisibility','off')
end

% Adding and formatting the lines of best fit to the Ra figure
fplot(@(x) linmaxra(1)*x + linmaxra(2),'-
.', 'Color', '#D50000', 'linewidth', 2)
fplot(@(x) linminra(1)*x + linminra(2),'-
.', 'Color', '#0034D5', 'linewidth', 2)
fplot(@(x) avgra(1)*x + avgra(2),'-.', 'Color', '#1AD500', 'linewidth',
2)
axis([0 max(sigmaindex) 0 max(maxra)])

```

```
% Adding and formatting the lines of best fit to the Ra figure
legend(['Upper Bound: y=' num2str(linmaxra(1)) 'x+'
num2str(linmaxra(2))], ['Lower Bound: y=' num2str(linminra(1)) 'x+'
num2str(linminra(2))], ['Average: y=' num2str(avgra(1)) 'x+'
num2str(avgra(2))], 'Location', 'northwest')
xlabel('Sigma (mm)')
ylabel('Ra (mm)')
title('Ra of Surface Generated for Input Sigma')

% End of the code. (??-'?)?
```



## C.5: Ra\_to\_Grit.m

```
function Equivalent_Grit = Ra_to_Grit(RaInquiry)
% This is a really quick and simple function to interpolate between
known
% values of Ra and the associated grit
% This data comes from https://www.microgroup.com/wp-
% content/uploads/...
% Grit-Finish-and-Estimated-RMS-and-Ra-Values.pdf

% Aluminum roughness values
AlRa = [4.3, 2.0, 1.4, .85, .70, .4, .3, .05];
% Corresponding sandpaper grits
Grit = [80 150 220 280 320 400 500 600];

% Interpolation between Ra values and Grit
Equivalent_Grit = interp1(AlRa, Grit, RaInquiry);
end
```

## C.6: Friction\_Test.m

```
% This code calculates the distance and coefficient of friction
resulting
% from two rough surfaces in contact under some normal force. This
% utilizes the modified Hertzian contact in LoadFun.m to calculate
these
% results.

close all
clear

% Specified standard deviations of the asperity distribution for the
rough
% surface generated
sigma1 = .75; % in microns
sigma2 = .75; % in microns

% Width of the surface generated. Note this surface will end up
equally
% width - 1 due to MATLAB's indexing
width = 10; % in mm

% Titles that the histograms and .stl figures will be named. These
must be
% input as a string (use the '')
title1 = 'Title1';
title2 = 'Title2';

% Resolution refers to the asperity density per square mm This
provides the step size between
% successive points. So to convert between Resolution (R) and
asperity
% density (p), use the formula  $p = R^{-2}$ 
resolution = .2; % in mm

% What normal force the code should iterate to achieve.
Fn = 1; % [N]

% This interpolateresolution specifies how many elements should be
created
% between successive asperities
interpolateresolution = 1;

% Runs the Surfaces.m function and collects the parameters desired for
% analysis
[Ra1,Rms1,Ra2,Rms2,L1,L2,LI1,LI2] =
Surfaces(sigma1,sigma2,width,title1,title2,resolution,interpolateresol
ution);
```

```

% Provides the equivalent grit (sandpaper) for the surface generated
GritEquivalent = Ra_to_Grit(Ra1);

max1 = max(L1);
min2 = min(L2);

% Material properties of Aluminum 6061 from matweb.com
E = 68.9e9; % [Pa / N/m^2]
v = 0.33;

% EStar is a modified Modulus of Elasticity considering both
interfacing
% materials. Since it is assumed both materials will be aluminum
6061,
% this simplification is made
EStar = 2*E/(1-v^2);

% Unit length is the distance between successive elements. In this
% situation, where we're considering the asperities only, the
distance in
% question is the resolution
UnitLength = resolution/1000; % convert to meters

% Secant method parameters
xl = -1; % Lower bound
xu = 1; % Upper bound
es = 0.000000000001; % Error Specification
maxit = 100; % Maximum Iterations

% distiter is intended to be used when the temporal dynamics of
asperity
% contact was to be examined with regard to kinetic friction. It is
% necessary in this code for LoadFun to run
distiter = 1;

% Initial Parameters being set for secant method
iter = 0;
xr = xl;
ea = 10;
a = zeros(1);
b = zeros(1);

% Secant method modified from "Applied Numerical Methods with MATLAB
for
% Engineers and Scientists" by Steven C. Chapra.
% Chapra's secant method has been modified to output the distance
% associated with the prescribed normal force. This is done using
the
% function LoadFun.m
while (1)
    xrold = xr;
    xr = (xl + xu)/2;

```

```

iter = iter + 1;
if xr ~= 0, ea = abs((xr - xrold)/xr) * 100; end
[f0l, s0l] = (LoadFun(L1, L2, xl, UnitLength, distiter));
[f0u, s0u] = (LoadFun(L1, L2, xr, UnitLength, distiter));
a(iter) = Fn - f0l;
b(iter) = Fn - f0u;
test = a(iter)*b(iter);
if test < 0
    xu = xr;
elseif test > 0
    xl = xr;
else
    ea = 0;
end
if ea <= es || iter >= maxit, break, end
end
d = xr; % output distance

% Coefficient of static friction (mu) is known to be equivalent to the
% shear force divided by the normal force
mu = s0u/f0u;
disp('Coeff. of Friction')
disp(mu)

% Create the heat maps of pressure and load on the surface using
% LoadFunHM.m
LoadFunHM(L1, L2, d, UnitLength, distiter);

% End of the code. (?'-')?

```

## C.7: Friction\_Test\_Int.m

```
% This code calculates the distance and coefficient of friction
resulting
% from two rough surfaces in contact under some normal force. This
% utilizes the modified Hertzian contact in LoadFun.m to calculate
these
% results.
% NOTE: This code is different from Friction_Test.m because it
utilizes
% the interpolated surface generated from Surfaces.m

close all
clear

% Specified standard deviations of the asperity distribution for the
rough
% surface generated
sigma1 = .1; % in microns
sigma2 = .1; % in microns

% Width of the surface generated. Note this surface will end up
equally
% width - 1 due to MATLAB's indexing
width = 10; % in mm

% Titles that the histograms and .stl figures will be named. These
must be
% input as a string (use the '')
title1 = 'Title1';
title2 = 'Title2';

% Resolution refers to the asperity density per square mm This
provides the step size between
% successive points. So to convert between Resolution (R) and
asperity
% density (p), use the formula  $p = R^{-2}$ 
resolution = .5; % in mm

% What normal force the code should iterate to achieve.
Fn = 100; % Normal Force to Achieve

% This interpolateresolution specifies how many elements should be
created
% between successive asperities
interpolateresolution = 2;

% Runs the Surfaces.m function and collects the parameters desired for
% analysis
```

```

[Ra1,Rms1,Ra2,Rms2,L1,L2,LI1,LI2] =
Surfaces(sigma1,sigma2,width,title1,title2,resolution,interpolateresol
ution);

% Provides the equivalent grit (sandpaper) for the surface generated
GritEquivalent = Ra_to_Grit(Ra1);

max1 = max(LI1);
min2 = min(LI2);

% Material properties of Aluminum 6061 from matweb.com
E = 68.9e9; % [Pa / N/m^2]
v = 0.33;

% EStar is a modified Modulus of Elasticity considering both
interfacing
% materials. Since it is assumed both materials will be aluminum
6061,
% this simplification is made
EStar = 2*E/(1-v^2);

% Unit length is the distance between successive elements. In this
% situation, where we're considering the interpolated elements, the
unit
% length is equivalent to the resolution (distance between
asperities)
% divided by the number of points of interpolation between elements
% (interpolateresolution)
UnitLength = (resolution/interpolateresolution)/1000; % convert to m

L1 = LI1;
L2 = LI2;

% Secant method parameters
xl = 0; % Lower Bound
xu = 1; % Upper Bound
es = 0.000000000001; % Error Specification
maxit = 100; % Maximum Iterations

% distiter is intended to be used when the temporal dynamics of
asperity
% contact was to be examined with regard to kinetic friction. It is
% necessary in this code for LoadFun to run
distiter = 1;

% Initial Parameters being set for secant method
iter = 0;
xr = xl;
ea = 100;
a = zeros(1);
b = zeros(1);

```

```

% Secant method modified from "Applied Numerical Methods with MATLAB
for
% Engineers and Scientists" by Steven C. Chapra.
% Chapra's secant method has been modified to output the distance
% associated with the prescribed normal force. This is done using
the
% function LoadFun.m
while (1)
    xrold = xr;
    xr = (xl + xu)/2;
    iter = iter + 1;
    if xr ~= 0,ea = abs((xr - xrold)/xr) * 100;end
    [f0l,s0l] = (LoadFunSimple(L1,L2,xl,UnitLength,distiter));
    [f0u,s0u] = (LoadFunSimple(L1,L2,xr,UnitLength,distiter));
    a(iter) = Fn - f0l;
    b(iter) = Fn - f0u;
    test = a(iter)*b(iter);
    if test < 0
        xu = xr;
    elseif test > 0
        xl = xr;
    else
        ea = 0;
    end
    if ea <= es || iter >= maxit,break,end
end
root = xr; % Output Distance

% Coefficient of static friction (mu) is known to be equivalent to the
% shear force divided by the normal force
mu = s0u/f0u;
disp('Coeff. of Friction')
disp(mu)

% Create the heat maps of pressure and load on the surface using
% LoadFunHM.m
LoadFunHM(L1,L2,xr,UnitLength,distiter);

% End of the code. ('?'-'')?

```

## C.8: Friction\_Test\_Evolve.m

```
% This code is nearly identical to Friction_Test.m, insofar as this
code
% aims to calculate the coefficient of friction between two rough
% surfaces. This code is modified such that a range of normal forces
are
% iterated through LoadFun.m such that a plot of the coefficient of
% friction vs the normal force may be generated

close all
clear

% Specified standard deviations of the asperity distribution for the
rough
% surface generated
sigma1 = 1; % in microns
sigma2 = 1; % in microns

% Width of the surface generated. Note this surface will end up
equally
% width - 1 due to MATLAB's indexing
width = 10; % in mm

% Titles that the histograms and .stl figures will be named. These
must be
% input as a string (use the '')
title1 = 'Title1';
title2 = 'Title2';

% Resolution refers to the asperity density per square mm This
provides the step size between
% successive points. So to convert between Resolution (R) and
asperity
% density (p), use the formula  $p = R^{-2}$ 
resolution = 1; % in mm

% What normal force the code should iterate to achieve.
Fn = 1; % Normal Force to Achieve

% This interpolateresolution specifies how many elements should be
created
% between successive asperities
interpolateresolution = 1;

% fact is the factor of iterations. This code calculates the evolution
of
% the static coefficient of friction as a function of applied normal
% force
fact = 10;
```



```

% Runs the Surfaces.m function and collects the parameters desired for
% analysis
[Ra1,Rms1,Ra2,Rms2,L1,L2,LI1,LI2] =
Surfaces(sigma1,sigma2,width,title1,...
    title2,resolution,interpolateresolution);

% Preallocate Arrays for Storage
mu = zeros(1);
zed = zeros(1);

% Beginning of the for loop that iterates through 100 applied loads
(normal
force) at intervals of fact
for z = 1:1:100
    Fn = z*fact; % Normal force

max1 = max(L1);
min2 = min(L2);

% Material properties of Aluminum 6061 from matweb.com
E = 68.9e9; % [Pa / N/m^2]
v = 0.33;

% EStar is a modified Modulus of Elasticity considering both
interfacing
% materials. Since it is assumed both materials will be aluminum
6061,
% this simplification is made
EStar = 2*E/(1-v^2);

% Unit length is the distance between successive elements. In this
% situation, where we're considering the asperities only, the
distance in
% question is the resolution
UnitLength = resolution/1000; % convert to meters

% Secant method parameters
xl = -1; % Lower bound
xu = 1; % Upper bound
es = 0.000000000001; % Error Specification
maxit = 100; % Maximum Iterations

% distiter is intended to be used when the temporal dynamics of
asperity
% contact was to be examined with regard to kinetic friction. It is
% necessary in this code for LoadFun to run
distiter = 1;

% Initial Parameters being set for secant method
iter = 0;
xr = xl;

```

```

ea = 10;
a = zeros(1);
b = zeros(1);

% Secant method modified from "Applied Numerical Methods with MATLAB
for
% Engineers and Scientists" by Steven C. Chapra.
% Chapra's secant method has been modified to output the distance
% associated with the prescribed normal force. This is done using
the
% function LoadFun.m
while (1)
    xrold = xr;
    xr = (xl + xu)/2;
    iter = iter + 1;
    if xr ~= 0, ea = abs((xr - xrold)/xr) * 100; end
    [f0l, s0l] = (LoadFun(L1, L2, xl, UnitLength, distiter));
    [f0u, s0u] = (LoadFun(L1, L2, xr, UnitLength, distiter));
    a(iter) = Fn - f0l;
    b(iter) = Fn - f0u;
    test = a(iter)*b(iter);
    if test < 0
        xu = xr;
    elseif test > 0
        xl = xr;
    else
        ea = 0;
    end
    if ea <= es || iter >= maxit, break, end
end
d = xr;
mu(z) = s0u/f0u; % Storage of coefficient of friction
zed(z) = Fn; % Storage of normal force
end

% Plots the coefficient of friction vs the normal force applied.
plot(zed, mu)
title('mu vs Force')
xlabel('Force (N)')
ylabel('mu')

% Create the heat maps of pressure and load on the surface using
% LoadFunHM.m
LoadFunHM(L1, L2, d, UnitLength, distiter);

% End of the code. ('?'-'')?

```

## C.9: Friction\_Test\_Int\_Evolve.m

```
% This code calculates the distance and coefficient of friction
resulting
% from two rough surfaces in contact under some normal force. This
% utilizes the modified Hertzian contact in LoadFun.m to calculate
these
% results.
% NOTE: This code is different from Friction_Test.m because it
utilizes
% the interpolated surface generated from Surfaces.m

close all
clear

% Specified standard deviations of the asperity distribution for the
rough
% surface generated
sigma1 = .1; % in microns
sigma2 = .1; % in microns

% Width of the surface generated. Note this surface will end up
equally
% width - 1 due to MATLAB's indexing
width = 10; % in mm

% Titles that the histograms and .stl figures will be named. These
must be
% input as a string (use the '')
title1 = 'Title1';
title2 = 'Title2';

% Resolution refers to the asperity density per square mm This
provides the step size between
% successive points. So to convert between Resolution (R) and
asperity
% density (p), use the formula  $p = R^{-2}$ 
resolution = .5; % in mm

% What normal force the code should iterate to achieve.
Fn = 100; % Normal Force to Achieve

% This interpolateresolution specifies how many elements should be
created
% between successive asperities
interpolateresolution = 2;

% Runs the Surfaces.m function and collects the parameters desired for
% analysis
```

```

[Ra1,Rms1,Ra2,Rms2,L1,L2,LI1,LI2] =
Surfaces(sigma1,sigma2,width,title1,title2,resolution,interpolateresol
ution);

% Provides the equivalent grit (sandpaper) for the surface generated
GritEquivalent = Ra_to_Grit(Ra1);

max1 = max(LI1);
min2 = min(LI2);

% Material properties of Aluminum 6061 from matweb.com
E = 68.9e9; % [Pa / N/m^2]
v = 0.33;

% EStar is a modified Modulus of Elasticity considering both
interfacing
% materials. Since it is assumed both materials will be aluminum
6061,
% this simplification is made
EStar = 2*E/(1-v^2);

% Unit length is the distance between successive elements. In this
% situation, where we're considering the interpolated elements, the
unit
% length is equivalent to the resolution (distance between
asperities)
% divided by the number of points of interpolation between elements
% (interpolateresolution)
UnitLength = (resolution/interpolateresolution)/1000; % convert to m

L1 = LI1;
L2 = LI2;

% Secant method parameters
xl = 0; % Lower Bound
xu = 1; % Upper Bound
es = 0.000000000001; % Error Specification
maxit = 100; % Maximum Iterations

% distiter is intended to be used when the temporal dynamics of
asperity
% contact was to be examined with regard to kinetic friction. It is
% necessary in this code for LoadFun to run
distiter = 1;

% Initial Parameters being set for secant method
iter = 0;
xr = xl;
ea = 100;
a = zeros(1);
b = zeros(1);

```

```

% Secant method modified from "Applied Numerical Methods with MATLAB
for
% Engineers and Scientists" by Steven C. Chapra.
% Chapra's secant method has been modified to output the distance
% associated with the prescribed normal force. This is done using
the
% function LoadFun.m
while (1)
    xrold = xr;
    xr = (xl + xu)/2;
    iter = iter + 1;
    if xr ~= 0,ea = abs((xr - xrold)/xr) * 100;end
    [f0l,s0l] = (LoadFunSimple(L1,L2,xl,UnitLength,distiter));
    [f0u,s0u] = (LoadFunSimple(L1,L2,xr,UnitLength,distiter));
    a(iter) = Fn - f0l;
    b(iter) = Fn - f0u;
    test = a(iter)*b(iter);
    if test < 0
        xu = xr;
    elseif test > 0
        xl = xr;
    else
        ea = 0;
    end
    if ea <= es || iter >= maxit,break,end
end
root = xr; % Output Distance

% Coefficient of static friction (mu) is known to be equivalent to the
% shear force divided by the normal force
mu = s0u/f0u;
disp('Coeff. of Friction')
disp(mu)

% Create the heat maps of pressure and load on the surface using
% LoadFunHM.m
LoadFunHM(L1,L2,xr,UnitLength,distiter);

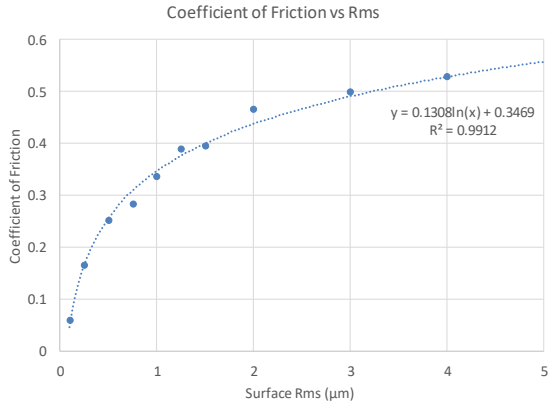
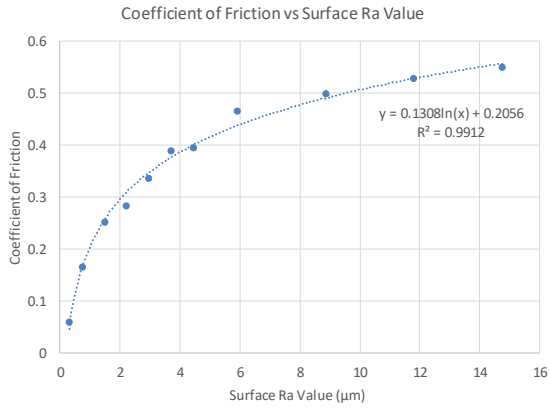
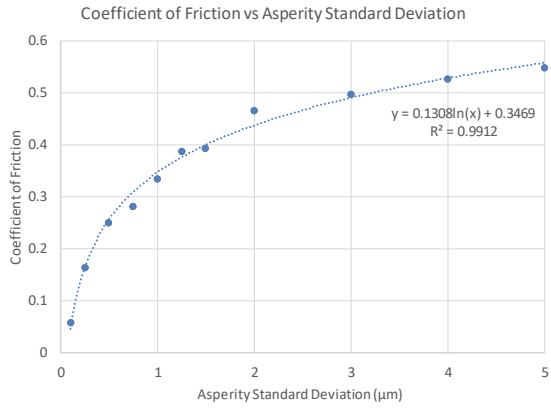
% End of the code. ('?'-'')?

```

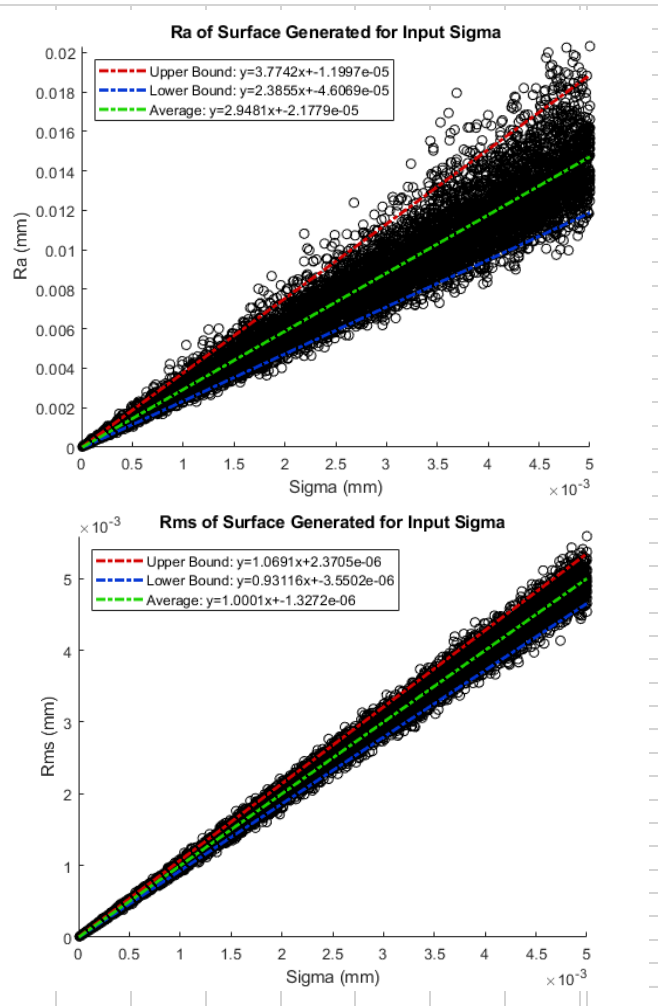
# Appendix D

## D.1: Surface Roughness vs Friction Calculations

Sigma	Beginning	End	Estimate	Load	Range	% SS	Sigma (μm)	Ra (μm)	Rms (μm)	Average E	Std. Estim	Range	Std. Range	% std/avg
0.1	0.036	0.048	0.043	60	0.012	0.895833	0.1	0.294788	0.100009	0.058267	0.012103	0.01075	0.008511	0.207712
0.1	0.0809	0.0769	0.079	50	0.004	1.027308	0.25	0.737003	0.250024	0.1645	0.016991	0.02525	0.020726	0.10329
0.1	0.0527	0.0513	0.0514	50	0.0014	1.001949	0.5	1.474028	0.500049	0.250333	0.033116	0.093667	0.10133	0.132287
0.1	0.0775	0.0575	0.06	70	0.02	1.043478	0.75	2.211053	0.750074	0.282333	0.029269	0.0865	0.075865	0.103668
0.1	0.0375	0.059	0.055	60	0.0215	0.932203	1	2.948078	1.000099	0.335	0.049497	0.157333	0.175186	0.147754
0.1	0.057	0.0626	0.0612	40	0.0056	0.977636	1.25	3.685103	1.250124	0.388333	0.057677	0.203417	0.225571	0.148525
Average	0.056933	0.059217	0.058267	55	0.01075	0.979735	1.5	4.422128	1.500149	0.39375	0.057874	0.236083	0.226015	0.146981
Std Dev	0.019137	0.010155	0.012103	10.48809	0.008511	0.056786	2	5.896178	2.000199	0.465833	0.061353	0.19725	0.134686	0.131705
Sigma	Beginning	End	Estimate	Load	Range	% SS	3	8.844278	3.000299	0.4975	0.081716	0.22	0.090554	0.164253
0.25	0.192	0.178	0.184	160	0.014	1.033708	4	11.79238	4.000399	0.528333	0.133778	0.278667	0.24633	0.253208
0.25	0.17	0.149	0.155	210	0.021	1.040268	5	14.74048	5.000499	0.549583	0.116752	0.318083	0.380228	0.212437
0.25	0.2	0.155	0.165	190	0.045	1.064516								
0.25	0.1405	0.143	0.143	280	0.0025	1								
0.25	0.228	0.172	0.185	170	0.056	1.075581								
0.25	0.142	0.155	0.155	220	0.013	1								
Average	0.17875	0.158667	0.1645	205	0.02525	1.035679								
Std Dev	0.034476	0.013545	0.016991	43.2435	0.020726	0.031606								
Sigma	Beginning	End	Estimate	Load	Range	% SS								
0.5	0.2	0.224	0.22	520	0.024	0.982143								
0.5	0.214	0.224	0.222	380	0.01	0.991071								
0.5	0.19	0.22	0.22	440	0.03	1								
0.5	0.38	0.26	0.27	380	0.12	1.038462								
0.5	0.366	0.268	0.28	470	0.098	1.044776								
0.5	0.54	0.26	0.29	580	0.28	1.115385								
Average	0.315	0.242667	0.250333	461.6667	0.093667	1.028639								
Std Dev	0.138926	0.022151	0.033116	79.09909	0.10133	0.049548								
Sigma	Beginning	End	Estimate	Load	Range	% SS								
0.75	0.36	0.32	0.33	730	0.04	1.03125								
0.75	0.246	0.285	0.284	820	0.039	0.996491								
0.75	0.205	0.31	0.3	540	0.105	0.967742								
0.75	0.285	0.275	0.27	450	0.01	0.981818								
0.75	0.46	0.24	0.25	930	0.22	1.041667								
0.75	0.36	0.255	0.26	830	0.105	1.019608								
Average	0.319333	0.280833	0.282333	716.6667	0.0865	1.006429								
Std Dev	0.092437	0.03089	0.029269	185.2206	0.075865	0.029095								
Sigma	Beginning	End	Estimate	Load	Range	% SS								
1	0.17	0.295	0.27	790	0.125	0.915254								
1	0.4175	0.365	0.365	780	0.0525	1								
1	0.385	0.3325	0.335	700	0.0525	1.007519								
1	0.14	0.31	0.285	890	0.17	0.919355								
1	0.382	0.338	0.355	880	0.044	1.050296								
1	0.85	0.35	0.4	890	0.5	1.142857								
Average	0.39075	0.33175	0.335	821.6667	0.157333	1.00588								
Std Dev	0.2543	0.025698	0.049497	77.82459	0.175186	0.085408								
Sigma	Beginning	End	Estimate	Load	Range	% SS								
1.25	0.28	0.4405	0.4	1000	0.1605	0.908059								
1.25	0.315	0.375	0.36	1000	0.06	0.96								
1.25	0.416	0.345	0.345	1000	0.071	1								
1.25	0.335	0.369	0.365	1000	0.034	0.98916								
1.25	0.6	0.335	0.36	1000	0.265	1.074627								
1.25	1.05	0.42	0.5	1000	0.63	1.190476								
Average	0.499333	0.38075	0.388333	1000	0.203417	1.020387								
Std Dev	0.293054	0.0416	0.057677	0	0.225571	0.099526								
Sigma	Beginning	End	Estimate	Load	Range	% SS								
1.5	0.8	0.4405	0.42	1000	0.3595	0.953462								
1.5	0.315	0.375	0.37	1000	0.06	0.986667								
1.5	0.418	0.345	0.345	1000	0.073	1								
1.5	0.335	0.369	0.3675	1000	0.034	0.995935								
1.5	0.61	0.33	0.36	1000	0.28	1.090909								
1.5	1.05	0.44	0.5	1000	0.61	1.136364								
Average	0.588	0.38325	0.39375	1000	0.236083	1.027223								
Std Dev	0.291997	0.047049	0.057874	0	0.226015	0.070389								
Sigma	Beginning	End	Estimate	Load	Range	% SS								
2	0.21	0.475	0.475	1000	0.265	1								
2	0.4325	0.424	0.43	1000	0.0085	1.014151								
2	0.32	0.41	0.41	1000	0.09	1								
2	0.78	0.43	0.47	1000	0.35	1.093023								
2	0.595	0.44	0.43	1000	0.155	0.977273								
2	0.84	0.525	0.58	1000	0.315	1.104762								
Average	0.529583	0.450667	0.465833	1000	0.19725	1.031535								
Std Dev	0.252519	0.042481	0.061353	0	0.134686	0.053626								



Sigma	Beginning	End	Estimate	Load	Range	% SS
3	0.31	0.55	0.55	1000	0.24	1
3	0.16	0.48	0.4	1000	0.32	0.833333
3	0.81	0.58	0.625	1000	0.23	1.077586
3	0.69	0.43	0.46	1000	0.26	1.069767
3	0.48	0.43	0.44	1000	0.05	1.023256
3	0.73	0.51	0.51	1000	0.22	1
Average	0.53	0.496667	0.4975	1000	0.22	1.000657
Std Dev	0.257604	0.06186	0.081716	0	0.090554	0.088547
Sigma	Beginning	End	Estimate	Load	Range	% SS
4	0.455	0.57	0.55	1000	0.115	0.964912
4	0.225	0.425	0.39	1000	0.2	0.917647
4	0.5	0.557	0.56	1000	0.057	1.005386
4	1.39	0.65	0.72	1000	0.74	1.107692
4	0.795	0.58	0.59	1000	0.215	1.017241
4	0.06	0.405	0.36	1000	0.345	0.888889
Average	0.570833	0.531167	0.528333	1000	0.278667	0.983628
Std Dev	0.473344	0.095782	0.133778	0	0.24633	0.078326
Sigma	Beginning	End	Estimate	Load	Range	% SS
5	0.56	0.465	0.47	1000	0.095	1.010753
5	0.425	0.6	0.61	1000	0.175	1.016667
5	0.14	0.54	0.45	1000	0.4	0.833333
5	0.579	0.5555	0.5575	1000	0.0235	1.0036
5	1.7	0.65	0.75	1000	1.05	1.153846
5	0.3	0.465	0.46	1000	0.165	0.989247
Average	0.617333	0.545917	0.549583	1000	0.318083	1.001241
Std Dev	0.555421	0.073458	0.116752	0	0.380228	0.10194
Sigma	Beginning	End	Estimate	Load	Range	% SS
7.5	0.6325	0.62	0.645	1000	0.0125	1.040323
7.5	0.05	0.51	0.45	1000	0.46	0.882353
7.5	1.75	0.68	0.7	1000	1.07	1.029412
7.5	1.19	0.74	0.84	1000	0.45	1.135135
7.5	1.35	0.8	0.9	1000	0.55	1.125
7.5	1.8	0.59	0.61	1000	1.21	1.033898
Average	1.12875	0.656667	0.690833	1000	0.625417	1.04102
Std Dev	0.678115	0.105198	0.162924	0	0.442466	0.090853

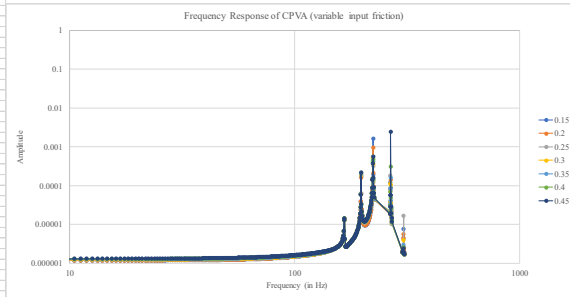
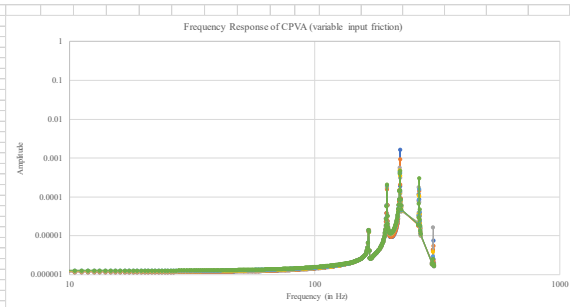






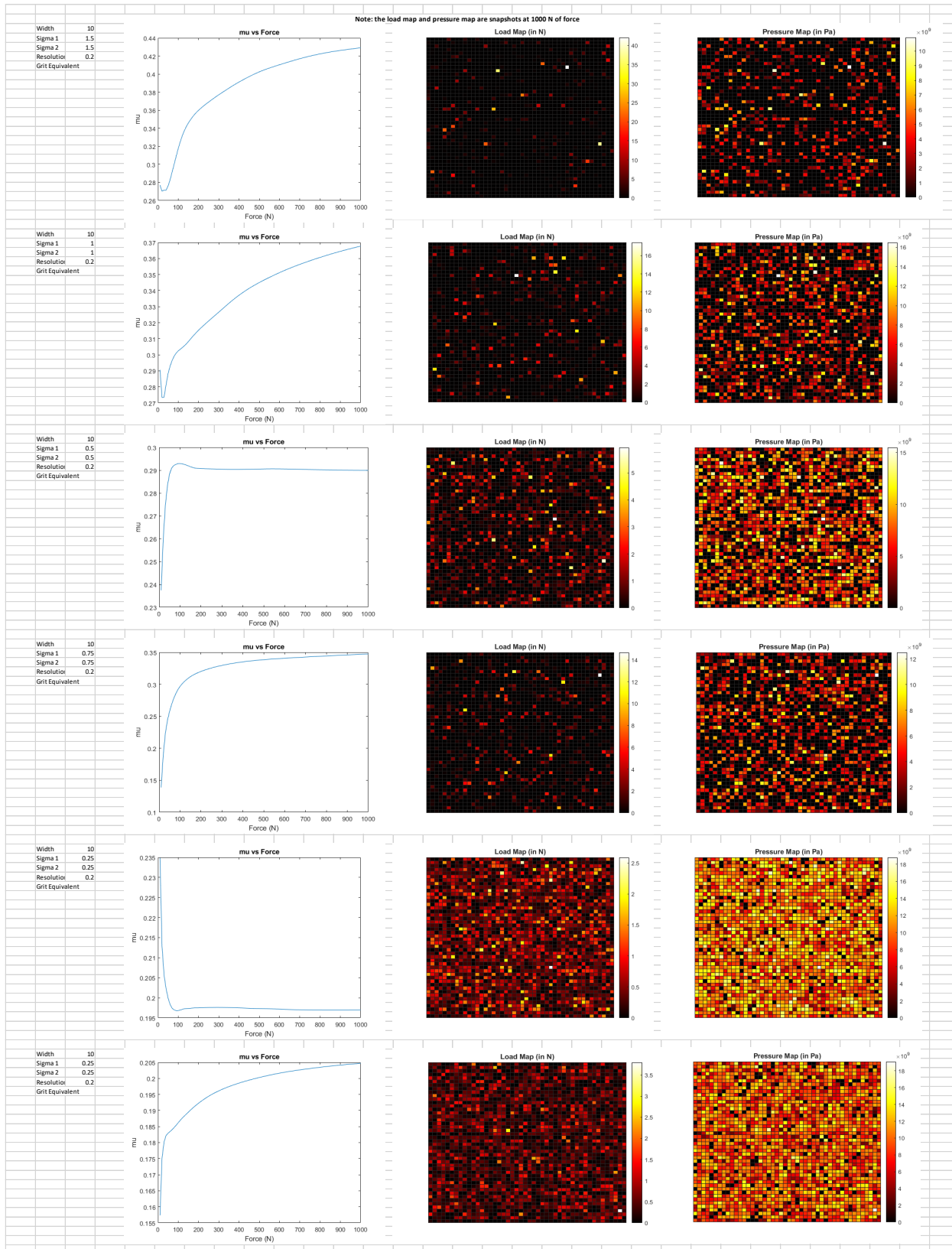
108.50	1.54E-06	1.54E-06	1.55E-06	1.58E-06	1.62E-06	1.65E-06	1.68E-06
109.20	1.55E-06	1.55E-06	1.57E-06	1.59E-06	1.63E-06	1.66E-06	1.69E-06
109.90	1.56E-06	1.56E-06	1.57E-06	1.59E-06	1.63E-06	1.66E-06	1.69E-06
110.60	1.56E-06	1.56E-06	1.58E-06	1.60E-06	1.63E-06	1.67E-06	1.69E-06
111.30	1.57E-06	1.57E-06	1.58E-06	1.60E-06	1.64E-06	1.67E-06	1.70E-06
112.00	1.58E-06	1.58E-06	1.59E-06	1.61E-06	1.65E-06	1.68E-06	1.71E-06
112.70	1.59E-06	1.59E-06	1.60E-06	1.62E-06	1.65E-06	1.69E-06	1.71E-06
113.40	1.59E-06	1.59E-06	1.60E-06	1.62E-06	1.66E-06	1.69E-06	1.72E-06
114.10	1.60E-06	1.60E-06	1.61E-06	1.63E-06	1.67E-06	1.70E-06	1.73E-06
114.80	1.61E-06	1.61E-06	1.62E-06	1.64E-06	1.67E-06	1.71E-06	1.74E-06
115.50	1.62E-06	1.62E-06	1.63E-06	1.64E-06	1.68E-06	1.71E-06	1.74E-06
116.20	1.62E-06	1.62E-06	1.64E-06	1.65E-06	1.69E-06	1.72E-06	1.75E-06
116.90	1.63E-06	1.63E-06	1.64E-06	1.66E-06	1.69E-06	1.73E-06	1.76E-06
117.60	1.64E-06	1.64E-06	1.65E-06	1.67E-06	1.70E-06	1.74E-06	1.77E-06
118.30	1.65E-06	1.65E-06	1.66E-06	1.67E-06	1.71E-06	1.74E-06	1.77E-06
119.00	1.66E-06	1.66E-06	1.67E-06	1.68E-06	1.72E-06	1.75E-06	1.78E-06
119.70	1.67E-06	1.67E-06	1.68E-06	1.69E-06	1.72E-06	1.75E-06	1.79E-06
120.40	1.67E-06	1.68E-06	1.69E-06	1.69E-06	1.73E-06	1.77E-06	1.80E-06
121.10	1.68E-06	1.68E-06	1.70E-06	1.70E-06	1.74E-06	1.77E-06	1.80E-06
121.80	1.69E-06	1.69E-06	1.70E-06	1.71E-06	1.75E-06	1.78E-06	1.81E-06
122.50	1.70E-06	1.70E-06	1.71E-06	1.72E-06	1.76E-06	1.79E-06	1.82E-06
123.20	1.71E-06	1.71E-06	1.72E-06	1.73E-06	1.76E-06	1.80E-06	1.83E-06
123.90	1.72E-06	1.72E-06	1.73E-06	1.74E-06	1.78E-06	1.81E-06	1.84E-06
124.60	1.73E-06	1.73E-06	1.74E-06	1.74E-06	1.78E-06	1.81E-06	1.85E-06
125.30	1.74E-06	1.74E-06	1.75E-06	1.75E-06	1.79E-06	1.82E-06	1.86E-06
126.00	1.75E-06	1.75E-06	1.76E-06	1.76E-06	1.80E-06	1.83E-06	1.86E-06
126.70	1.76E-06	1.76E-06	1.77E-06	1.77E-06	1.81E-06	1.84E-06	1.87E-06
127.40	1.77E-06	1.77E-06	1.78E-06	1.78E-06	1.82E-06	1.85E-06	1.88E-06
128.10	1.78E-06	1.78E-06	1.80E-06	1.79E-06	1.82E-06	1.86E-06	1.89E-06
128.80	1.79E-06	1.79E-06	1.81E-06	1.81E-06	1.83E-06	1.87E-06	1.90E-06
129.50	1.80E-06	1.80E-06	1.82E-06	1.82E-06	1.84E-06	1.88E-06	1.91E-06
130.20	1.82E-06	1.82E-06	1.83E-06	1.83E-06	1.85E-06	1.89E-06	1.92E-06
130.90	1.83E-06	1.83E-06	1.84E-06	1.84E-06	1.86E-06	1.90E-06	1.93E-06
131.60	1.84E-06	1.84E-06	1.85E-06	1.85E-06	1.87E-06	1.91E-06	1.94E-06
132.30	1.85E-06	1.85E-06	1.86E-06	1.86E-06	1.88E-06	1.92E-06	1.95E-06
133.00	1.87E-06	1.87E-06	1.88E-06	1.88E-06	1.89E-06	1.93E-06	1.96E-06
133.70	1.88E-06	1.88E-06	1.89E-06	1.89E-06	1.90E-06	1.94E-06	1.97E-06
134.40	1.89E-06	1.89E-06	1.90E-06	1.90E-06	1.91E-06	1.95E-06	1.99E-06
135.10	1.91E-06	1.91E-06	1.92E-06	1.92E-06	1.92E-06	1.96E-06	2.00E-06
135.80	1.92E-06	1.92E-06	1.93E-06	1.93E-06	1.93E-06	1.97E-06	2.01E-06
136.50	1.94E-06	1.94E-06	1.94E-06	1.94E-06	1.95E-06	1.98E-06	2.02E-06
137.20	1.96E-06	1.96E-06	1.96E-06	1.96E-06	1.96E-06	2.00E-06	2.03E-06
137.90	1.97E-06	1.97E-06	1.98E-06	1.98E-06	1.98E-06	2.01E-06	2.04E-06
138.60	1.99E-06	1.99E-06	1.99E-06	1.99E-06	1.99E-06	2.02E-06	2.05E-06
139.30	2.01E-06	2.01E-06	2.01E-06	2.01E-06	2.01E-06	2.03E-06	2.07E-06
140.00	2.02E-06	2.02E-06	2.02E-06	2.02E-06	2.02E-06	2.05E-06	2.08E-06
140.70	2.04E-06	2.04E-06	2.05E-06	2.05E-06	2.05E-06	2.06E-06	2.09E-06
141.40	2.06E-06	2.06E-06	2.07E-06	2.07E-06	2.07E-06	2.07E-06	2.11E-06
142.10	2.08E-06	2.08E-06	2.09E-06	2.09E-06	2.09E-06	2.09E-06	2.12E-06
142.80	2.10E-06	2.10E-06	2.11E-06	2.10E-06	2.10E-06	2.10E-06	2.14E-06
143.50	2.12E-06	2.12E-06	2.13E-06	2.13E-06	2.13E-06	2.12E-06	2.15E-06
144.20	2.14E-06	2.14E-06	2.15E-06	2.15E-06	2.15E-06	2.15E-06	2.16E-06
144.90	2.16E-06	2.16E-06	2.17E-06	2.17E-06	2.17E-06	2.17E-06	2.18E-06
145.60	2.19E-06	2.19E-06	2.19E-06	2.19E-06	2.19E-06	2.19E-06	2.19E-06
146.30	2.21E-06	2.21E-06	2.22E-06	2.22E-06	2.22E-06	2.21E-06	2.21E-06
147.00	2.23E-06	2.23E-06	2.24E-06	2.24E-06	2.24E-06	2.24E-06	2.24E-06
147.70	2.26E-06	2.26E-06	2.27E-06	2.27E-06	2.27E-06	2.26E-06	2.26E-06
148.40	2.29E-06	2.29E-06	2.29E-06	2.29E-06	2.29E-06	2.29E-06	2.29E-06
149.10	2.31E-06	2.31E-06	2.32E-06	2.32E-06	2.32E-06	2.32E-06	2.32E-06
149.80	2.34E-06	2.34E-06	2.35E-06	2.35E-06	2.35E-06	2.35E-06	2.35E-06
150.50	2.37E-06	2.37E-06	2.38E-06	2.38E-06	2.38E-06	2.38E-06	2.38E-06
151.20	2.40E-06	2.40E-06	2.41E-06	2.41E-06	2.41E-06	2.41E-06	2.41E-06
151.90	2.44E-06	2.44E-06	2.44E-06	2.44E-06	2.44E-06	2.44E-06	2.44E-06
152.60	2.47E-06	2.47E-06	2.48E-06	2.48E-06	2.48E-06	2.48E-06	2.48E-06
153.30	2.51E-06	2.51E-06	2.52E-06	2.52E-06	2.52E-06	2.52E-06	2.52E-06
154.00	2.55E-06	2.55E-06	2.56E-06	2.56E-06	2.56E-06	2.56E-06	2.56E-06
154.70	2.59E-06	2.59E-06	2.60E-06	2.60E-06	2.60E-06	2.60E-06	2.60E-06
155.40	2.64E-06	2.64E-06	2.65E-06	2.65E-06	2.65E-06	2.65E-06	2.65E-06
156.10	2.69E-06	2.69E-06	2.70E-06	2.70E-06	2.70E-06	2.70E-06	2.70E-06
156.80	2.74E-06	2.74E-06	2.75E-06	2.75E-06	2.75E-06	2.75E-06	2.75E-06
157.50	2.80E-06	2.80E-06	2.81E-06	2.81E-06	2.81E-06	2.81E-06	2.81E-06
158.20	2.87E-06	2.87E-06	2.88E-06	2.88E-06	2.88E-06	2.88E-06	2.88E-06
158.90	2.94E-06	2.94E-06	2.96E-06	2.96E-06	2.96E-06	2.96E-06	2.96E-06
159.60	3.03E-06	3.03E-06	3.04E-06	3.04E-06	3.05E-06	3.05E-06	3.05E-06
160.30	3.13E-06	3.13E-06	3.14E-06	3.14E-06	3.15E-06	3.15E-06	3.15E-06
161.00	3.24E-06	3.24E-06	3.25E-06	3.25E-06	3.26E-06	3.26E-06	3.26E-06
161.70	3.40E-06	3.41E-06	3.43E-06	3.43E-06	3.43E-06	3.43E-06	3.43E-06
162.40	3.60E-06	3.61E-06	3.63E-06	3.63E-06	3.64E-06	3.64E-06	3.64E-06
163.10	3.85E-06	3.86E-06	3.89E-06	3.89E-06	3.91E-06	3.91E-06	3.91E-06
163.80	4.28E-06	4.28E-06	4.32E-06	4.33E-06	4.33E-06	4.34E-06	4.34E-06
164.50	4.97E-06	4.98E-06	5.03E-06	5.04E-06	5.04E-06	5.07E-06	5.08E-06
165.20	5.51E-06	5.51E-06	5.56E-06	5.57E-06	5.57E-06	5.61E-06	5.62E-06
165.90	6.33E-06	6.33E-06	6.40E-06	6.40E-06	6.40E-06	6.43E-06	6.43E-06
166.60	7.48E-06	7.48E-06	7.56E-06	7.56E-06	7.56E-06	7.59E-06	7.59E-06
167.30	8.98E-06	8.98E-06	9.07E-06	9.07E-06	9.07E-06	9.09E-06	9.09E-06
168.00	1.07E-05	1.07E-05	1.08E-05	1.08E-05	1.08E-05	1.08E-05	1.08E-05
168.70	1.28E-05	1.28E-05	1.29E-05	1.29E-05	1.29E-05	1.29E-05	1.29E-05
169.40	1.53E-05	1.53E-05	1.54E-05	1.54E-05	1.54E-05	1.54E-05	1.54E-05
170.10	1.84E-05	1.84E-05	1.84E-05	1.84E-05	1.84E-05	1.84E-05	1.84E-05
170.80	2.21E-05	2.21E-05	2.22E-05	2.22E-05	2.22E-05	2.22E-05	2.22E-05
171.50	2.79E-05	2.79E-05	2.79E-05	2.79E-05	2.79E-05	2.79E-05	2.79E-05
172.20	3.58E-05	3.58E-05	3.59E-05	3.59E-05	3.59E-05	3.59E-05	3.59E-05
172.90	4.69E-05	4.69E-05	4.70E-05	4.70E-05	4.70E-05	4.70E-05	4.70E-05
173.60	6.25E-05	6.25E-05	6.26E-05	6.26E-05	6.26E-05	6.26E-05	6.26E-05
174.30	8.38E-05	8.38E-05	8.39E-05	8.39E-05	8.39E-05	8.39E-05	8.39E-05
175.00	1.12E-04	1.12E-04	1.12E-04	1.12E-04	1.12E-04	1.12E-04	1.12E-04
175.70	1.50E-04	1.50E-04	1.51E-04	1.51E-04	1.51E-04	1.51E-04	1.51E-04
176.40	2.00E-04	2.00E-04	2.00E-04	2.00E-04	2.00E-04	2.00E-04	2.00E-04
177.10	2.64E-04	2.64E-04	2.64E-04	2.64E-04	2.64E-04	2.64E-04	2.64E-04
177.80	3.55E-04	3.55E-04	3.57E-04	3.57E-04	3.57E-04	3.56E-04	3.56E-04
178.50	4.84E-04	4.84E-04	4.86E-04	4.86E-04	4.86E-04	4.86E-04	4.86E-04
179.20	6.54E-04	6.54E-04	6.56E-04	6.56E-04	6.56E-04	6.56E-04	6.56E-04
179.90	8.78E-04	8.78E-04	8.80E-04	8.80E-04	8.80E-04	8.80E-04	8.80E-04
180.60	1.17E-03	1.17E-03	1.17E-03	1.17E-03	1.17E-03	1.17E-03	1.17E-03
181.30	1.56E-03	1.56E-03	1.57E-03	1.57E-03	1.57E-03	1.57E-03	1.57E-03
182.00	2.07E-03	2.07E-03	2.07E-03	2.07E-03	2.07E-03	2.07E-03	2.07E-03
182.70	2.73E-03	2.73E-03	2.73E-03	2.73E-03	2.73E-03	2.73E-03	2.73E-03
183.40	3.58E-03	3.58E-03	3.59E-03	3.59E-03	3.59E-03	3.59E-03	3.59E-03
184.10	4.75E-03	4.75E-03	4.76E-03	4.76E-03	4.76E-03	4.76E-03	4.76E-03
184.80	6.28E-03	6.28E-03	6.29E-03	6.29E-03	6.29E-03	6.29E-03	6.29E-03
185.50	8.32E-03	8.32E-03	8.33E-03	8.33E-03	8.33E-03	8.33E-03	8.33E-03
186.20	1.09E-02	1.09E-02	1.09E-02	1.09E-02	1.09E-02	1.09E-02	1.09E-02
186.90	1.43E-02	1.43E-02	1.43E-02	1.43E-02	1.43E-02	1.43E-02	1.43E-02
187.60	1.86E-02	1.86E-02	1.86E-02	1.86E-02	1.86E-02	1.86E-02	1.86E-02
188.30	2.49E-02	2.49E-02	2.49E-02	2.49E-02	2.49E-02	2.49E-02	2.49E-02
189.00	3.35E-02	3.35E-02					

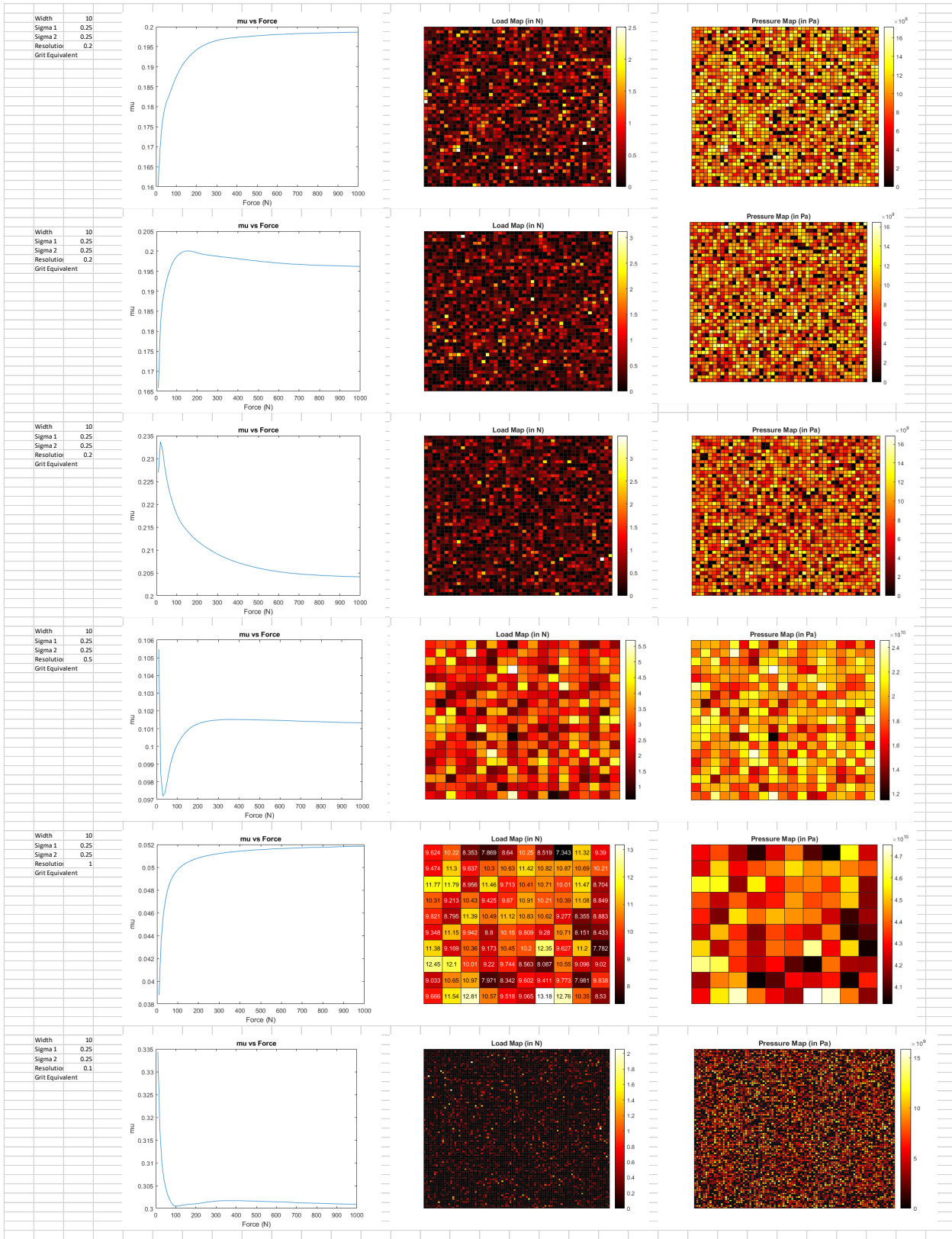
219.10	2.72E-05	2.81E-05	3.94E-05	4.02E-05	4.06E-05	4.11E-05	4.15E-05
219.80	3.25E-05	3.32E-05	4.82E-05	4.87E-05	4.93E-05	4.97E-05	5.01E-05
220.50	4.07E-05	4.07E-05	6.18E-05	6.24E-05	6.29E-05	6.33E-05	6.36E-05
221.20	5.41E-05	5.39E-05	8.73E-05	8.76E-05	8.79E-05	8.79E-05	8.74E-05
221.90	8.03E-05	7.79E-05	0.000104	0.000104	0.000104	0.000104	0.000104
222.60	1.54E-04	1.43E-04	0.000104	0.000104	0.000104	0.000104	0.000104
223.30	1.64E-03	9.39E-04	0.000104	0.000104	0.000104	0.000104	0.000104
224.00	1.91E-04	2.09E-04	0.000104	0.000104	0.000104	0.000104	0.000104
224.70	9.07E-05	9.45E-05	0.000104	0.000104	0.000104	0.000104	0.000104
225.40	9.97E-05	8.53E-05	0.000104	0.000104	0.000104	0.000104	0.000104
226.10	4.86E-05	4.54E-05	0.000104	0.000104	0.000104	0.000104	0.000104
226.80	1.95E-05	1.84E-05	0.000104	0.000104	0.000104	0.000104	0.000104
227.50	3.41E-05	3.03E-05	0.000104	0.000104	0.000104	0.000104	0.000104
228.20	1.29E-04	7.95E-05	0.000104	0.000104	0.000104	0.000104	0.000104
228.90	8.67E-05	1.42E-04	0.000104	0.000104	0.000104	0.000104	0.000104
229.60	3.28E-05	3.88E-05	0.000104	0.000104	0.000104	0.000104	0.000104
229.80	2.07E-05	2.29E-05	0.000104	0.000104	0.000104	0.000104	0.000104
229.50	1.53E-05	1.64E-05	0.000104	0.000104	0.000104	0.000104	0.000104
230.20	1.23E-05	1.28E-05	0.000104	0.000104	0.000104	0.000104	0.000104
230.90	1.04E-05	1.07E-05	0.000104	0.000104	0.000104	0.000104	0.000104
231.60	2.07E-05	2.06E-05	0.000104	0.000104	0.000104	0.000104	0.000104
232.40	2.11E-06	2.08E-06	0.000104	0.000104	0.000104	0.000104	0.000104
233.10	2.29E-05	2.17E-05	0.000104	0.000104	0.000104	0.000104	0.000104
233.80	2.54E-05	2.48E-05	0.000104	0.000104	0.000104	0.000104	0.000104
234.50	4.33E-06	4.48E-06	0.000104	0.000104	0.000104	0.000104	0.000104
235.20	7.68E-06	5.51E-06	0.000104	0.000104	0.000104	0.000104	0.000104
235.90	2.56E-06	2.37E-06	0.000104	0.000104	0.000104	0.000104	0.000104
236.60	2.95E-06	3.88E-06	0.000104	0.000104	0.000104	0.000104	0.000104
237.30	1.87E-06	1.82E-06	0.000104	0.000104	0.000104	0.000104	0.000104



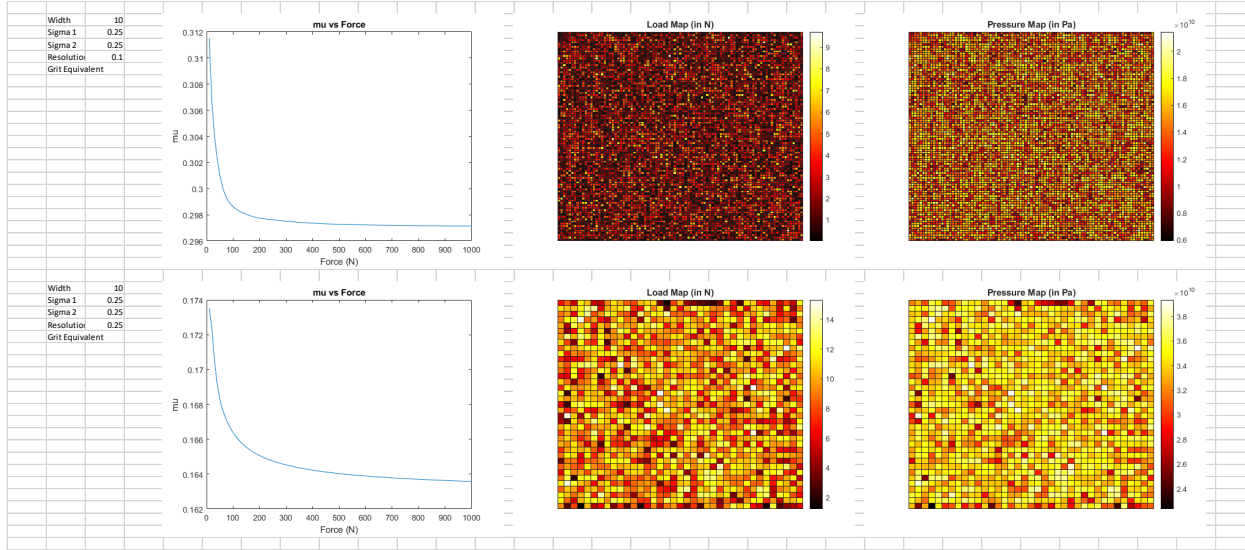
# D.3: Examination of the Influence of Resolution and Radius on the Contact Model

## D.3.1: Maximum Instantaneous Radius Examination

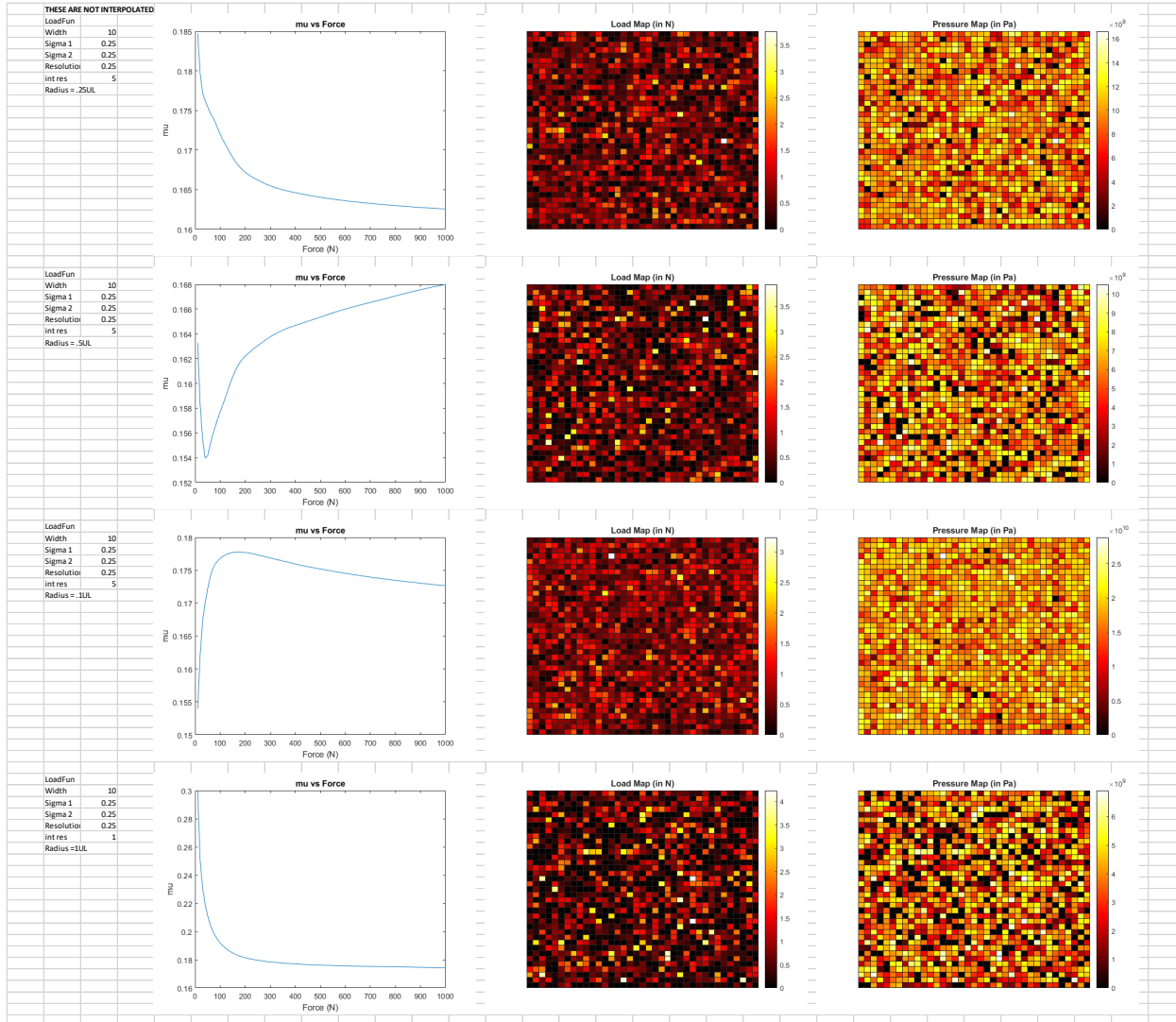




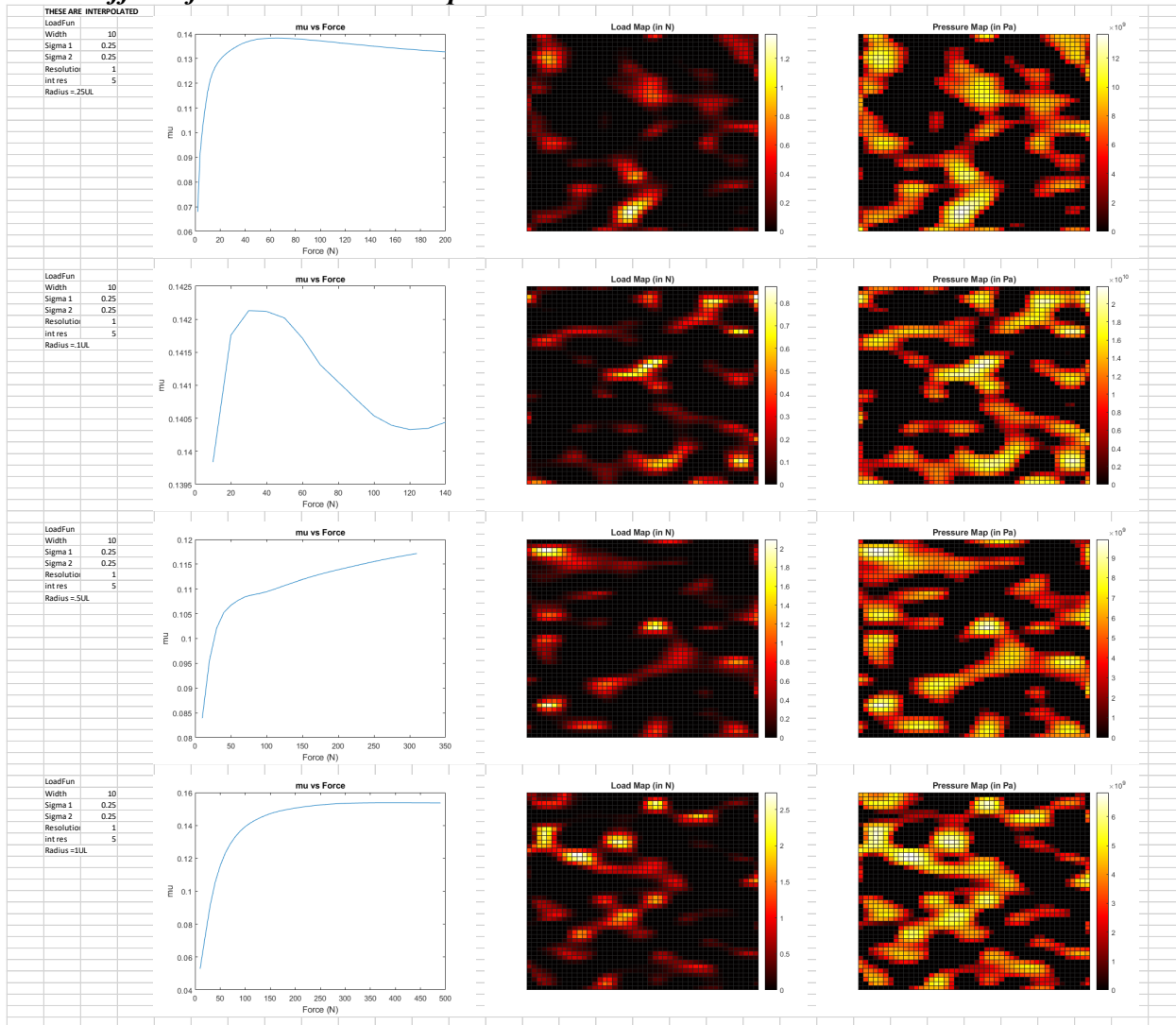
### D.3.2: Minimum Instantaneous Radius Examination



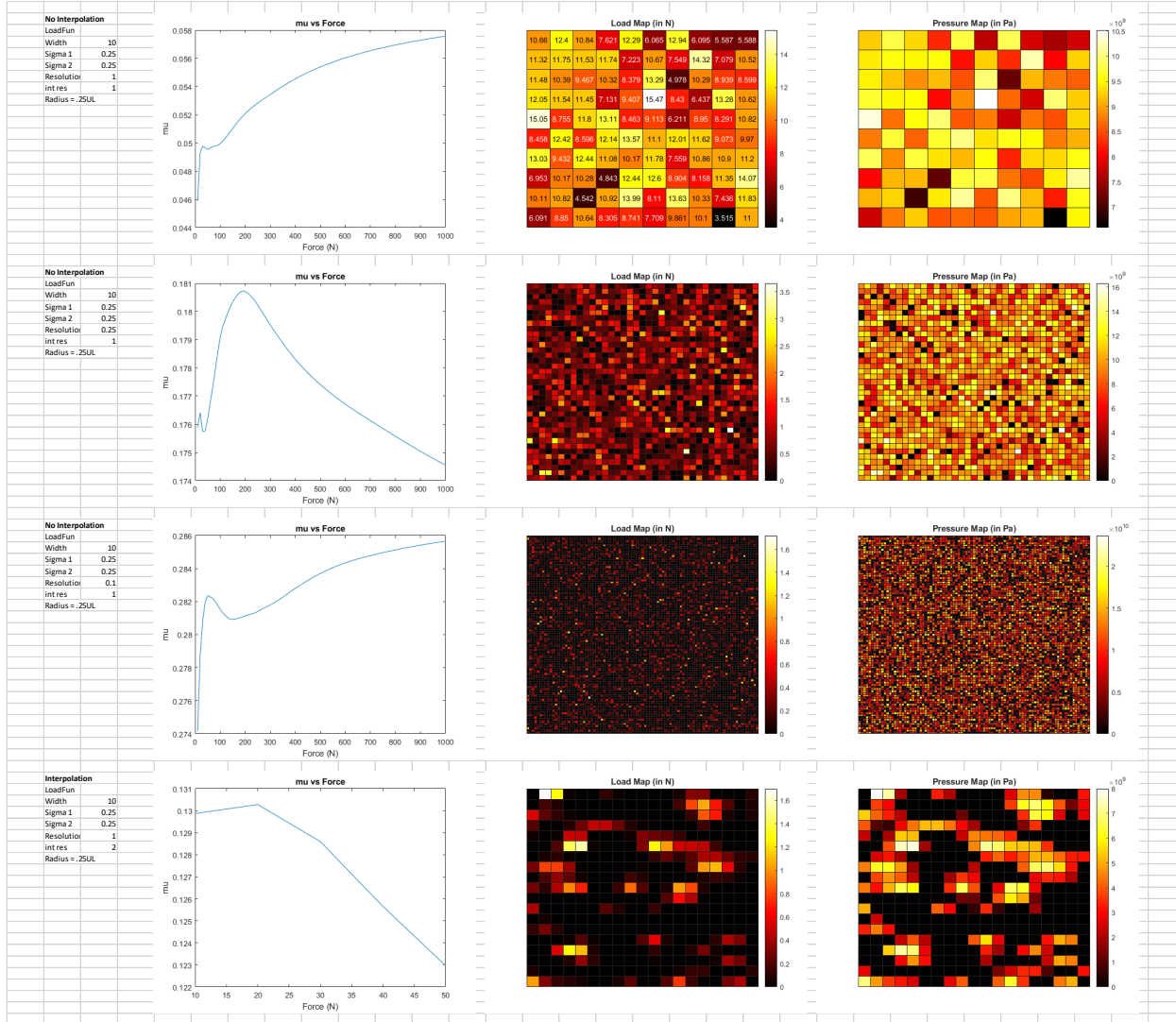
### D.3.3: Effect of Radius on Asperity Only Model



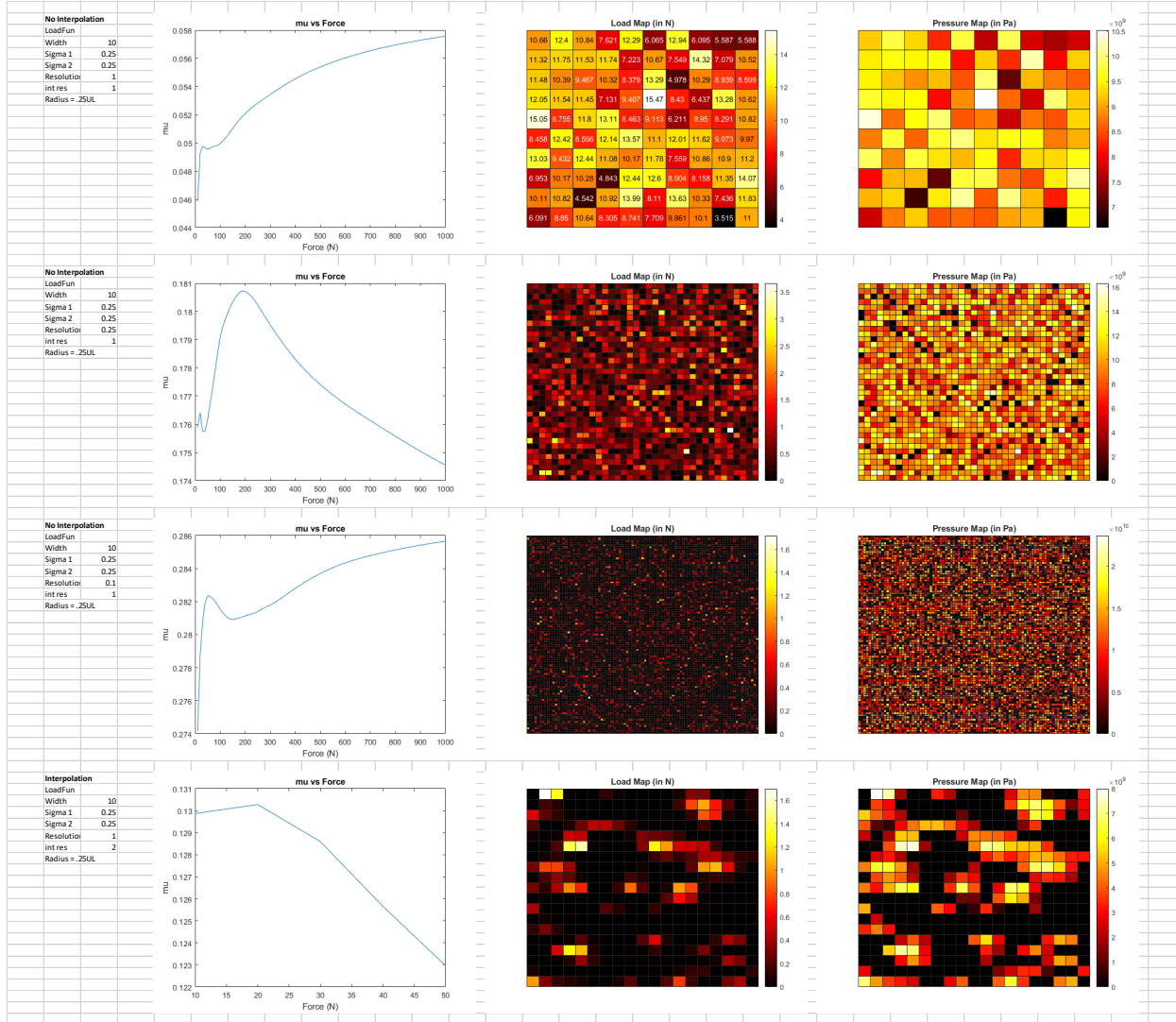
### D.3.4: Effect of Radius on the Interpolated Model



### D.3.5: Effect of Resolution on the Asperity Only Model



### D.3.6: Effect of Resolution on the Interpolated Model





## D.4: Correlation Between Clamping Force and Torque for a 4-40 Screw

		4-40 screw	
Torque in-lb	Clamping Force lb	Coefficient of friction	Bolt Diameter (in)
1	19.84126984	0.45	0.112
2	39.68253968		
3	59.52380952		
4	79.36507937		
5	99.20634921		
6	119.047619		
7	138.8888889		
8	158.7301587		
9	178.5714286		
10	198.4126984		
11	218.2539683		
12	238.0952381		
13	257.9365079		
14	277.7777778		
15	297.6190476		
16	317.4603175		
17	337.3015873		
18	357.1428571		
19	376.984127		
20	396.8253968		
21	416.6666667		
22	436.5079365		
23	456.3492063		
24	476.1904762		
25	496.031746		
26	515.8730159		
27	535.7142857		
28	555.5555556		
29	575.3968254		
30	595.2380952		
31	615.0793651		
32	634.9206349		
33	654.7619048		
34	674.6031746		
35	694.4444444		
36	714.2857143		
37	734.1269841		
38	753.968254		
39	773.8095238		
40	793.6507937		
41	813.4920635		
42	833.3333333		
43	853.1746032		
44	873.015873		
45	892.8571429		
46	912.6984127		
47	932.5396825		
48	952.3809524		
49	972.2222222		
50	992.0634921		
Coefficient of friction Eq			
<a href="https://www.engineeringtoolbox.com/friction-coefficients-d_778.html">https://www.engineeringtoolbox.com/friction-coefficients-d_778.html</a>			
Clamping force eq			
<a href="https://engineering.stackexchange.com/questions/8324/calculation-of-clamping-force-from-bolt-torque">https://engineering.stackexchange.com/questions/8324/calculation-of-clamping-force-from-bolt-torque</a>			

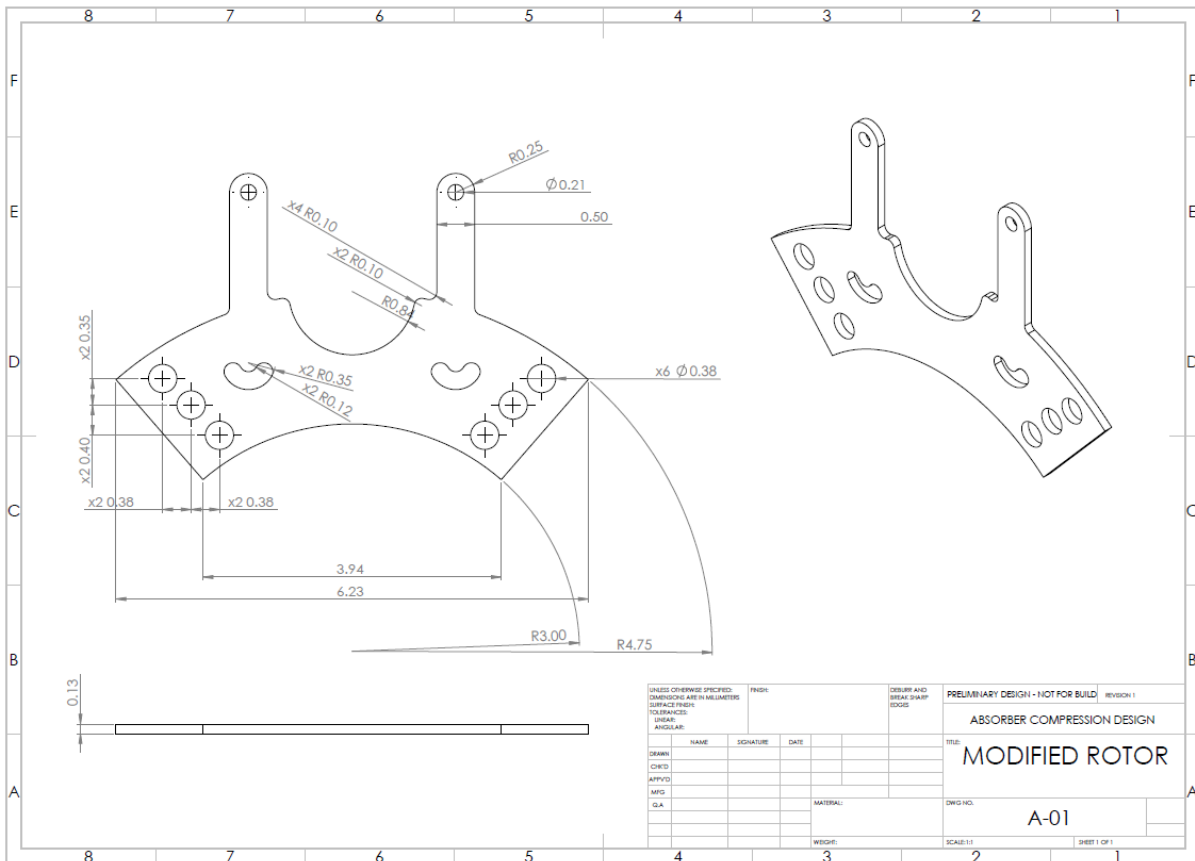
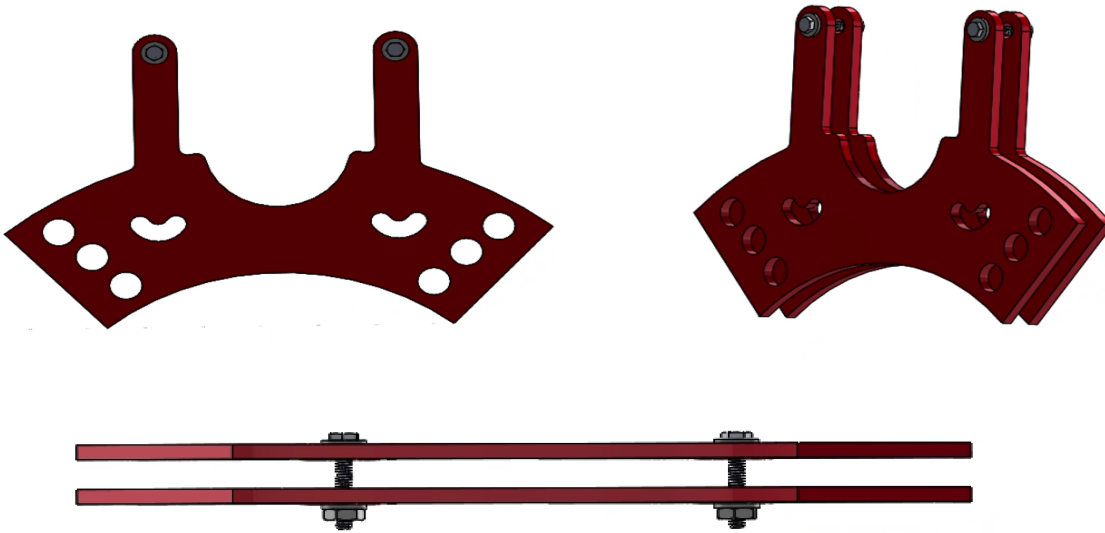
## D.5: Final Weeks Deliverables Map

Week :	Week 1					Week 2					Week 3	
Weekday	Wednesday	Thursday	Friday	Saturday	Sunday	Monday	Tuesday	Wednesday	Thursday	Friday	Saturday	Sunday
DATE	4/8/2020	4/9/2020	4/10/2020	4/11/2020	4/12/2020	4/13/2020	4/14/2020	4/15/2020	4/16/2020	4/17/2020	4/18/2020	4/19/2020
	Scheduling Rest of Capstone											
	Assinging duties											
			Make graph of sigma vs coeff									
					Complete Literature Review - CPVA Fundamentals - Friction Fundamentals - Applicable Procedures (Sandblasting)							
					Friction/Computations							
					Sandblasting/Generating Friction							
					CPVA Fundamentals							
					Project Schedule							
					Teamwork							
					Technical communication skills							
					Project schedule (postmortem)							
					Ethical Standards							
					Industrial/Commercial Standards							
					Professional Societies, codes, and standards							
					Safety							
						Meeting						
						Talk about Powerpoint						
						Design Constraints						
								Cost Analysis				
								Meeting				
									Polish Design Methodology			
										Meeting		
										Complete Ansys Models		
										Ansys Models		
										Talk about powerpoint		
											Design Constraints (design methodology)	
											Design Workflow (design methodology)	
											Each person needs to finish writing about their design section	
											describe how the ansys model is made (design)	
											Complete writing design solution (mostly ansys stuff)	
											finish writing results	
											MATLAB	
											Friction results	
											Summary/Conclusion	
											Recommendations	

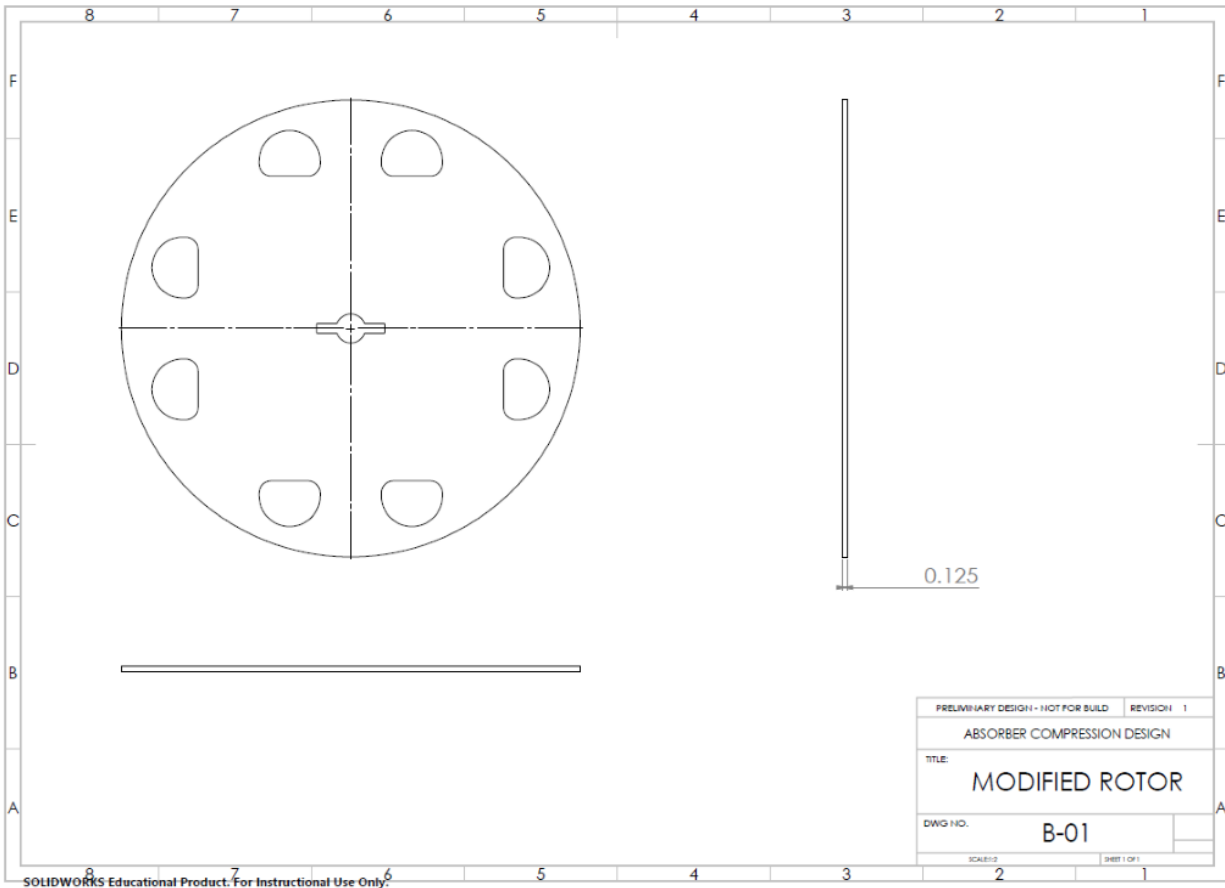
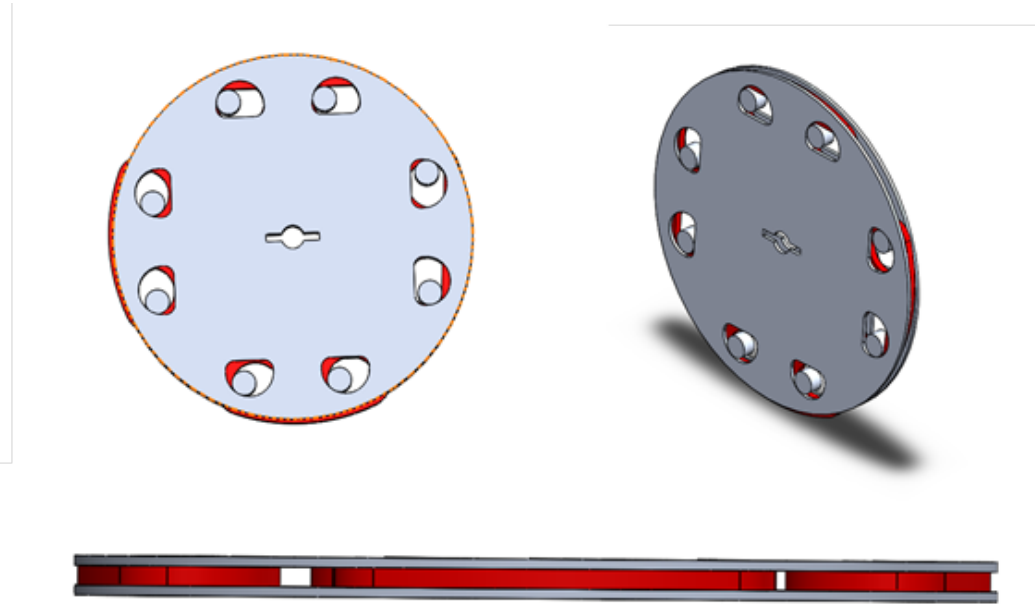


# Appendix E

## E.1: DESIGN A. Rotor Compressing Design

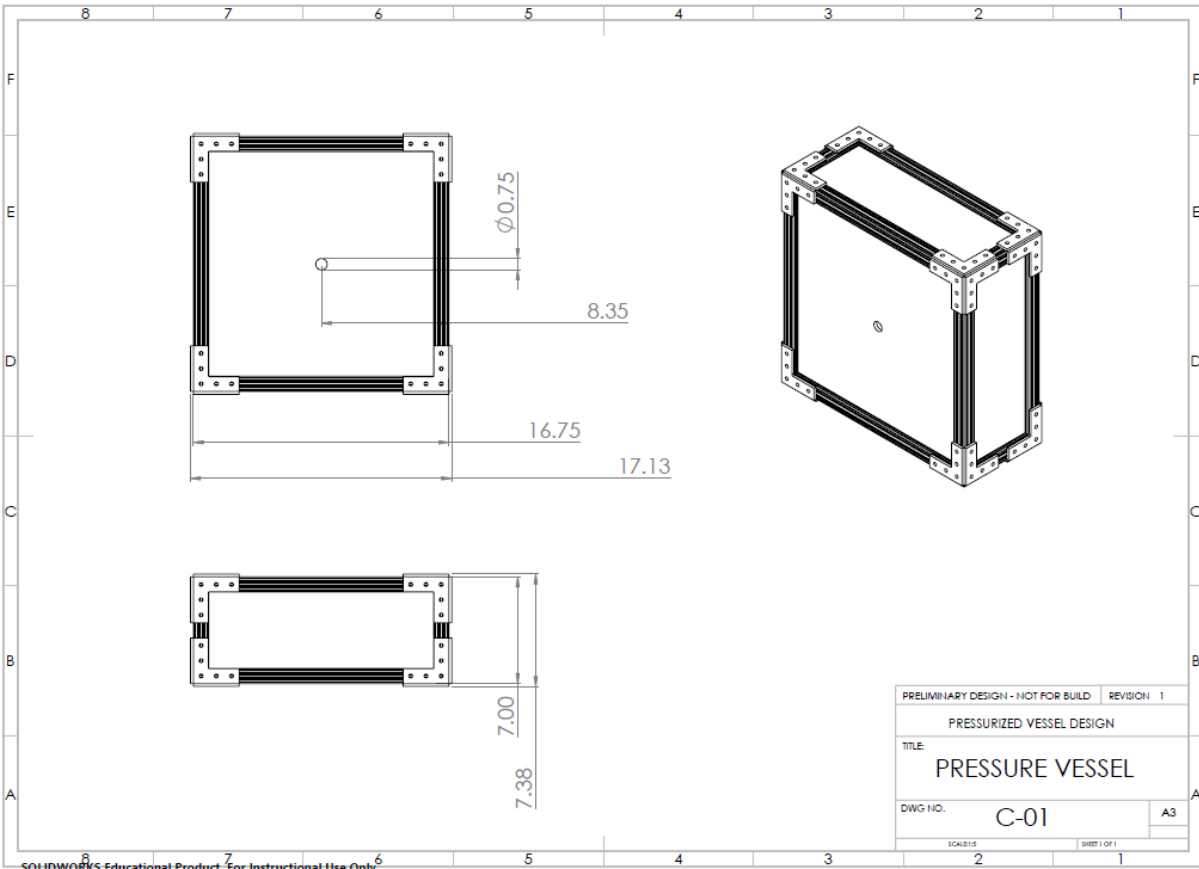
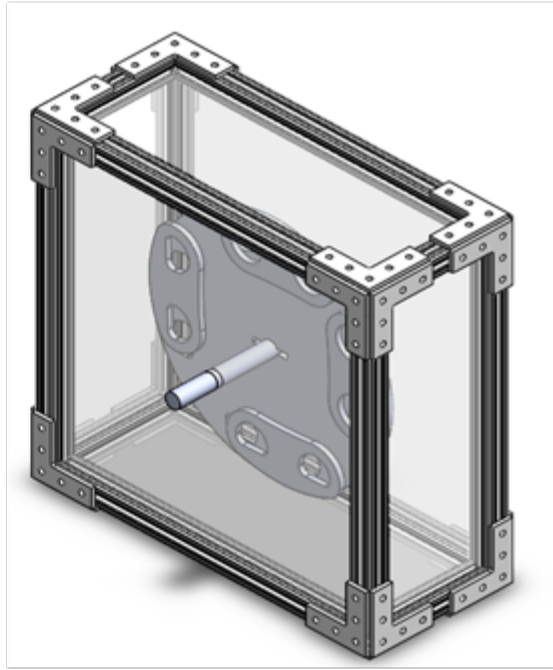
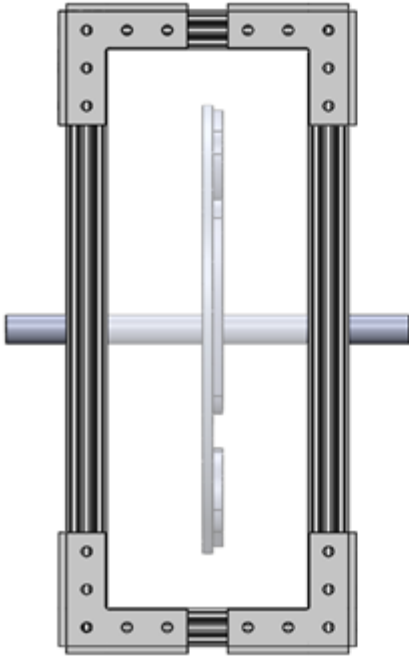


## E.2: DESIGN B. Absorber Compressing Design

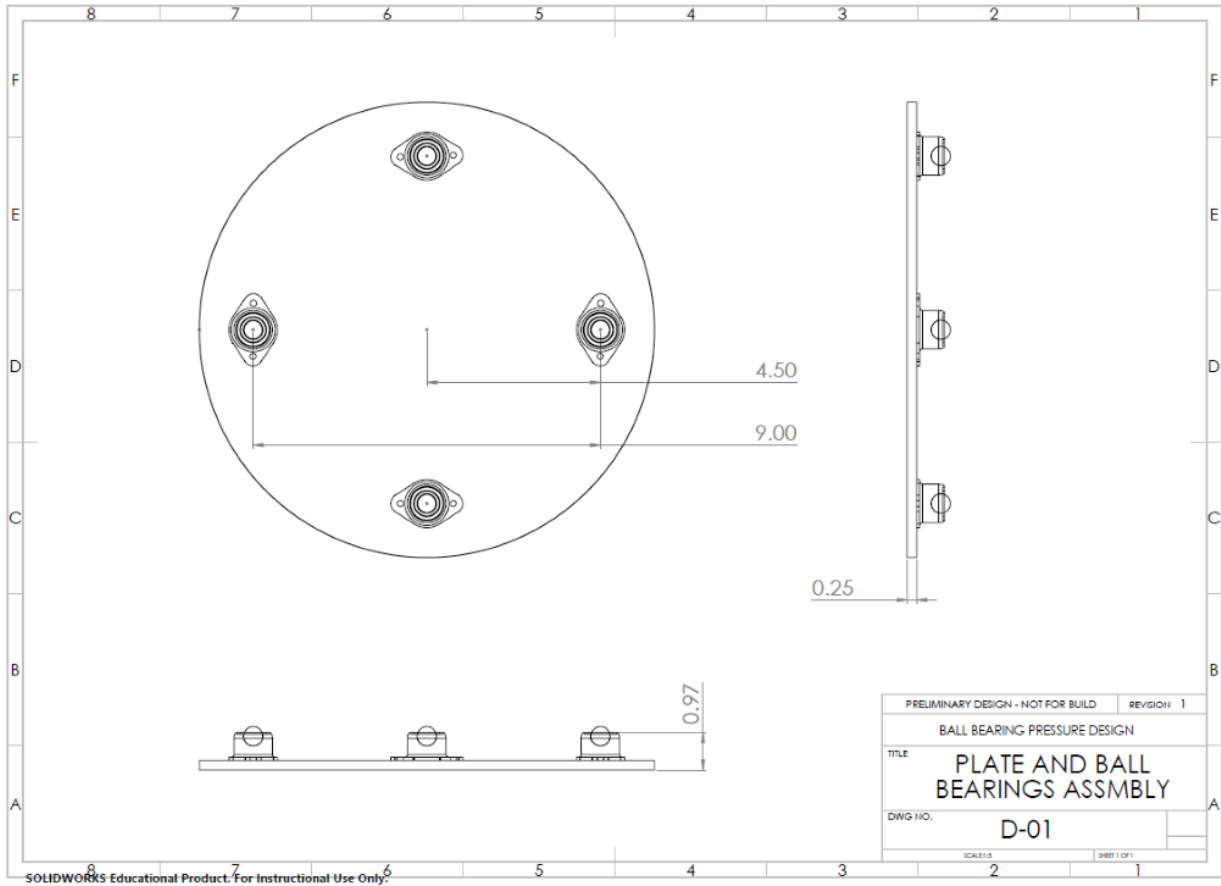
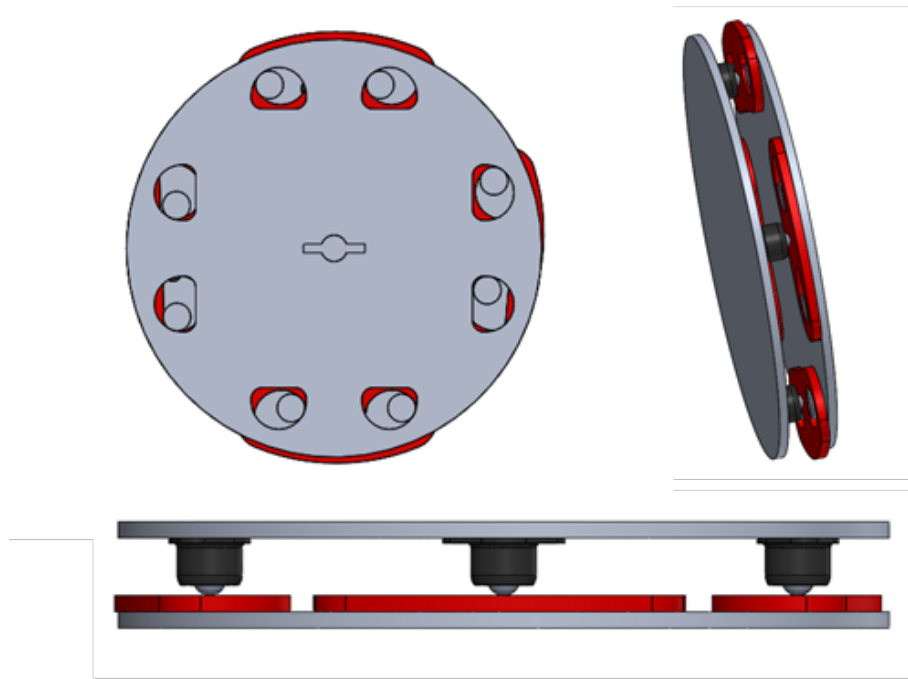


SOLIDWORKS Educational Product. For Instructional Use Only.

### E.3: DESIGN C. Pressurized Vessel Design



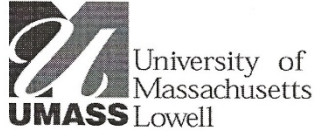
### E.4: DESIGN D. Ball Bearing Pressure Design



SOLIDWORKS Educational Product. For Instructional Use Only.

# Appendix F

## F.1: Materials Order February 14, 2020



Department of Mechanical Engineering  
One University Avenue  
Lowell, Massachusetts 01854

### Capstone Materials & Supplies Order Form

*To be completed by Requester*

**Student Name(s):** Nicholas McLaughlin, Alina Berkowitz, Stefanie Evans, Sean Freeman

**Course Section:** 809

**Capstone Instructor:** Professor Murat Inalpolat

**Date:** 2/14/2020

**Description of Supplies:**

Part Name	Part Number	Quantity	Unit Price	Extended Cost	Supplier	Estimated Shipping Cost
Multipurpose 6061 Aluminum Sheet 1/8" Thick, 6" x 12"	89015K236	2	\$16.63	\$33.26	McMaster-Carr	N/A
Multipurpose 6061 Aluminum 1/4" Thick x 2-1/2" Wide, 3 Feet Long	8975K68	2	\$16.44	\$32.88	McMaster-Carr	N/A
Stainless Steel Spade-Head Thumb Screw 8-32 Thread Size, 3/8" Long	91745A192	1	\$9.38	\$9.38	McMaster-Carr	N/A
General Purpose Tap Plug Chamfer, Uncoated High-Speed Steel, 8-32 Thread Size	26955A33	1	\$4.61	\$4.61	McMaster-Carr	N/A
Black-Oxide High-Speed Steel Drill Bit Wire Gauge 29, 2-7/8" Overall Length	2901A203	1	\$1.86	\$1.86	McMaster-Carr	N/A
<b>Subtotal</b>						\$81.99



---

*To be completed by Department Staff (G. Bousquet or B. O'Brien)*

**I certify that the total Bill of Materials of this project (including shipping estimate) is below the \$500 Department allotment, or otherwise approved by the Department Chair and that all items are from an approved UMass Lowell vendor.**

**Department Staff Signature:** \_\_\_\_\_ **Date:** 2/18/20

---

*To be completed by Capstone Instructor*

**I certify that the capstone project, including this form and associated attachments, has satisfactorily completed the design review and is approved to use/arrange the described resources.**

**Capstone Instructor Signature:** \_\_\_\_\_ **Date:** 2/18/20

---

*Capstone student(s) should submit this form to the department staff to order the materials & supplies only after signed by both the Department Staff and Capstone Instructor. Students should retain a copy of this form to include in Capstone Final Report.*

*This completed form must be received by March 20, 2020 to request departmental purchases.*



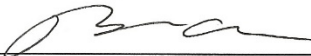
[zMktNREFPRVAYNE5RQiZ3aWRnZXROYW1IPXNwX2F0ZiZhY3Rpb249Y2xpY2tSZWRpc  
mVjdCZkb05vdExvZ0NsaWNrPXRydWU=](https://www.amazon.com/Sandpaper-Furniture-Finishing-Automotive-Polishing/dp/B01LZ6TG05/ref=lp_552594_1_4?s=power-hand-tools&ie=UTF8&qid=1582744535&sr=1-4)

**Item 4 Link:** [https://www.amazon.com/Sandpaper-Furniture-Finishing-Automotive-Polishing/dp/B01LZ6TG05/ref=lp\\_552594\\_1\\_4?s=power-hand-tools&ie=UTF8&qid=1582744535&sr=1-4](https://www.amazon.com/Sandpaper-Furniture-Finishing-Automotive-Polishing/dp/B01LZ6TG05/ref=lp_552594_1_4?s=power-hand-tools&ie=UTF8&qid=1582744535&sr=1-4)

---

*To be completed by Department Staff (G. Bousquet or B. O'Brien)*

**I certify that the total Bill of Materials of this project (including shipping estimate) is below the \$500 Department allotment, or otherwise approved by the Department Chair and that all items are from an approved UMass Lowell vendor.**

**Department Staff Signature:**  **Date:** 2/26/20

---

*To be completed by Capstone Instructor*

**I certify that the capstone project, including this form and associated attachments, has satisfactorily completed the design review and is approved to use/arrange the described resources.**

**Capstone Instructor Signature:**  **Date:** 2/26/20

---

*Capstone student(s) should submit this form to the department staff to order the materials & supplies only after signed by both the Department Staff and Capstone Instructor. Students should retain a copy of this form to include in Capstone Final Report.*

*This completed form must be received by March 20, 2020 to request departmental purchases.*

## **Appendix G**

# **Preliminary Coupon Friction Test Procedure**

**Design of Auxiliary Subsystems for an Automotive Drivetrain Test Rig**

Nicholas McLaughlin

Sean Freeman

Alina Berkowitz

Stefanie Evans

Revision A

# TABLE OF CONTENTS

<b>REVISIONS</b> .....	3
<b>1.0 OVERVIEW</b> .....	3
1.1 SCOPE.....	3
1.2 REQUIREMENTS.....	3
1.3 DEFFINITIONS AND ACCRONYMS.....	3
<b>2.0 TEST CONDITIONS</b> .....	3
2.1 ENVIRONMENT.....	3
2.2 SAFETY REQUIREMENTS.....	3
2.3 TEST EQUIPMENT.....	3
2.4 TEST SET UP.....	3
<b>3.0 TESTING SEQUENCE</b> .....	4
3.1 FRICTION TEST.....	4
<b>4.0 CONCLUSIONS</b> .....	4
4.1 FRICTION TEST CONCLUSIONS.....	4

## REVISIONS

<b>VERSION</b>	<b>DATE</b>	<b>AUTHOR</b>	<b>NOTES</b>
A	2/10/2020	S. Freeman	Initial Release

## 1.0 OVERVIEW

The purpose of this document is to detail the test procedure for the preliminary coupon friction test of UMass Lowell Mechanical Engineering Capstone project “*Design of Auxiliary Subsystems for an Automotive Drivetrain Test Rig*”.

### 1.1 SCOPE

The purpose of this test is to gain an understanding of the friction forces experienced by 6061 Aluminum Alloy coupons of metal with different surface roughness. This will serve to aid in the design of a subsystem capable of varying frictional forces on a Centrifugal Pendulum Vibration Absorber (CPVA) for an automotive drivetrain. The test being performed is to drag varying roughness aluminum coupons across a surface of known roughness, with an instrument to measure the force required to move the coupon.

### 1.2 REQUIREMENTS

Measurements of force, surface roughness and weight of the coupons are to be recorded. Coupons are to be varying degrees of roughness, and several trials of the tests are to be conducted to ensure accuracy.

### 1.3 DEFINITIONS AND ACRONYMS

<b>Acronyms</b>	<b>Definitions</b>
CPVA	Centrifugal Pendulum Absorber

## 2.0 TEST CONDITIONS

### 2.1 ENVIRONMENT

Standard lab conditions at UMass Lowell’s Baseball Laboratory unless otherwise specified.

### 2.2 SAFETY PRECAUTIONS

Ensure that all personal in attendance are following policies specified by the Composite lab. All lab equipment is to be handled with caution, and returned when testing is complete.

## 2.3 TEST EQUIPMENT

- Aluminum Coupons with varying surface roughness
- Instrument to measure force
- Table with known surface roughness
- String/Line to fix instrument to coupons
- Laptop to record data

## 2.4 TEST SET UP

Testing apparatus will be the same friction test set up for baseballs in UMass Lowell's baseball testing laboratory, modified to accommodate aluminum coupons. This test uses a two vertical supports to move a horizontal arm with controlled velocity and force, while measuring the resulting force applied to the arm. A line is attached at one end to the arm, runs through a pulley to convert all motion to horizontal, and the other end attached to the test subject. When the test is started the arm moves upward, resulting in the test subject being dragged across a surface, and the resulting force is measured by the arm. Testing apparatus can be seen in Figure 1.



Figure 1. Testing Apparatus for Friction Test

## 3.0 TESTING SEQUENCE

### 3.1 FRICTION TEST PROCEDURE

- 1.) Record Surface roughness of table, calibration of force instrument, mass of each coupon to be tested

- 2.) Secure coupon with tow line to instrument and ensure test is set up as described in Section 2.4 Test Set Up, complying to all conditions and rules of the baseball lab.
- 3.) Run the pre-programmed code to apply force onto coupon until it is in motion
- 4.) Record force necessary to move coupon.
- 5.) Repeat steps 2-4 for additional coupons to be tested.
- 6.) Break down test fixture and return all materials to composite lab

## **4.0 CONCLUSIONS**

### **4.1 FRICITION TEST CONCLUSIONS**

All Forces, Masses and surface roughness will be recorded. A successful test is defined as successfully obtaining understanding on how the force needed to move coupons varies with surface roughness of the coupons. Additionally, predictions and designs of how to apply this to the drivetrain testing rig will be determined.